

JOURNAL OF FACADE DESIGN & ENGINEERING

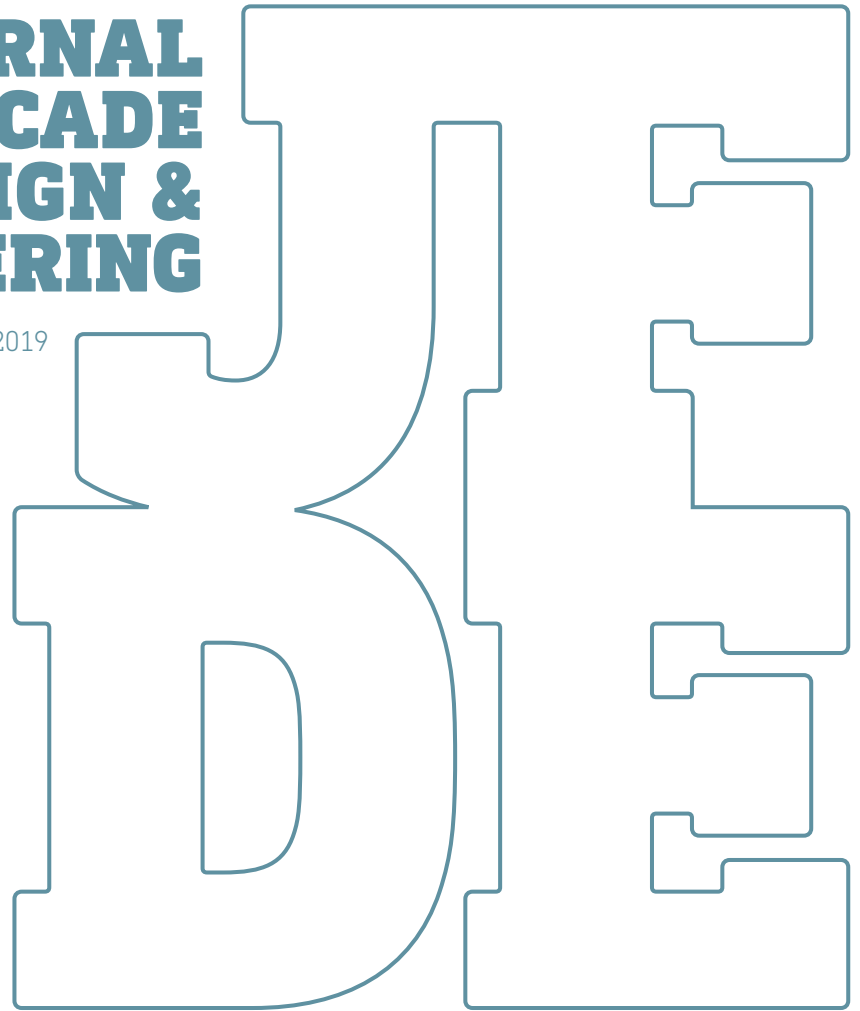
VOLUME 7 / NUMBER 1 / 2019

SPECIAL ISSUE POWERSKIN 2019

EDITORS IN CHIEF ULRICH KNAACK AND TILLMANN KLEIN
GUEST EDITORS THOMAS AUER AND JENS SCHNEIDER
SUPPORTED BY THE EUROPEAN FACADE NETWORK

**JOURNAL
OF FACADE
DESIGN &
ENGINEERING**

VOLUME 7 / NUMBER 1 / 2019



EDITORS IN CHIEF ULRICH KNAACK AND TILLMANN KLEIN
GUEST EDITORS THOMAS AUER AND JENS SCHNEIDER
SUPPORTED BY THE EUROPEAN FACADE NETWORK

SPECIAL ISSUE
POWERSKIN
2019

JFDE Journal of Facade Design and Engineering

JFDE presents new research results and new proven practice of the field of facade design and engineering. The goal is to improve building technologies, as well as process management and architectural design. JFDE is a valuable resource for professionals and academics involved in the design and engineering of building envelopes, including the following disciplines:

- Architecture
- Building Engineering
- Structural design
- Climate design
- Building Services Engineering
- Building Physics
- Design Management
- Facility Management

JFDE will – initially - be directed at the scientific community, but it will also feature papers that focus on the dissemination of science into practice and industrial innovations. In this way, readers explore the interaction between scientific developments, technical considerations and management issues.

Publisher

TU Delft Open
TU Delft / Faculty of Architecture and the Built Environment
Julianalaan 134, 2628 BL Delft, The Netherlands

Contact

Thaleia Konstantinou
JFDE-BK@tudelft.nl
+ 31 (0)6 48 27 26 43
<http://jfde.tudelft.nl/>

Policies

Peer Review Process – The papers published in JFDE are double-blind peer reviewed.

Open Access – JFDE provides immediate Open Access (OA) to its content on the principle that making research freely available to the public supports a greater global exchange of knowledge.

Licensed under a Creative Commons Attribution 4.0 International License (CC BY 4.0).

Indexation – JFDE is indexed in the Directory of Open Access Journals (DOAJ), Google Scholar, Inspec IET and Scopus.

Publication Ethics – Editors, authors and publisher adopt the guidelines, codes to conduct and best practices developed by the Committee on Publication Ethics (COPE).

Copyright Notice – Author(s) hold their copyright without restrictions.

Design & layout

Design – Sirene Ontwerpers, Rotterdam

Layout – Nienke Blaauw, TU Delft

Cover image

Pavilion of Africa. Expo Milan. Italy. @Ulrich Knaack

ISSN 2213-302X (Print)
ISSN 2213-3038 (Online)
ISBN 978-94-6366-127-0



Editorial board

Editors in Chief

Ulrich Knaack
Tillmann Klein
Delft University of Technology, The Netherlands

Guest editors

Thomas Auer (TU Munich, Munich, Germany)
Jens Schneider (TU Darmstadt, Darmstadt, Germany).

Editors

Thaleia Konstantinou (Delft University of Technology, The Netherlands)
Alejandro Prieto Hoces (Delft University of Technology, The Netherlands)

Associate Editors

Daniel Aelenei (Universidade Nova de Lisboa, Lisbon, Portugal), Enrico de Angelis (Polytechnico Milano, Milan, Italy), Julen Astudillo (TECNALIA Research & Innovation, San Sebastian, Spain), Carlo Battisti (IDM Südtirol - Alto Adige, Italy), Anne Beim (Royal Danish Academy of Fine Arts, Copenhagen, Denmark, Denmark), Jan Belis (Ghent University, Belgium), Jan Cremers (Hochschule für Technik Stuttgart (HFT), Germany), Andy van den Dobbelaere (Delft University of Technology, Delft, the Netherlands), Paul Donnelly (Washington University, St. Louis, USA), Chris Geurts (TNO, Delft, Netherlands), Mikkel K. Kragh (University of Southern Denmark, Odense, Denmark), Klaus Kreher (Lucerne University of Applied Sciences and Art, Lucerne, Switzerland), Bert Lieverse (Association of the Dutch Façade Industry, Nieuwegein, The Netherlands), Steve Lo (University of Bath, Bath, United Kingdom), Andreas Luible (Lucerne University of Applied Sciences and Art, Lucerne, Switzerland), Enrico Sergio Mazzucchelli (Politecnico di Milano ABC Department, Italy), David Metcalfe (Centre for Window and Cladding Technology, United Kingdom), Mauro Overend (University of Cambridge, Cambridge, United Kingdom), Uta Pottgiesser (University of Antwerp, Antwerp, Belgium), Josemi Rico-Martinez (University of the Basque Country, Donostia- San Sebastian, Spain), Paolo Rigone (UNICMI, Milan, Italy), Holger Strauss (Hartmann&Hauss, Germany), Jens Schneider (University of Darmstadt, Darmstadt, Germany), Holger Techen (University of Applied Sciences Frankfurt, Frankfurt, Germany), Nil Turkeri (Istanbul Technical University, Istanbul, Turkey), Claudio Vásquez-Zaldívar (Pontificia Universidad Católica de Chile, Santiago, Chile), Aslihan Ünlü Tavil (Istanbul Technical University, Istanbul, Turkey), Stephen Wittkopf (Lucerne University of Applied Sciences and Art, Lucerne, Switzerland).

Submissions

All manuscripts and any supplementary material should be submitted to the Editorial Office (JFDE-BK@TUDelft.nl), through the Open Journal System (OJS) at the following link: <http://jfde.tudelft.nl/>

Author Guidelines

Detailed guidelines concerning the preparation and submission of manuscripts can be found at the following link:
<https://journals.open.tudelft.nl/index.php/jfde/about/submissions>



Contents

- v **Editorial PowerSkin 2019**
- 001 **Trombe Curtain Wall Façade**
Thomas Wüest, Andreas Luible
- 013 **Comparative Overview on LCA Software Programs for Application in the Façade Design Process**
Rebecca Bach, Negar Mohtashami, Linda Hildebrand
- 027 **A Study on the Impact of Climate Adaptive Building Shells on Indoor Comfort**
Jacopo Gaspari, Emanuele Naboni, Caterina Ponzio, Adele Ricci
- 041 **SMP Prototype Design and Fabrication for Thermo-responsive Façade Elements**
Jungwon Yoon
- 063 **Auxetic Structures and Advanced Daylight Control Systems**
Yun Kyu Yi, Ryan Sharston, Dua Barakat
- 075 **Impacts on the Embodied Energy of Rammed Earth Façades During Production and Construction Stages**
Lisa Nanz, Martin Rauch, Thomas Honermann, Thomas Auer
- 089 **Bio-inspired Transparent Microfluidic Platform as Transformable Networks for Solar Modulation**
Mark E Alston, Uta Pottgiesser, Ulrich Knaack
- 101 **The PLUG-N-HARVEST Façade: A Second Skin with Active and Passive Components**
Verena Dannapfel, Tanja Osterhage, Maike Klein, Rita Streblow, Marius Vontein, Dirk Müller, Markus Kuhnhenne

Editorial PowerSkin 2019

This issue of the Journal of Façade Design and Engineering is a result of the second façade conference, PowerSkin, held on January 17th 2019, in the context of the building trade fair 'BAU' in Munich. The conference was organized collaboratively by TU Munich, TU Darmstadt, and TU Delft. All three universities conduct high-impact research and education in the field of building envelopes.

The conference featured a mix of practice and education experiences, as well as scientific contributions, and aimed to answer the key question of the 2019 conference: How can digital tools and methods promote changes that aim towards the decarbonisation of the built environment and the improvement of well-being? The 2019 conference focused on the envelope as an integral part of the building and its energy system, as well as the main driver to create comfort. Thus, the envelope is understood in its condition of being a complex interface to the social, economic, and climatic environment in which we build our cities. The interaction between these topics, the influences they create, and the digital tools that have been developed and used to design and engineer building envelopes are the main focus points of each of the papers published in this issue.

We thank our guest editors Thomas Auer (TU Munich) and Jens Schneider (TU Darmstadt), and their respective teams, who have been key partners in creating this special issue.

The editors in chief,

Tillmann Klein
and
Ulrich Knaack.

DOI 10.7480/jfde.2019.1.3025

Trombe Curtain Wall Façade

Thomas Wüest¹, Andreas Luible²

- 1 Competence Centre Building Envelope, Institute of Civil Engineering, Lucerne University of Applied Sciences and Arts, Horw, Switzerland, email: thomas.wueest@hslu.ch
- 2 Competence Centre Building Envelope, Institute of Civil Engineering, Lucerne University of Applied Sciences and Arts, Horw, Switzerland

Abstract

In times of energy use awareness, decarbonisation, and resource efficiency, the performance of well-known façade components must be pushed beyond current limits through innovative designs and new combinations in construction. This paper presents an unconventional redesign of a double skin façade (DSF), based on Trombe wall principles, to enlarge solar gains in heating seasons and avoid overheating issues in summertime. The DSF variant is equipped with a thermal storage mass in the DSF cavity and interior insulation. The thermal mass, in this case concrete, is of a dark colour for high solar absorption, whereas the shading device is highly reflective. In contrast to traditional Trombe wall systems, this TCW is not supposed to actively heat interior space or transfer thermal energy. Instead, the TCW aims to regulate heat flux within the façade level by the management of solar thermal energy fluxes. The potential to reduce buildings' heat losses through solar energy use is shown and compared to a traditional external thermal insulation composite system (ETICS) with an appropriate insulation thickness for renovation purposes in Switzerland. The U-Value is therefore considerably lower, 0.25 instead of 0.41 for the TCW. Due to the innovative design and fully transient operation, a highly detailed and flexible simulation tool is needed to analyse and assess the façade performance. The decision to simulate the novel system was made for Modelica-Dymola, with its object-oriented, equation-based simulation language. The simulations of both TCW and ETICS show potential for heat loss reduction due to solar energy storage on every orientation. However, the TCW shows a high solar energy usage due to its 'natural' overheating tendency. Furthermore, heat losses are significantly lower than the U-Value predicts and, in some cases, even lower than the ETICS heat losses. In addition, due to its lower use of material and lower weight, the system can be used as a curtain wall system instead of traditional DSFs, which have higher heat losses in winter and higher solar gains in summer.

Keywords

Passive façade, Low-Tec, energy efficiency, adaptive façade, performance gap, adaptive g-Value

DOI 10.7480/jfde.2019.1.2619

1 INTRODUCTION

In recent decades, there has been a constant rise in awareness of energy. According to the International Energy Agency (2013), the largest energy consumer is the building sector, which is responsible for one-third of global energy consumption and carbon dioxide emissions. If energy efficiency is not improved, the energy demand is expected to rise by 50% by 2050. However, the EU Energy Roadmap 2050 (European Commission, 2012) states that the buildings that will be in use in 2050 are being designed and built now. To achieve those energy goals, higher energy efficiency in new and existing buildings plays a key role. In addition, Zero Energy Buildings (ZEB) should become the standard for new buildings.

Achieving high energy efficiency in buildings is a complex process with various influences. The role of its envelope, as a physical separator between controlled and uncontrolled environments, is an important factor. A façade controls the energy and mass transfer between indoors and outdoors, making it one of the most promising solutions for the improvement of energy consumption in buildings. Therefore, improved façades will lead to lower energy demand for cooling and heating. Furthermore, the façade can support HVAC systems and reduce their size. Undoubtedly, more efficient HVAC installations also contribute to a building's energy savings. However, the façade still makes the highest demands on HVAC energy. As Perino & Serra (2015) emphasise, new and more revolutionary concepts and technologies to achieve a ZEB or nearly ZEB standard need to be developed.

Various research efforts in the area of energy efficient and / or adaptive façades are in progress. While some focus on the limits of available simulation tools (Loonen, 2010), others explore the potential of smart materials, such as a Phase Change Material (PCM) filled double glazing unit (Goia, Zinzi, Carnielo, & Serra, 2015) or other smart windows (Casini, 2015) for improving the energy efficiency of buildings. Furthermore, kinematic (Schleicher et al., 2011; Suralkar, 2011) solutions are being researched. However, the possibilities of active or passive solar energy use within façades are also under exploration. For this topic, a review of Quesada Rousse, Dutil, Badache, & Hallé (2012) gives a good overview of opaque solar façades, which have significant potential to reduce heating loads.

Thermally active solar façades usually need fans or pumps to distribute the solar thermal gains for heating, cooling, or storage purposes. Passive systems instead utilise natural processes of heat transfer (conduction, convection, radiation). The most popular solar walls are Trombe walls and its variants. Trombe walls are rather simple construction elements; they consist of an external glass layer and an internal, high absorptive thermal mass, divided by an air gap, which uses the greenhouse effect. Active or passive controllable flaps enable the natural airflow to be controlled and, therefore, the internal heat gain. Hu, He, Ji, & Zhang, (2017), Quesada et al. (2012), and Omrany, Ghaffarianhoseini, Ghaffarianhoseini, Rhaahemifar, & Tookey (2016) agree that Trombe walls (TW) have the potential to significantly reduce a building's energy consumption.

However, most TWs are often considered as massive, thick walls that allow significant thermal transfer to the room. This study introduces a new TW façade with solar thermal storage, which can be used as "lightweight" curtain wall façade element. In contrast to earlier attempts, this new TW façade renounces to "heat" interior spaces; instead, its purpose is to passively balance out thermal heat gains on the façade level. In addition, this study aims to use low-tech solutions as far as possible. Due to the low-tech principle, this feasibility study of a Trombe curtain wall element is strongly related to currently available materials and elements.

The façade is based on non-ventilated Double Skin Façade (DSF) elements with a high reflective shading device. The inner Insulated Glazing Unit (IGU) layer of traditional DSFs is replaced by a 50mm thermal mass and 75mm internal insulation. This configuration allows it to control heat fluxes through the façade on seasonal, daily, or hourly levels. While the “natural” overheating tendency of DSFs is used to load the thermal storage in heating seasons, the high reflective shading device, in cooperation with the thermal mass, reduces overheating in cooling seasons. This enables the Trombe Curtain wall (TCW) system to actively employ an adaptive g-Value.

In this paper, the performance of the new TCW prototype is compared to a traditional external thermal insulation composite system and shows the potential of solar energy use to reduce heating demands of buildings. This is an extract of the original project “Solar Energy Balanced Façade” (SEBF), in which the façade element is partly transparent and the TCW element is used as a parapet.

2 METHODOLOGY

To investigate the thermal performance of this new TCW prototype, a detailed dynamic calculation model must be applied. Unfortunately, most Building Performance Simulation (BPS) tools are not supposed to investigate such a dynamic system in a detailed way. Therefore, the decision was made to use Modelica, an object-orientated, equation-based language that can describe physical systems in various domains.

Detailed descriptions of the various advantages of equation-based modelling with Modelica can be found in Wetter (2011). One of the features is the possibility to encapsulate physical functions into classes, which can be tested separately and reused to build up systems that are more complex. In addition, the user can concentrate on describing the physical constraints instead of describing the intended performance.

Because of its high level of detail, the study is undertaken only at a façade level.

2.1 MODELLING APPROACH

The Trombe wall system is divided into its four main elements described in the simulation model (see Fig. 1): B) external glass layer; C) air cavity with shading device; D) thermal mass; E) insulation layer.

The external glazing (Fig 1.B) is modelled as a pane with two surface nodes and a centre node, connected by two conduction elements. The mass of the glazing is concentrated at the centre node, where the solar heat gain is applied. So far, these are standard Modelica library elements with extended parameters to simplify model changes and encapsulation. The implemented optical model uses direct radiation, diffuse radiation, and the angle of incidence to calculate the Fresnel corrected reflection and transmission of the glazing.

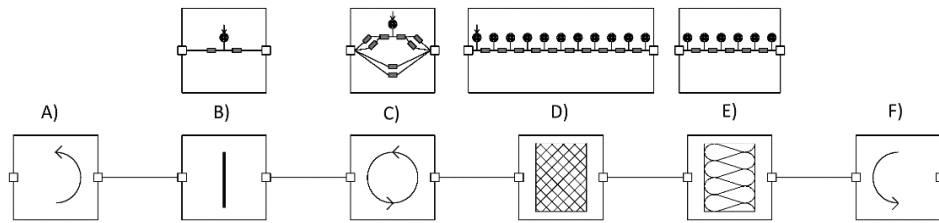


FIG. 1 Modelica model scheme for the four main components of the Trombe wall system. Bottom row, from left to right: A) external surface heat transfer, B) single glazing element, C) air cavity, D) storage mass, E) insulation, and F) interior surface transfer. Upper row: detailed scheme

For the air gap model, two models are combined: a) air gap without shading and b) air gap with shading. Both possible heat fluxes are completely modelled by one (or two) convective and radiative (standard) conduction elements based on the ISO 15099 formulation (Section 8.3.2.2 and 8.4.3.1). The shading device is modelled in the same manner as the single glazing, two conductors, one mass, and heat gain elements. Due to the small thickness (1mm) and high conductivity ($\lambda=160\text{W/mK}$) of aluminium, this is regarded as a valid simplification. All conduction elements in the air gap were connected to the shading control by a shading area factor (0...1). In case of activation or deactivation of the shading device, a critical damping element smoothens the transition from open to closed, or vice versa. The optical model is also connected to the shading area factor to calculate transmission, reflection, and solar heat gain on the shading mass.

The wall is divided into 10 equidistant conductors and 11 masses, nine of which represent $1/10^{\text{th}}$ of the total thickness with the final two representing $1/20^{\text{th}}$ of the total thickness as surface elements. The solar heat gain is applied to the outer surface mass, depending on the surface's characteristics. The insulation layer is a simplified wall model in which only five conductors are used instead of 10. This also applies to the masses, four of which represent $1/5^{\text{th}}$ and two represent $1/10^{\text{th}}$ of the surface.

Internal and external surface heat exchange is modelled according to EN 15099 with a radiation temperature equal to air temperature. The definition of those basic elements allows the main components to be reconnected to a comparison model of a standard insulated wall system (see Section 2.3).

2.2 ELEMENT DESCRIPTION

For the investigations shown in this paper, the results are based on elements of 2.5m^2 , with 1m width and 2.5m height. To compare the results, two elements are considered: the Trombe curtain wall element and a standard insulated wall for renovation purposes (SIA 380/1, 2009).

The Trombe curtain wall (TCW) element consists of:

- 6mm external glazing
- 150mm air gap (shading mounted centrally)
- Shading device (1mm aluminium)
- 50mm of concrete
- 75mm insulation
- U-Value: 0.44 / 0.41 W/(m²K) (without and with shading)

The second wall, a usual external thermal insulation composite system (ETICS);

- 15mm plaster
- 150mm insulation
- 150mm concrete
- U-Value 0.25 W/(m²K)

2.3 MATERIAL PROPERTIES

Each material used is considered in terms of “common” values from practice, according to related literature (see Table 1). This is not to distort the results of the comparison with standard façades. The adjustment of material properties and therefore the improvement of the façade performance are topics for further investigations.

MATERIAL	ρ [-]	τ [-]	λ [W/(mK)]	ρ [kg/m ³]	c_p [J/(kgK)]	ϵ [-]	d [mm]
Glass (orthogonal)	0.08	0.82	1.0	2700	750	0.84	6
Insulation	0.5	0	0.04	80	600	0.9	75
Concrete	0.8	0	2.1	2400	1000	0.9	150 / 50
Plaster	0.5	0	0.87	1600	1000	0.9	15
Shading device	0.85	0	160	2800	880	0.9	1

TABLE 1 Material properties

2.4 BOUNDARY CONDITIONS

Internal air temperature is set to 22 °C, and influences of occupancy, which lead to temperature variations, are not considered here. The climatic outdoor conditions are given by a standard design year for Zürich (CH) on an hourly basis from METEONORM. All parameters, such as temperature, wind speed, façade irradiation, and sun position, are interpolated linearly from hourly values.

2.5 SHADING CONTROL

The TCW makes use of solar gains in cold periods and prevents overheating during warmer periods, for which a customised shading control is responsible.

First, the shading control must decide whether it is a heating or cooling period. Therefore, the mean value of external air temperature over 24 hours is used as deciding factor. If the mean outside temperature is below 12 °C, which is more or less the heating limit temperature in Switzerland, the ‘heat gain’ mode is activated. Consequently, the ‘avoid heat gain’ mode is enabled for mean temperatures above 12°C. For mean outside temperatures higher than 15°C, the system enlarges night time heat losses.

To prevent heat losses, the shading is activated at night time (global radiation < 25 W/m²) with a mean outside temperature below 15°C as an additional thermal resistance. During daytime with

solar irradiation $>25 \text{ W/m}^2$ and mean outside temperatures below $12 \text{ }^\circ\text{C}$, the high absorptive thermal storage accumulates solar energy.

To avoid solar gains, the high reflective shading device is activated on days with mean outside temperatures above 12°C . In addition, during nights with mean outside temperatures above 15°C , the shading device is disabled to enlarge heat losses and 'pre-cool' the thermal storage.

This TCW control strategy is determined to react to seasonal needs. At the moment, this is undoubtedly a simplified approach to prove the feasibility of the system for the Central European climate. Further investigation to define the right set points and, perhaps, additional input parameters is in progress.

3 RESULTS

In this chapter, the simulation results are presented. To begin with, the systems are simulated in a detailed transient manner without solar gains in order to compare it to the U-Value calculation. Based on those "no-sun" results, the solar energy potential for each façade system in the four main orientations is presented. Finally, the orientation-dependent transient results are compared directly.

3.1 NON-SOLAR RESULTS

Based on Chapters 2.2 and 2.3, the U-Value of the TCW system is 64% higher. The transient simulation, without solar gains, shows similar results to the simplified calculation (see Table 2). However, the shading control system within the TCW façade receives the same data and therefore provides the same control output as when solar gains occur. The relatively higher heat losses in summer months (June to September) is due to the night-cooling mode and therefore the discharged thermal storage. Furthermore, the shading device is closed during "sunny" hours and reduces daily heat gains due to higher outside temperatures.

	JAN	FEB	MAR	APR	JUN	JUL	AUG	SEP	OCT	NOV	DEC
Massive	-9.2	-8.0	-7.6	-5.6	-3.9	-2.1	-1.6	-1.7	-3.2	-5.0	-7.3
Trombe	-15.0	-13.0	-12.4	-9.4	-6.6	-3.9	-3.1	-3.2	-5.7	-8.5	-11.9
%	163%	163%	163%	167%	171%	185%	194%	192%	179%	170%	164%

TABLE 2 Heat flux through façade elements per month, without solar influences in [kWh] per element

The U-Value prediction is confirmed and an overheating of the DSF is, due to the lack of solar irradiation, not observed.

3.2 SOLAR ENERGY POTENTIAL FOR THE ETICS

The solar potential is strongly dependent on orientation (available solar irradiation) and solar absorption. In this study, the solar absorption coefficient of the massive wall system is assumed to be

0.5, which is relatively high for painted surfaces and low for bricks. However, it is an average value to demonstrate the solar potential and to provide a comparison with the Trombe wall system.

As shown in Fig. 2, the solar irradiance has an influence on all façade orientations. For the four main directions (North = 0°, East = 90°, South = 180°, and West = 270°), a reduction of at least 2% and increases up to 135% in the monthly energy losses are observed, where a reduction of 100% means that no energy losses occur and values over 100% mean that gains occur. For the heating demand, the winter months (December to February) are considered. Within this time range, North, East, and West façades show a reduction of less than 10%. The South facing wall, shows a significant reduction of 9% to 17%. For the summer period, East, South, and West can turn into zero or even plus energy façades.

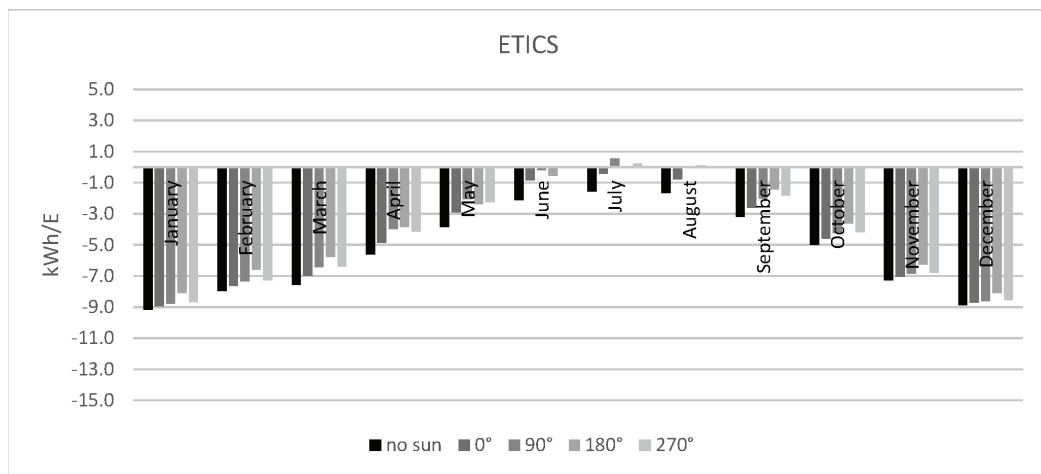


FIG. 2 Monthly energy losses of the ETICS wall element

3.3 SOLAR ENERGY POTENTIAL TCW

The TCW system is proposed to increase solar gains during heating season and to prevent overheating in cooling periods. The material properties in Section 2.2 and shading control strategy in Section 2.3 support this performance.

Fig. 3 presents the monthly energy losses for TCW under identical boundary conditions as the ETICS. The reduction in energy losses of a North facing TCW in the winter months are at least 14%, with maximum of 29%. South and West facing walls perform between 21% and 60% compared to the system without solar gains. The South facing TCW reduces heat losses in a range between 59% and 111%. This means that a South facing TCW produced solar gains in February instead of losses. Over all, the TCW presents a highly effective use of available solar energy in wintertime. This is mostly due to the exploitation of the DSFs overheating tendency.

Additionally, due to the highly reflective shading device, overheating and unwanted solar gains during the cooling period are mainly avoided. The maximum reduction in heat losses reaches 160% for the East facing TCW in July. The results in Fig. 3 support the claim that the TCW energy balance is seasonally adaptive.

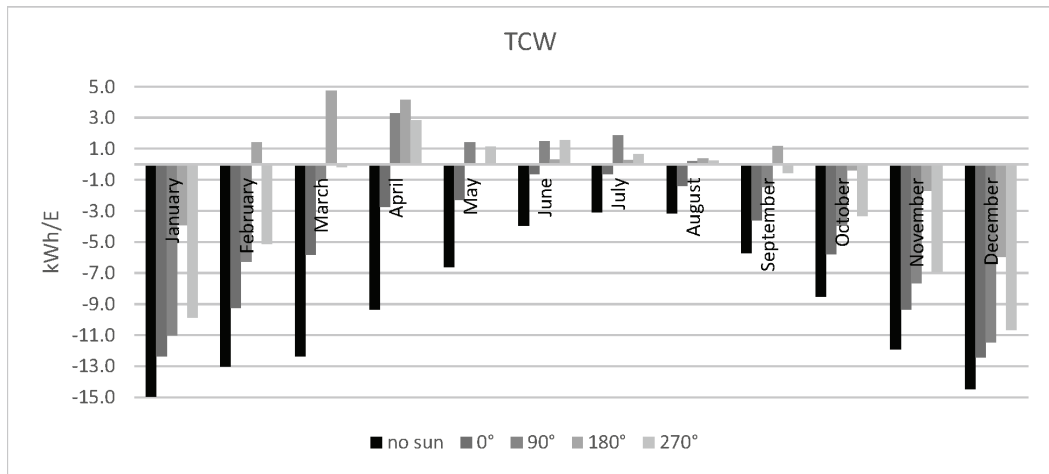


FIG. 3 Monthly energy losses of the TCW façade element

3.4 TCW AND ETICS COMPARISON

For a comprehensive performance evaluation, the transient results of TCW and ETICS are compared directly. As mentioned in Chapters 2.3 and 3.1, the TCW is supposed to lose 64% more heat than the ETICS. Whereas the ETICS is still a static construction, the TCW is seasonally adaptive.

Figs. 4 to 7 present the monthly energy balance of TCW and ETICS for the four main directions. North, East, and West facing TCWs still perform worse than ETICS in wintertime. The northern TCW's energy loss is only about 21% to 43% higher than the ETICS. For East and West directions, the TCW loses a maximum of 25% more energy than the ETICS. The southern TCW performs consistently better than the ETICS.

In Spring and Autumn, the TCW system on all orientations is more efficient than the ETICS. Even North facing façades (Fig. 4) show lower heat losses in March and April, while the East and West facing ones (Figs. 5 and 7) show lower heat losses than in the February to October period. The South facing elements, depicted in Fig. 6, demonstrate even positive energy balances in February to April.

The summer performance of the TCW shows no significant overheating problem when compared to the ETICS façade. In many cases, the energy balance is on a similar level. Only East and West façades show significantly higher heat gains up to 1.9 kWh instead of 0.6 kWh for an ETICS element (July, East, see Fig. 5).

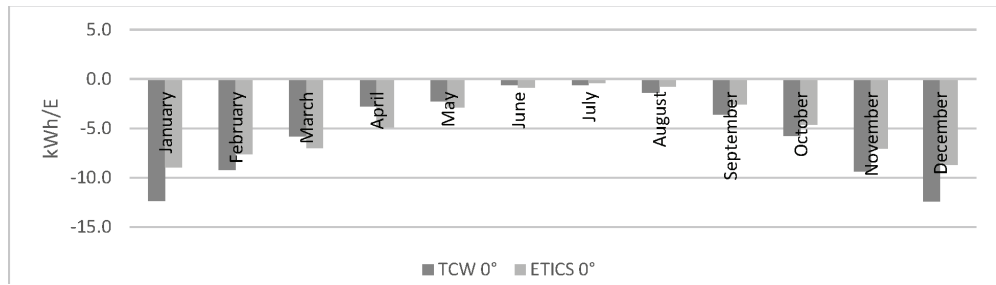


FIG. 4 Monthly energy losses of TCW and ETICS with solar gains for North orientation

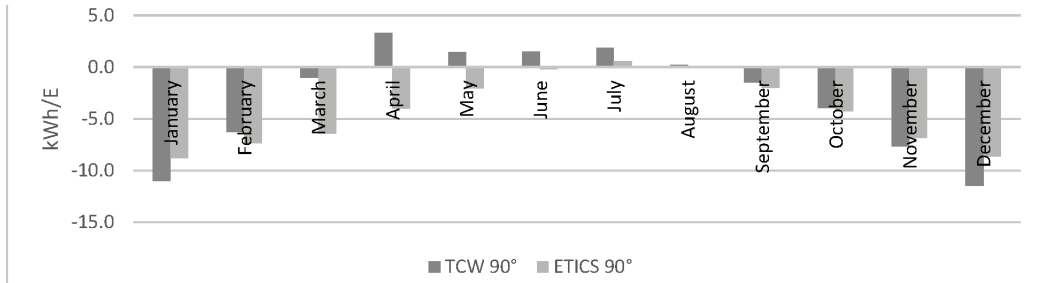


FIG. 5 Monthly energy losses of TCW and ETICS with solar gains for East orientation

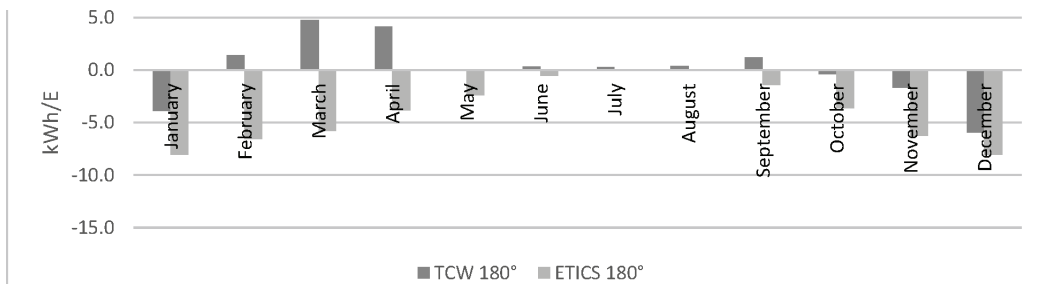


FIG. 6 Monthly energy losses of TCW and ETICS with solar gains for South orientation

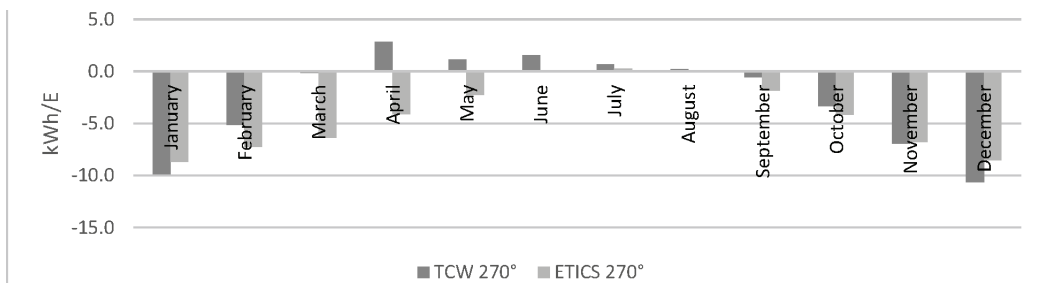


FIG. 7 Monthly energy losses of TCW and ETICS with solar gains for West orientation

4 DISCUSSION & CONCLUSIONS

Undoubtedly, the comparison between those two façade elements seems to be “unfair”. On the one hand, we have twice the amount of insulation and, on the other hand, a DSF system that is predicted to overheat in summertime. Following these arguments, the TCW system’s energy performance has no chance. Goia, Romeo, & Perino (2017) showed that simplified metrics (U- and g-Values) are not always suitable for determining the performance of advanced façades.

The presented results show that both systems, TCW and ETICS, can benefit from solar irradiation to reduce heat losses. In case of the ETICS, the reductions during heating seasons are constantly low, with the exception of South facing walls, whereas the TCW system presents a continuously high use of solar energy. The TCW presents higher solar gains than the ETICS, due to the utilisation of DSF’s tendency to overheat to charge the thermal storage within the cavity. In summertime, both systems, TCW and ETICS, show considerably lower heat losses or even solar gains. However, the g-Value of the TCW with closed shading is below 0.02, which is hardly reachable in a dynamic environment. Furthermore, this is still one quarter of a traditional fully glazed Closed Cavity Façade (CCF) (Rudolf, 2015).

This paper has shown that even if the TCW U-Value is significantly higher, the transient energy simulation shows a high potential for solar thermal energy use to reduce energy losses of buildings at the façade level. The TCW construction tries to exploit the full potential of the used materials by using an unconventional redesign of a DSF system. In addition, the lower material usage leads to lower weight, which makes it feasible to be used as curtain wall system. However, the material properties have not yet been tuned to their limits.

To sum up, even if the system’s potential is not yet fully revealed, the TCW’s potential to contribute to the future energy challenges in the building sector is evident. Further investigations on shading control, material selection, optical, and radiative properties shall study additional enhancements of the system during each season.

The main SEBF project is still in progress. The first simplified laboratory tests on small-scale function models confirmed that the main simulation components are operating correctly. A 1:1 mock-up with a TCW parapet is currently being built to perform measurements and validate the simulation model. More detailed experiments to improve the SEBF / TCW system and the simulation model are planned in the future.

Acknowledgements

The authors gratefully acknowledge the funding provided by the Swiss National Science Foundation (SNF Grant No. IZCNZ0-174562) and support of the Lucerne University of Applied Sciences and Arts.

References

- Casini, M. (2015, April 30). Smart windows for energy efficiency of buildings. *International Journal of Civil and Structural Engineering - IJCSSE*, 2(1), pp. 230-238.
- European Commission. (2012). *Energy Roadmap 2050*. Luxembourg: Publications Office of the European Union. doi:10.2833/10759
- Goia, F., Romeo, M., & Perino, M. (2017). Simplified metrics for advanced window systems. Effects on the estimation of energy use for space heating and cooling. *Energy Procedia* 122, pp. 613-618.
- Goia, F., Zinzi, M., Carnielo, E., & Serra, V. (2015). Spectral and angular solar properties of a PCM-filled double glazing unit. *Energy and Buildings* (87), pp. 302-312.
- Hu, Z., He, W., Ji, J., & Zhang, S. (2017). A review on the application of Trombe wall system in buildings. *Renewable and Sustainable Energy Reviews* 70, pp. 976-987.

- International Energy Agency (2013). *Transition to Sustainable Buildings - Strategies and Opportunities to 2050*. Paris: International Energy Agency.
- Loonen, R. (2010). *Climate Adaptive Building Shells*. Eindhoven: Technische Universiteit Eindhoven.
- Omran, H., Ghaffarianhoseini, A., Ghaffarianhoseini, A., Rhaahemifar, K., & Tookey, J. (2016). Application of passive wall systems for improving the energy efficiency in buildings: A comprehensive review. *Renewable and Sustainable Energy Reviews* 62, pp. 1252-1259.
- Perino, M., & Serra, V. (2015). Switching from static to adaptable and dynamic building envelopes: A paradigm shift for the energy efficiency in buildings. *Journal of Façade Design and Engineering* (3), pp. 143-163.
- Quesada, G., Rousse, D., Dutil, Y., Badache, M., & Hallé, S. (2012). A comprehensive review of solar façades. Opaque solar façades. *Renewable and Sustainable Energy Reviews* 16, pp. 2820-2832.
- Rudolf, B. (2015). Closed Cavity Fassaden und D3-Fassaden: Geschlossene zwei- und dreischalige Fassaden [Closed Cavity and D3 Facades: closed double and triple layered facades]. *Bauphysik [Building Physics]* (37), pp. 244-249.
- Schleicher, S., Lienhard, J., Poppinga, S., Masselter, T., Speck, T., & Knippers, J. (2011). *Adaptive Façade Shading Systems Inspired by Natural Elastic Kinematics*. London: International Adaptive Architecture Conference.
- SIA 380/1. (2009). SIA 380/1 Thermische Energie im Hochbau [Thermal Energy in Building Construction]. Zürich: Schweizer Ingenieur- und Architektenverein [Swiss society of Engineers and Architects].
- Suralkar, R. (2011). Solar Responsive Kinetic Façade Shading Systems inspired by plant movements in nature. In Proceedings of Conference: People and Buildings held at the offices of Arup UK, 23rd.
- Wetter, M. (2011). A View on Future Building System Modeling and Simulation. In J. L. Hensen, & R. Lamberts, *Building Performance Simulation for Design and Operation*. London UK: Routledge.

Comparative Overview on LCA Software Programs for Application in the Façade Design Process

Rebecca Bach¹, Negar Mohtashami², Linda Hildebrand²

1 Faculty of Architecture, RWTH Aachen University, Aachen, Germany, email: rbach@rb.arch.rwth-aachen.de

2 Faculty of Architecture, RWTH Aachen University, Aachen, Germany

Abstract

Façades impact the environmental performance of a building by their passive contribution to operational energy demand and by embodied energy and emissions during each life cycle phase. LCA is a method widely used to quantify the environmental contribution. The use of LCA software programs in façade planning can guide design decisions and contribute to environmental optimisation.

A large amount of LCA software programs have been developed so far, all of which differ in their focus and requirements. This paper aims to address these differences and investigate the capability and suitability of these programs for façade design. It is structured in four sections. The first part introduces LCA in the building and façade design context. The second part introduces categories to understand the different capabilities of LCA software products. Hereafter, eleven products are evaluated based on these categories. The fourth part focuses on the suitability of software products for simple or complex façades. The study concludes that there are different software choices available for almost every level of user knowledge. While Gabi, Simapro, and Umberto require users to work to a high level of proficiency, software programs like eLCA, CAALA, and 360 Optimi do not require much user knowledge over LCA, but provide a range of other opportunities.

Keywords

Life Cycle Assessment, LCA software programs, façade design, environmental impact

DOI 10.7480/jfde.2019.1.2657

1 INTRODUCTION - DEVELOPMENT OF LCA IN ARCHITECTURE AND FAÇADE ENGINEERING

In the 1960s, life cycle assessment (LCA) flows were initially calculated for the depletion of resources and the generation of energy. (Guinée et al., 2011; Jensen, Hoffman, Møller, & Schmidt, 1998) Decades later, a broad range of information was developed for the building materials. The environmental assessment of buildings mostly gained attention in the 1970s when more careful calculations for operational energy demand were required due to the oil crisis. The number of green building certificates has increased significantly in the last three decades, alongside a growing awareness of a building's different life cycle phases. The production phase of a building's life cycle – along with the end-of-life scenarios – were integrated in the sustainability assessments and received increasing attention. Environmental Product Declaration (EPD) provided information for building materials according to the ISO standard 14025 (DIN, 2011). The variety of databases and software programs that have been developed so far provide the user with the opportunity to devise environmental decisions at different planning phases. Many metrics and standards have since been developed to quantify the environmental impacts of buildings. Life Cycle Assessment (LCA) is considered to be one of the most prevalent and reliable methods to date (Klöppfer & Grahl, 2009).

Against the background of a design and planning process which includes increasingly more information, software products become faster at processing complex data. The developments to support building information models provide the opportunity to include ecological information in the planning process with a comparably small workload.

Successful LCA software tools reflect both development in the building planning process and variations in applying the LCA method. In the last two decades, a large variety of LCA software products were introduced to the building industry and the number is growing. The overall goal of this paper is to encourage the application of LCA as a means to reduce the environmental impact of the façade. As both the façade and the LCA method are complex in nature, the application of LCA software products is intended to be encouraged here, by providing the means to understand the potential of specific software products. Furthermore, the goal is to explain the capabilities of software products and refer them to planning situations. This paper provides categories to understand the scope of software products and support to choose the most suitable LCA products by explaining different purposes of LCA software products. On the basis of this overview, façade planners can examine the suitability of the individual programs in terms of their own previous knowledge and the complexity of their design.

2 METHODOLOGY

The research follows the question: Which LCA software programs are more suitable for façade engineering according to different user experiences and different degrees of complexity in façade design?

In order to answer this, the paper is structured in four parts. The first introduces façade design and its environmental dimension. Here, findings from other studies regarding the ecological impact of façade typology are described (Hildebrand, 2014). The ecological scope and user experience is characterised by seven categories in the second part. These are based on the evaluation of software products published in Bach and Hildebrand (2018). In the second part, the categories are briefly

introduced. After that, a comparison model is developed based on six of these categories. The model is based on a radar graph in which the six categories are spread along the axes and by travelling from the centre to the outer layers, the comprehensiveness of the said criteria increases. In the third part, the model is applied to eleven LCA tools which have been chosen among the 26 evaluated software products as the most useful in the façade context. The result is a set of graphs that provide the ability to be compared. The fourth part reflects the LCA software products regarding the user's experience and planning tasks with different extents of complexity.

3 LCA IN FAÇADE DESIGN

3.1 ENVIRONMENTAL IMPACT OF FAÇADES

The relevance of the material and construction contribution to the overall ecological performance of buildings increased with sinking (non-renewable) energy consumption during the usage period. The building's substance was identified as having potential to further decrease the negative effect of the built environment to the natural environment. In the last 20 years, a variety of studies on building and building element level have been published in which different planning alternatives or built examples are compared to one another. For example, in Blanchard and Reppe, (1998) the authors presented the ratio of operational and embodied energy for a typical American home. Finnveden et al. (2009) reviews the differences in LCA methods; Guardigli, Monari, and Bragadin (2011) use LCA to evaluate construction alternatives; Lasvaux, Habert, Peuportier, and Chevalier (2015) address the topic of generic and product specific LCA flows; Lüdemann and Feig (2014) present an overview of software products; Meex, Hollberg, Knapen, Hildebrand, and Verbeeck (2018) investigate the application of LCA tools in the architectural context; and Takano, Winter, Hughes, and Linkosalmi (2014) compare different databases used for LCA.

As there are no benchmarks for the ecological performance (for the building substance) available, in LCA planning alternatives are compared to one another. Studies like Villares et al. (2017) and Hildebrand, (2014) state that LCA at early planning phases gives neither final nor accurate results, but it can have a great impact on the environmental performance especially when comparing alternatives. It is recommended that the solution showing the lower results (most commonly considering primary energy rather than renewable, also called embodied energy, and the global warming potential which is also called embodied carbon) should be realised.

Among the building elements, generally the building structure accounts for the highest ecological impact due to its high weight. Its impact can be significantly reduced with a lighter construction made from renewable materials. By optimising the cross section, only smaller reductions are possible. Most typically, the building's envelope accounts for less environmental impact in comparison to the building structure. However, due to the variety in typology and material, the bandwidth for environmental impact is very broad (Hildebrand, 2014). Fig.1 shows the impact of the façade typology; light façades, like a wooden post-and-beam construction, consisting of one structural layer, accounts for the lowest amount of embodied energy. Solid façades, like masonry or concrete façades with one layer are heavier and show higher values. Double- façades with a high proportion of aluminium or steel construction show the highest amount of embodied energy. This

evaluation shows the relevance of the typology for the environmental impact of façades. With the choice for one typology, the span of impact is predefined.

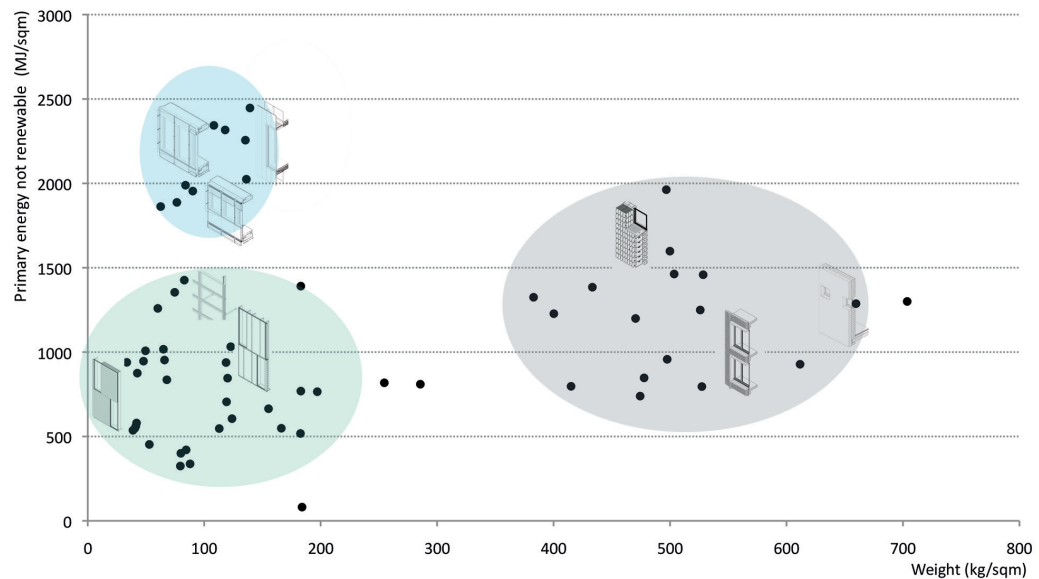


FIG. 1 Embodied energy in different façade typologies. (blue: double façades; green: post-and-beam construction; grey: solid façades) (Hildebrand, 2014)

3.2 SOFTWARE PROGRAMS TO ASSESS ENVIRONMENTAL PERFORMANCE

In façade design, energy demand is impacted by the passive properties of the façade. So far, there are various software programs such as EnergyPlus, TRANSYS, OpenStudio, etc. developed specifically to calculate the energy performance of a building during its operation. While, on building level, the link between embodied and operational energy can be found (for example, Caala), it is rarely found at building element level. In the context of façade design, trade-offs between operational and embodied energy are possible. A link between the two can be useful. This calls for the close cooperation of façade engineer, architect, and HVAC engineer. Integrated software solutions are not part of this paper. In order to contribute to bridging the disciplines, this paper presents the differences in LCA software programs.

In this context, a consideration of operational energy can inform about the relevance of embodied energy and carbon dioxide. For a building with high operational energy (supplied by non-renewable energy sources), it makes sense to reduce the energy efficiency first before optimising the building substance. For buildings with low (non-renewable) energy demands, such as nearly zero energy buildings, the optimisation of the building substance can contribute to an improved overall environmental performance. The application of LCA software programs in façade development, without the context of the building, can also contribute to a better environmental performance. It can be used to optimise the amount of material used in a façade element and/or to choice of a specific material with a low environmental impact. Furthermore, it can be useful to check whether the combination of products supports a circular production chain and whether reuse or recycling is possible.

LCA in the building sector is relatively new. However, some façade companies have picked up on this development and provided life cycle data for their products. The motivations for an architect or façade engineer to include a LCA in the planning process may include the following:

- review the façade concept in terms its ecological impact
- decide upon the façade typology and quantify its scope
- compare different planning alternatives
- optimise the construction and material choice in the façade
- review the performance of new materials regarding their ecological performance.

Currently, two ways of integrating LCA in the planning process can be observed: either an external LCA expert is involved or an engineer in the company performs the LCA. For the planning process, the internal solution offers advantages as changes can be easily incorporated. Regarding the choice of an LCA software, the user's level of knowledge - whether they are a LCA professional or planner - is decisive. Beyond this, LCA can be motivated by auditing for a green building certificate. In this case, the building is assessed with regard to its ecological performance and evaluated in a reference system. It is not integrated in the planning process, but conducted when it is completed.

In order to approach façade engineering in the context of this paper, the range of planning tasks is simplified into more simple and more complex façades. While simple façades consist of a small range of materials and standard construction typology, complex façade systems include a high degree of diversity on technical aspects, construction type, and material choice. Solid or layered façades are typical simple façades. Double façades or customised façade elements account for complex façades.

4 CATEGORIES TO CHARACTERISE LCA SOFTWARE PRODUCTS

In order to create a proper basis for the comparison of different programs, it is first needed to determine suitable categories to differentiate the programs based on them. In the following, categories to differentiate software products are introduced based on those described in Bach and Hildebrand (2018), in which a more elaborate description can be found. For this study, all categories are adopted with two exceptions: the level (building, component, material) is not discussed as the focus here is on façades that belong to the group of components. The accessibility is also excluded as this paper addresses architects and façade engineers for which this criterion is less relevant than for students. Here, optimisation is included as working hours are very relevant in the commercial context.

1 Origin

The origin of a software program can be categorised by the developer, country of origin, and year of publication. The developer can be a research institution or a company, which can be a hint in terms of its accessibility and scope. The country is relevant in regard to the national background, as it indicates the use of the national database. The year of publication indicates the actuality. Programs that have been available on the market for many years have already gone through several optimisation cycles, whereas programs that are still in the beta phase usually address current research results and problems in order to close gaps in earlier programs.

2 Required user knowledge

LCA software tools are designed for different user profiles: no previous knowledge of LCA, basic knowledge, and expert knowledge. Programs developed for users with expert knowledge usually have highly editable pre-settings, so that the assessment can be adjusted. These programs are mainly used in research and consulting. Programs for users with little or no previous knowledge in the LCA include limited access to change settings.

3 Data source

Software products have either a predefined database, which cannot be changed, or they are open to different databases or single data sets. Often, databases refer to a national context which makes the choice for any particular one relevant, as, for instance, the share of renewable energy varies, which leads to different primary energy coefficients in different countries.

4 Entry format

LCA calculations are based on mass and volume related data. The input of this data can be supplied in spreadsheet and geometric-based format. Geometric-based programs require 3D-geometric data input. Software programs based on spreadsheet format require the manual entry of mass or volume related data, which must be calculated separately in a previous step.

5 Optimisation

The ideal application of LCA includes an optimisation, which can either be conducted manually (LCA results are analysed, changes in the planning are made, and LCA is conducted again) or computational (LCA is conducted and a computational optimisation follows). Usually, spreadsheet programs require manual iteration. For 3D programs with access to LCA, an optimisation is easier to include but until now has seldom been found.

6 Default settings

Default settings provide a basic structure to facilitate the applicability and execution of the LCA for the user. The more default settings are specified, the faster and easier the first statements can be made. For higher accuracy, it can be useful to adjust to specific situations. This includes the settings of the database, the life cycle phases, and the considered life span.

7 Life cycle phases

In general, LCA is divided into three groups of life cycle phases: production, use phase, and end-of-life. Standard EN 15804 (DIN, 2012) differentiates them into 17 stages. There are few programs that look at all these phases. In general, a distinction can be made between three levels: programs that consider only part of the production process: A1-A3; others that also include part of the deconstruction and recycling process: A1-A3, C3-C4, D; and programs that consider parts of all life cycle phases: A1-A3, B6, C3-C4, D.

The categories discussed above describe the essential characteristics of an LCA software program and help to identify the most suitable choice for a specific application. In the following, they are embedded in a model and applied to each program individually.

5 MODEL DEVELOPMENT AND SOFTWARE COMPARISON

In this section, different LCA programs are analysed according to the categories described in the previous chapter. To do so, a chart was structured, in which the discussed categories in the previous section are spread along the chart's axes. The inner circle represents relatively limited and less accurate statements about LCA, whereas the outer circle illustrates a more holistic, broad and more detailed analysis. As a consequence, by traveling from the inner circle to the outer one, the LCA software provides more comprehensive, reliable calculations, which also require more a professional level of working knowledge. On the other hand, software programs closer to the inner circle provide simple comparisons and quick statements with less effort.

The 'origin' criterion is excluded from comparison since it is a region-based characteristic which the user has to select based on their project and it does not represent the level of comprehension of a software. As a result, the remaining six categories were spread along the chart for comparison. In some categories, there are two steps and in others, there are three steps of comprehensiveness. In the following, the software programs are introduced in the order of their development.

The German Ganzheitliche Bilanzierung (GaBi) [Holistic Assessment] (Fig.2, right) and the Dutch Simapro programs (Fig.2, middle) are regarded as the earliest software, having been introduced in the early 90s. Following that, Umberto (Fig. 2, left) was developed to address material assessment. Today, GaBi, Simapro, and Umberto have evolved into (LCA-) expert tools based on very detailed information. Moreover, they provide the ability to edit many different settings within the program to adjust it more to the project condition. They are mainly used to assess products (for example for the Environmental Products Declarations), and are highly detailed and relatively accurate in their calculations. However, their complexity and high user knowledge requirements make it more difficult for building sector users to handle them. Fig. 2 shows the similarity of these software in the six studied criteria.

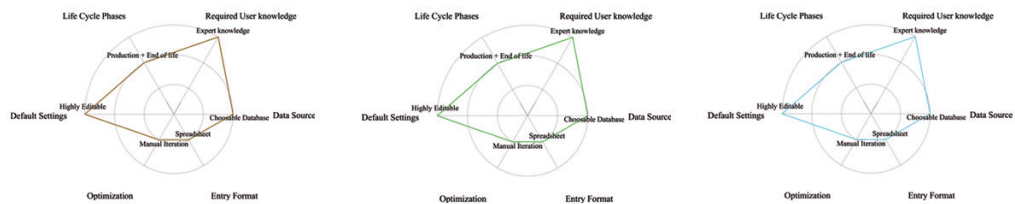


FIG. 2 Analysis of the early LCA tools and their similar functionality (from right to left: Gabi, Simapro, Umberto)

The focus of the German software Legep (Fig. 3), released in 2005, is on building materials; the entry format is spreadsheet based. To increase the number of users, the Open LCA program (Fig. 4) provides free access and includes a broad variety of databases (which are only partly free of charge). Athena (Fig. 5), established in Canada, is focused on material selection, by using the US units of building materials.

The spreadsheet-based tool eLCA predefines its entry mask and provides a large amount of default settings, which allows for easy calculation at the building element level. eLCA (Fig. 6) is able to compare planning alternatives to strengthen the application as a basis for decision-making, rather than simply documenting the results. This free tool motivated the integration of LCA for the German context.

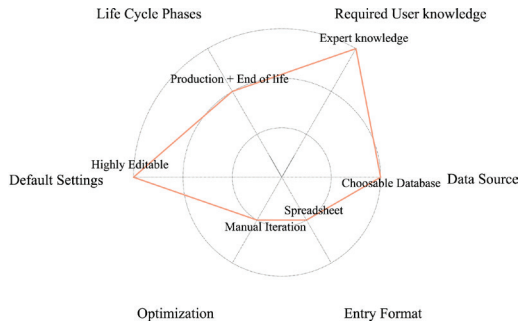


FIG. 3 Application of model on Legep software program

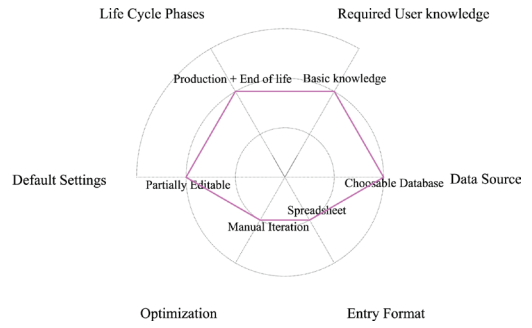


FIG. 4 Application of model on Open LCA software program

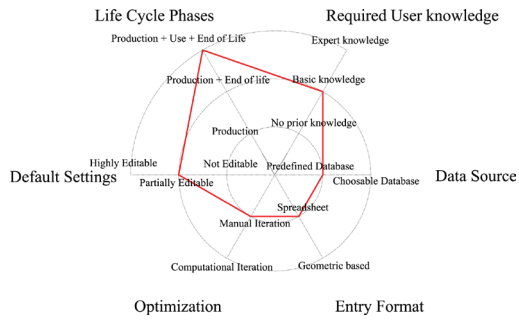


FIG. 5 Application of model on Athena software program

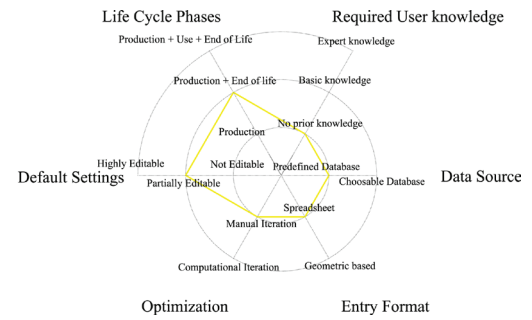


FIG. 6 Application of model on eLCA software program

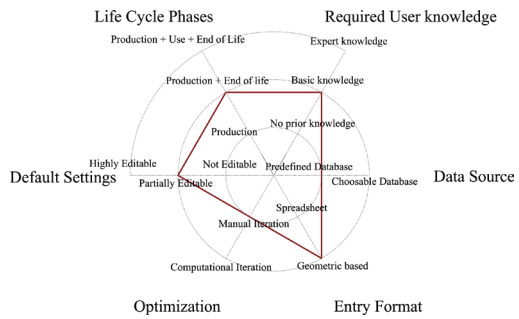


FIG. 7 Application of model on Tally software program

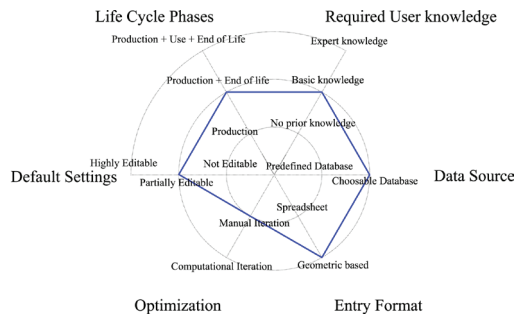


FIG. 8 Application of model on 360 Optimi software program

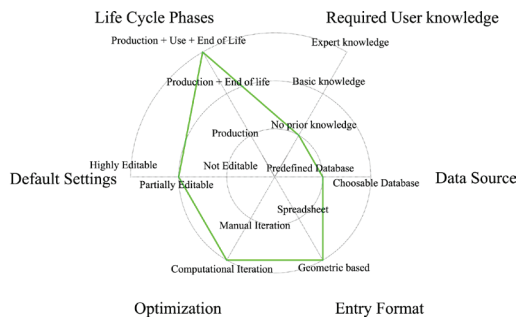


FIG. 9 Application of model on CAALA software program

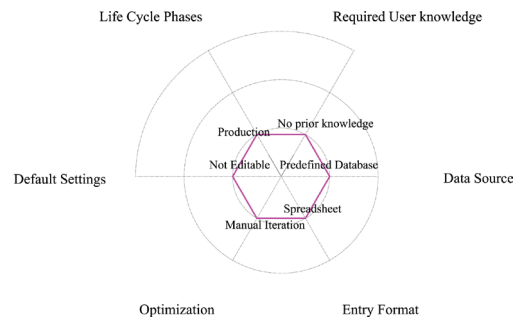


FIG. 10 Application of model on BEES software program

The software programs Tally (Fig. 7) and 360 Optimi (Fig. 8) provide the link between 3D data and different LCA databases. On the other hand, CAALA (Fig. 9) connects to Ökobau.dat and includes an optimisation feature, which assesses the ecological impact of the building fabric and relates it to a simplified (operational) energy calculation. A growing number of add-ons for computer programs like Revit (Autodesk) or Rhinoceros (McNeel) are also available, while software programs like BEES (Fig.10) use a much more simple, and non-editable interface to provide an easy platform.

Fig. 11 depicts the overall comparison of all the eleven analysed LCA software programs. The comparison also reflects that most of the software programs available focus on the production and end-of-life phases of a building's lifespan, and only Athena and CAALA take the use-phase into account. The comparison also illustrates that there are different software choices available for almost every level of user knowledge. While Gabi, Simapro, Umberto, and Legep require a high level of user proficiency, there are still software programs like CAALA and 360 Optimi that do not require much user knowledge of LCA, but still provide a good range of other opportunities. Although BEES (Fig. 10) is considered to be a program that requires no prior knowledge, it has fewer editable options and therefore provides less accurate statements. Similarly, eLCA is a tool that provides more editable options, which makes it an easy-to-use tool for designing simple façades.

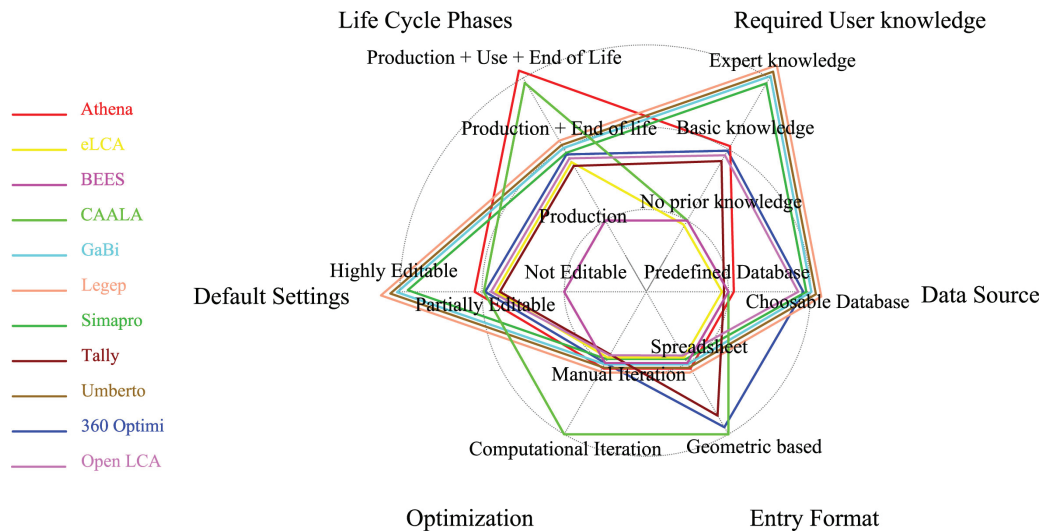


FIG. 11 Comparison of eleven LCA tools based on façade engineering aspects

It is also understandable from the graph, in terms of default settings, that the more editable options the programs provide, the higher the level of user knowledge required. This inevitably leads to a switch to less editable (and therefore less accurate) software when an inexperienced user tries out LCA tools. Therefore, it is more challenging to choose an appropriate software when there is a shift towards partially editable software, as these offer different capabilities when compared to one another. For example, Tally and CAALA provide good optimisation with a geometric based entry, while 360 Optimi is recommended when there is a need to be able to choose from different data sources.

While the graph shows a balanced distribution of the type of data sources that different software use, it is clearly visible that still most of them use spreadsheets rather than geometric entries. Greater use of spreadsheets makes it difficult for designers to work with the software programs as this group

normally works with 3D geometries in their projects. Moreover, use of 3D geometries often provides the ability for an easier recalculation of environmental impact of a façade when there is need to change an element. As a result, modifications and optimisation in geometry-based software are more convenient for the user.

All in all, the almost symmetrical, widespread graphs indicate that there are many different tools for addressing different criteria at different building levels. Therefore, it is crucial to advise users on what software to choose, when it comes to planning the façade, which is the main core of the following chapter.

6 SOFTWARE CLASSIFICATION FOR FAÇADE DESIGN

When preparing a LCA study, it is essential to consider the context in which it will be carried out. When selecting a LCA software and the corresponding database, the national context as well as the actuality and degree of elaboration of the program should be taken into account. The selection of the life cycle phases considered is important for the comparability of the studies. Differences in the method of LCA over the last two decades can be observed. In the beginning, only the production phase was considered. Later, generic End-of-Life scenarios for material groups were introduced, which found broad application. Considering or excluding the End-of-Life can impact the LCA significantly. For a comparison between a customised and a prefabricated façade element, the exclusion can favour the first one, as material can be reduced for a specific building and values can be lower. Including the capability for application in multiple usage cycles may require that an element be oversized for its current use. For this, including specific End-of-Life scenarios is useful.

The categories' entry format and optimisation process provide information about the basic structure of the tools. For BIM-based and architectural planning processes, programs with a 3D geometry-based entry format with computational optimisation processes are recommended. These programs prevent errors due to manual entries and transfer errors. Otherwise, these categories depend on the preferences of the user.

The category 'default settings' goes closely together with required user knowledge: the more editable the settings of a program are, the more expert knowledge is needed and vice versa. For example CAALA, which is currently in the Beta phase, shows the greatest number of default settings that are currently non-exchangeable. In this way, design decisions regarding the cubature and material choice can be optimised and the LCA methodology can help to reduce the environmental impact of a building. For research and consulting purposes, it is mostly the established spreadsheet programs, which have highly editable default settings and thus require expert user knowledge, that are being used.

All in all, the most essential criterion for choosing a software tool is the required user knowledge. Programs should be chosen depending on the planner's knowledge level on LCA. Looking at the development of LCA software programs, the younger ones are 3D geometry-based, while the more established programs work with spreadsheets. 3D based programs or building information models tend to show advantages in decreasing the working time as it supports an integrated, rather than an iterative, planning process.

In Fig. 12, the evaluated software tools are classified into an overview according to the criteria 'required user knowledge' and the planning assignment. Most of the evaluated LCA programs are suitable for simple to slightly complex façade planning. They mainly differ in their requirements in terms of the user's previous knowledge and their scope. CAALA, 360 Optimi, and Tally are suitable for simple to slightly complex designs. They require very little to no prior user knowledge. Data input takes place via geometric drawings and CAALA offers a computational iteration process. Thus, they can be easily integrated during the design process. Athena and Legep are similar, both being used in simple to slightly complex façade designs. The default settings of these programs are partly to highly editable, so previous knowledge to expert knowledge, in case of Legep, is needed. As Fig. 6 of Chapter 5 states, eLCA is partly editable but the database is not selectable. The pre-structure of eLCA is specifically created for building components, which makes it partly suitable for complex façade designs with little prior user knowledge. However, it is necessary to insert the data manually, which can be time-consuming when dealing with a large number of individual building elements. Against the background of the increasing amount of information linked to building volume, 3D software tools that provide reference points between information and building materials are increasingly more common (Building Information Modelling – BIM). This offers the chance to connect ecological data and include it in the early design stage, rather than during the phase of construction when the scope of intervention regarding environmental impact reduction is limited.

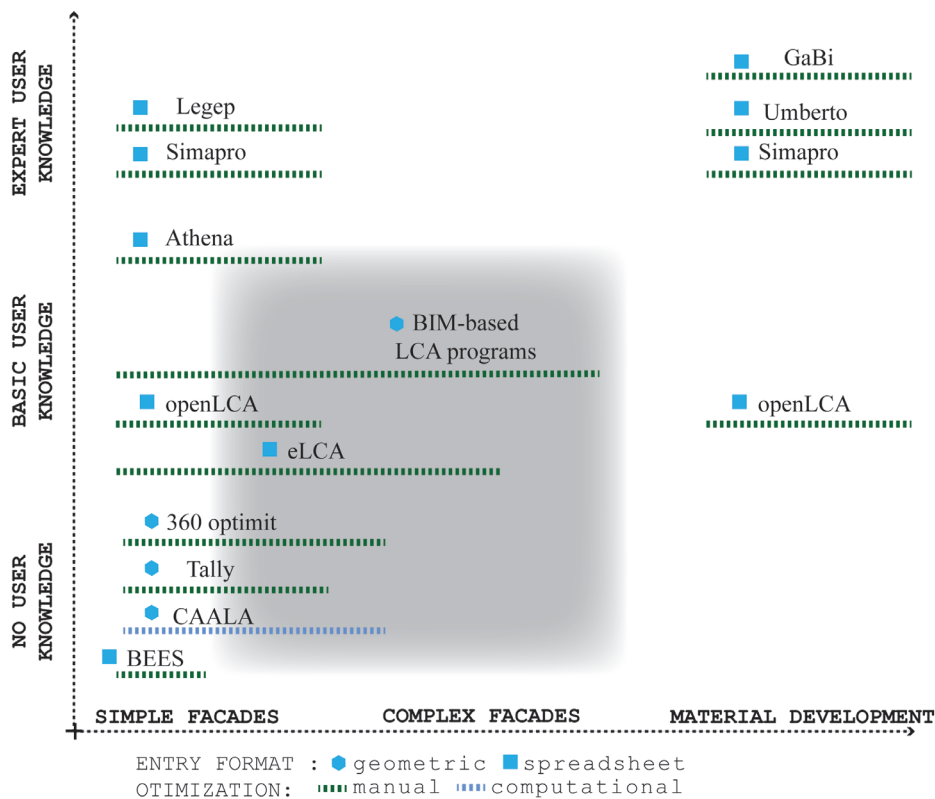


FIG. 12 LCA Software products organised according to user knowledge and planning assignment. The grey field marks the most suitable products for façade design and engineering.

In addition to the axis alignment from simple to complex façade design, the aspect 'Material Development' was added to this axis in Fig.12. Depending on the desired level of detail of the assessment, material development can be carried out for both simple and complex façade designs.

At this level, there are the programs GaBi, Simapro, and Umberto, which were mainly developed for calculations on material level. It is possible to perform LCAs for façades and buildings using these programs. However, this involves a great deal of effort because there are no pre-structures for components or building elements, so everything would have to be designed in small scale at material level.

This graph shows that the evaluated LCA calculation programs, which are among the most common tools in the construction sector, are mostly suitable for simple façade designs. The scope of the software programs is displayed as a green or blue dottedline, as it can be used for different purposes. It is used to demonstrate the range. The form of the blue dot shows the entry format, either geometric or spreadsheet. For the highly complex façade designs, software tools from façade manufacturers, for example, were developed. Since they are not publicly accessible, they could not be evaluated within the scope of this paper. Nevertheless, these manufacturer-specific programs are currently very well suited for assessing complex façade designs, because these tools are specially customised for the planners' needs. Their default settings and pre-structure were developed to calculate façade systems at every level of complexity and they already have the specific data sets of the company's components and elements included. This can be an advantage, when the façade typology and the product are defined and only details like dimension change. Earlier in the design process, programs with access to generic data provide variety.

Otherwise, interfaces can be developed to integrate the LCA processes into the façade design program. For example, the plugin Tortuga was developed for the integration of LCA in Grasshopper processes. Such programs are currently being developed and are still in the optimisation phases.

7 CONCLUSION

The façade typology already predefines a certain environmental range. While light post-and-beam construction accounts for the lowest amount of embodied energy and emissions, solid single layered façades show slightly higher values. Double façades with high metal and glass content result in high environmental impact. This study provided an overview on the categories that façade planners should consider when selecting a program. The paper showed different existing LCA software products, which are suitable for different levels of user knowledge. It was demonstrated that a number of software are available for simpler façade design, such as eLCA or CAALA. Whereas Gabi, Simapro, Umberto, and Legep require high levels of user proficiency. If material innovation requires the LCA for a specific material, GaBi, Legep, or Umberto are suitable. In this regard, an (external) person with expert knowledge on LCA is required due to the complexity of the programs (highly editable). For complex façades, the link between a 3D geometric model and information shows the highest potential, since most of the programs still use spreadsheets rather than geometric entries. The growing number of tools in this field shows high potential for planners with basic knowledge of LCA.

The study also reveals that most of the software programs available focus on the production and end-of-life phases of a building's lifespan, and only Athena and CAALA embed the use-phase into their analysis at building level. Taking into account that there is currently a severe gap in considering both embodied and operational energy at the same time, it becomes clear that more effort is required to develop software choices that address both simultaneously and through all life cycle phases, including the use-phase to provide a more holistic environmental analysis.

Acknowledgements

The categories were developed in the context of the EU Horizon Project KLABS (Knowledge Labs for Sustainable and Resilient Environments) and functioned here as a basis for the focus on façade design and engineering.

References

- Bach, R., & Hildebrand, L. (2018). Review on tools for assessment of buildings' environmental performance. In S. Kosanovic, T. Klein, T. Konstantiou, A. Fikfak, & L. Hildebrand (Eds.), *Sustainable and resilient building design - Approaches, methods and tools* (Vol. 5). Delft: BK Books.
- Beuth. (2006). *Environmental management - Life cycle assessment - Principles and framework* (ISO 14040:2006); German and English version EN ISO 14040:2006 (Vol. 14040). Berlin: Beuth.
- Blanchard, & Reppe. (1998). *Life Cycle Analysis of a Residential Home in Michigan*. Michigan: University of Michigan
- Finnveden, G., Hauschild, M. Z., Ekvall, T., Guinée, J., Heijungs, R., Hellweg, S., . . . Suh, S. (2009). Recent developments in Life Cycle Assessment. *Journal of Environmental Management*, 91, 1-21.
- Guardigli, L., Monari, F., & Bragadin, M. A. (2011). Assessing Environmental Impact of Green Buildings through LCA Methods: A comparison between Reinforced Concrete and Wood Structures in the European Context. *Procedia Engineering*, 21(0), 1199-1206. doi:<http://dx.doi.org/10.1016/j.proeng.2011.11.2131>
- Guinée, J., Heijungs, R., Huppes, G., Zamagni, A., Masoni, P., Buonamici, R., . . . Rydberg, T. (2011). Life Cycle Assessment: Past, Present, and Future. *Environmental Science & Technology*, 45(1), 90-96.
- Hildebrand, L. (2014). *Strategic investment of embodied energy during the architectural planning process*. Delft University of Technology, Rotterdam.
- Jensen, A. A., Hoffman, L., Møller, B. T., & Schmidt, A. (1997). *Life Cycle Assessment-A guide to approaches, experiences and information sources*. Retrieved from <https://www.eea.europa.eu/publications/GH-07-97-595-EN-C>
- Klöpffer, W., & Grahl, B. (2009). *Wirkungsabschätzung Ökobilanz [LCA]* pp. 195-354. Wiley-VCH Verlag GmbH & Co. KGaA.
- Lasvaux, S., Habert, G., Peuportier, B., & Chevalier, J. (2015). Comparison of generic and product-specific Life Cycle Assessment databases: application to construction materials used in building LCA studies. *The International Journal of Life Cycle Assessment*, 20(11), 1473-1490. doi:10.1007/s11367-015-0938-z
- Lüdemann, L., & Feig, K. (2014). Comparison of software solutions for Life Cycle Assessment (LCA) – a software ergonomic analysis. *Logistics Journal*.
- Meex, E., Hollberg, A., Knapen, E., Hildebrand, L., & Verbeeck, G. (2018). Requirements for applying LCA-based environmental impact assessment tools in the early stages of building design. *Building and Environment*, 133, 228-236. doi:<https://doi.org/10.1016/j.buildenv.2018.02.016>
- Nagus. (2006). Environmental labels and declarations – Type III environmental declarations – Principles and procedures (ISO 14025:2006) *ISO/TC 207/SC 3 „Environmental Labelling“* (Vol. 14025). Berlin: Normenausschuss Grundlagen des Umweltschutzes (NAGUS) im DIN.
- Takano, A., Winter, S., Hughes, M., & Linkosalmi, L. (2014). Comparison of life cycle assessment databases: A case study on building assessment. *Building and Environment*, 79 (Supplement C), 20-30. doi:<https://doi.org/10.1016/j.buildenv.2014.04.025>
- Villares, M., Isildar, A., Giesen, C. C. V. D. & Guinée, J. B. (2017). Does ex ante application enhance the usefulness of LCA? A case study on an emerging technology for metal recovery from e-waste. *International Journal of Life Cycle Assessment; Issue 10*.
- Young, R. F. (2007). *Crossing boundaries in urban ecology: Pathways to sustainable cities* (Doctoral thesis). Retrieved from ProQuest Dissertations Thesis database. (UMI No. 327681). For more information see: <http://www.library.cornell.edu/resrch/citmanage/apa>

A Study on the Impact of Climate Adaptive Building Shells on Indoor Comfort

Jacopo Gaspari¹, Emanuele Naboni², Caterina Ponzio³, Adele Ricci⁴

1 School of Engineering and Architecture, Alma Mater Studiorum University of Bologna, Italy

2 The Royal Danish Academy of Fine Arts, Copenhagen, Denmark

3 IUAV, University of Venice, Italy

4 School of Engineering and Architecture, Alma Mater Studiorum University of Bologna, Italy, adele.ricci1@gmail.com

Abstract

Energy savings and indoor comfort are widely considered to be key priorities in the current architectural design trends. Additionally, the well-being and satisfaction of end users is a relevant issue when a human-centred perspective is adopted. The application of Climate Adaptive Building Shells (CABS) compared to conventional façades offers appropriate opportunities for tackling these challenges. This paper reports the outcomes of a study performed on CABS in order to optimise the indoor comfort while calibrating the configuration of a dynamic façade module. The horizontal louvres of the adaptive façade are moved by an actuator that exploits the expansion of a thermo-active resin as it melts, by its absorption of energy. The actuation mechanism depends on the outdoor air temperature conditions and does not require a supply of energy. The performed simulation evidenced a decrease of approximately 4°C indoors when the dynamic module is fully efficient (21st June at 12 p.m.). Furthermore, the lux level is always within the comfort range for an office building (500-2000 lux) during both winter and summer scenarios. The optimised solution shows a substantial gain for energy performance and environmental sustainability. Moreover, the uniformity of distribution of daylight illuminance across the entire space is another associated advantage, giving interesting insights into potentials for architectural façade design.

Keywords

adaptive façade, parametric design, daylight, energy efficiency, building shells

DOI 10.7480/jfde.2019.1.2778

1 INTRODUCTION AND OBJECTIVES

The building envelope usually represents the boundary between the indoor and outdoor environments, becoming a key and complex system to achieve optimal comfort and wellness standards for end users. This is certainly a relevant issue, considering that in today's society most people spend over 90% of their time inside buildings. The use of Climate Adaptive Building Shells allows for conditions to be improved to users' satisfaction, while simultaneously decreasing the need for equipment. However, most of these systems are still very complex and expensive, and they require supplied energy to operate. Intrinsically controlled systems applied to kinetic façades enable the merging of the sensor and the motion actuator into the same component, allowing for its kinetic elements to move without requiring supplied energy. The level of sustainability of CABS depends on the difference between energy supplied and energy saved. A large amount of energy is usually required to activate the actuators and sensors used in adaptive façade systems (Barozzi, Lienhard, Zanelli, & Monticelli, 2016). To make allowances for sustainability of the whole system, operational costs must also be carefully considered. A large amount of buildings still have louvres and shutters fixed outside windows; if manually activated these elements are low-energy and low-cost devices.

If these elements are re-designed in an innovative way, they allow for an adaptive environment without complex automatic systems. Potential perks of the reduction in operating energy supplied by the system should overcome the additional capital and carbon costs of the system itself. The high construction cost and technological complexity that characterise CABS are still unresolved in terms of their limits (Barozzi et al., 2016). Nowadays, CABS belongs to quite a restricted area of application and the aim of this study is to try to take a step towards widening the opportunities for their use. For this reason and for the reasons we have pointed out above, the façade's design was focused on reducing operational energy while trying to keep the technological complexity under control (Boake, 2014).

The study was driven by the idea of adopting a relatively conventional solution and re-designing it to adapt its potential advantages to a simple but effective adaptable façade system. Since the introduction of energy simulation software, the integration of parametric design and performance simulation allows designers to test the efficiency of a system. In this specific case, the use of energy simulation models has allowed the thermal and light conditions of the indoor environment to be monitored, and the testing of the efficiency of the façade as a whole. In conclusion, the aim of this work is to design a passive kinetic façade with intrinsic control and study its effects on indoor comfort through a replicable design method based on parametric design and simulation tools.

2 BACKGROUND AND METHODOLOGY

As recent literature shows, successful building performance simulation has been considered as 'the right type of virtual experiment with the right model and tool' (Godfried, 2011). For this reason, there is a great demand for tools and instruments that can be used in the design process of kinetic façades (Nielsen, Svendsen & Bjerreg, 2011; Shen & Tzempelikos, 2012). Accordingly, the work of Ayman and Yomna (2016) on parametric-based designs for kinetic façades applied to daylight performances, aims to provide a toolkit for daylight control inside buildings, combining different software programs such as Grasshopper and Diva. Similarly, the study of Loonen, Trčka, Cóstola, & Hensen (2010) explores the potential role that building performance simulation plays in designing CABS by taking the window technology Smart Energy Glass as a case study and coupling TRNSTS and DAYSIM to

build a model for performance simulations. From the beginning of the study, the focus was set on the need to keep both luminous and thermal aspects together, to obtain a tool that would consider the two major aspects that influence the indoor comfort. For this reason, the research targets a series of design problems: design integration through tool development, and design process improvement through the incorporation of physics-based modelling and real-world dynamics.

2.1 GENERAL DESIGN PROCESS

A method marked by parametric design, dynamic simulations, and in-situ measurements has been developed, in order to monitor the tool's validity. The method allowed for the evaluation of the effects of the façade on indoor comfort.

The study can be divided into three phases:

- design of the thermal and luminous simulation model;
- testing of the model: on-site physical measurements and comparison with the simulation model results; and
- testing of the façade.

Mean radiant temperature (°C) and illuminance levels (lux) were assumed as key parameters for the investigation.

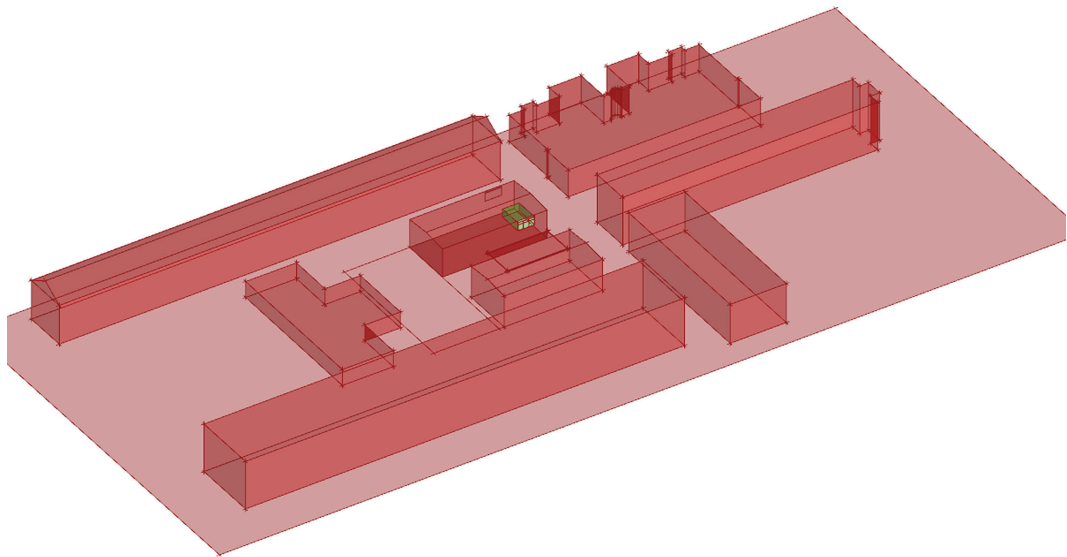


FIG. 1 Simulation model with all buildings modelled (red) and the thermic zone (green)

A simulation model to reproduce the real environment of measurement was set. Measured experiments were conducted in a full-scale test room designed as daylight laboratory at The Royal Academy of Fine Arts in Copenhagen (Denmark). Illuminance values were measured and simulated at two points: P1 located at 1.5 m and P2 at 5.5 m from the window. A luxometer was placed in P1 and P2 at a height of 0.8 m, like the height of a worktop, such as a desk or a small table. Mean radiant temperature (MRT) was measured and simulated at 1.5 m from the window as a main heat dispersion source on P2 at a height of 1.1 m, the centre of gravity of a man standing (Fig. 4).

The room was considered as a sealed environment, and measurement was done while keeping windows and doors closed so that no heating or cooling system would generate convective air movements. Air speed measurements carried out hourly on P1 and P2 with a hot-wire anemometer were always below 0.1 m / s (measuring tool technical specifications are outlined below in Section 2.4). We decided not to take into account electricity consumptions for this phase of the research. All luminous contributions are due to natural daylight as the electrical system was not switched on. The façade was designed as a set of horizontal louvres that shields the sun via a downwards-rotative movement. The façade is kinetic and intrinsically controlled as it is moved by a passive movement actuator, which turns the sun-blinds in response to the outside temperature. Façade technology will be explained in detail in Section 4. The geometry of the louvres was shaped using Grasshopper-Honeybee (McNeel Europe, n. d.) and embedded into the simulation workflow as a shading device. Honeybee is an environmental design plug-in for Grasshopper that connects Radiance and Energyplus, which we used for the simulation model design (Davidson, 2013). This model was used for comparing simulated data with measured data and to monitor the façade's effects on the indoor comfort of the mock-up.

2.2 MODEL DEFINITION AND SIMULATION

The simulation model's thermal and luminous behaviour must be similar to real conditions if it is to return values comparable with those which are measured. For this reason, the modelled room's dimensions are the same as the daylight laboratory. The room communicates with the outside through a completely glazed closing surface. The room was inserted into the campus building and only one wall was modelled as being exposed to the outdoors. It was modelled following its real dimensions, orientation, and thermal and luminous properties. The room is oriented to the east. Copenhagen EnergyPlus weather file (.EPW file extension) was downloaded on September 27, 2017 (U. S. Department of Energy, n. d.) and inserted in the model. The light room is considered as a thermal zone formed by the union of the various Honeybee surfaces, joined together by the 'Honeybee_CreateHBZones' command. Each surface was set to have certain thermal and light properties. The thermal properties were determined through the assignment to the surface of a 'Honeybee_EP Construction', while luminous ones were assigned using 'Honeybee_RadianceOpaqueMaterial' (for opaque partitions) and 'Honeybee_RadianceGlassMaterial' (for a window). A list of thermal and luminous parameters is included in the following tables.

The room was free of any cooling or heating systems and free from artificial lighting equipment. The thermal zone inside the simulation model was set as a sealed environment; measurements were made keeping doors and windows closed and there were no heating or cooling systems inside the test room that would generate convective movements. Since nobody was working inside the lab while the measurements were taken, the thermal load due to the occupants was considered null. Context buildings were added to the thermal simulation as 'Honeybee_EPContextSurfaces', and reflectance values of surrounding materials were also settled (Table 3).

With 'Honeybee_GenerateClimateBasedSky', a sky was created with radiation values calculated according to the weather file at a specific time of the year. Illuminance on points of the simulated space, P1 and P2 (which corresponded to P1 and P2 in the measured space) was calculated by connecting the 'Honeybee grid-based simulation' to the command running the Radiance simulation. According to Jakubiec and Reinhart (2011), the following input was inserted in the simulation model to achieve good accuracy for daylight modelling results.

ROOM'S COMPONENTS	TRANSMITTANCE (U-VALUE) [W/M2K]
Exterior wall	0.98
Exterior window	4.43
Interior floor, ceiling	1.44
Interior walls	2.58
Exterior roof	1.45

TABLE 1 Input parameters for thermal simulations

RADIANCE MATERIALS	REFLECTANCE VALUE
Ceiling	0.98
Interior walls	4.43
Floor	1.44
Shadings (Kinetic Façade)	2.58
TRANSMITTANCE VALUE	
Window	0.65

TABLE 2 Materials' properties used for Radiance daylight model

RADIANCE MATERIALS	REFLECTANCE VALUE
External ground	0.20
Aged asphalt	0.10
Buildings (brick cladding)	0.25

TABLE 3 Materials' properties used for Radiance daylight model

SIMULATION PARAMETER	VALUE
Ab – ambient bounces	5
Ad – ambient divisions	1024
As – ambient supersamples	16
Ar – ambient resolution	256
Aa – ambient accuracy	0.10

TABLE 4 Input parameters for thermal simulations

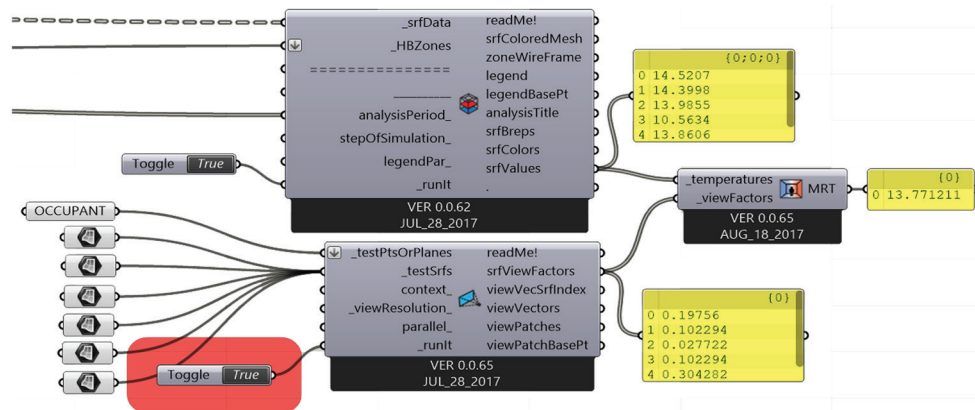


FIG. 2 Illustration of the parametric logic of the room's model within the Grasshopper Algorithm, MRT workflow calculation

With EnergyPlus simulation, the surface temperature of the test room's walls was evaluated. 'Ladybug_MRTCalculator' then elaborated these temperatures. Therefore, MRT on P2 has been simulated by the software (Fig. 2).

The façade structure has been included in the model, and its effects on indoor comfort monitored through simulated values of illuminance and MRT. Previous set parameters have been considered constant during the façade's design process.

2.3 SIMULATION SCENARIO

To verify the effectiveness of the new façade design, three shells' configurations were simulated for two days of the year: December 21st and June 21st (Fig.3). The winter and summer solstices were chosen because they are accepted to be the worst and best days, respectively, in terms of air temperature and hours of daylight. Configurations are dependent on the external air temperature because the movement actuator moves according to the temperature (see Section 4).

- Configuration 0: No shells.
- Configuration 1: Sun-shutters inclined at 0°, horizontal position, when the air temperature is below 16 °C and motion actuators are at rest.
- Configuration 2: Sun-shutters inclined at 45° compared to Configuration 1, when the outside air temperature is higher than 24 °C.

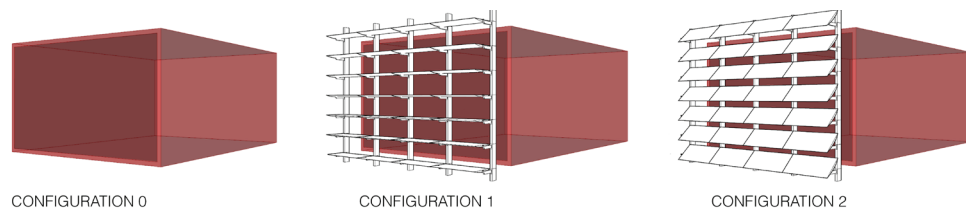


FIG. 3 3D model of the system configurations

2.4 TESTING THE MODEL

In-situ measured parameters were compared with the results of energy simulations. Measured experiments were conducted in November 2017 in a full-scale test room (Fig. 4) designed as a daylight laboratory. The room is inside the KADK campus, consisting of several buildings connected by open spaces belonging to the university. As Fig. 4 shows, the room is a rectangular space with a fully glazed wall, facing southeast.

The objective of this testing phase was to understand and monitor the thermal and luminous conditions of the room, air temperature, and relative humidity, MRT, illuminance, and solar radiation. To collect an adequate amount of climatic data, three climatic stations were placed inside the room, and a further one was placed outside. As Fig. 4 and Fig. 5 explain, the two indoor points were located at 1.1 m and 0.8 m above floor level and 2.7 m from side walls. P1 and P2 were positioned at 5.5 m and 1.5 m, respectively, from the window (Fig.5). The outdoor measurement station (P3) was instead fixed on the railing, 1.1 m above the floor level, on the same virtual line of P1 and P2.

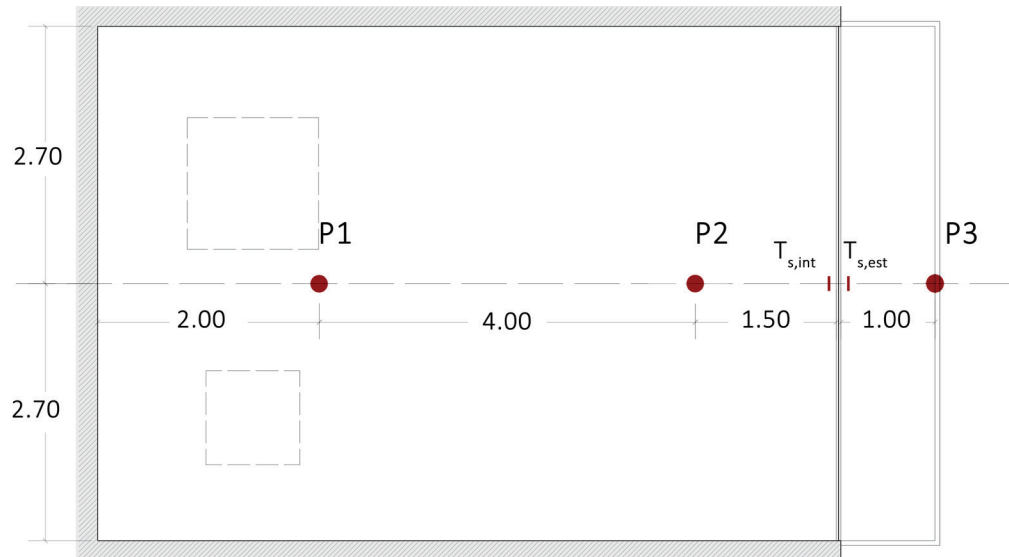


FIG. 4 Floor plan of the room with points of measurements (red dots – P1, P2, P3) and sensors for the surface temperature of the glass (red lines)



FIG. 5 Overview of the stations in the test room (P2 indoor and P3 outdoor) during the measurement phase

During this first phase, the following tools were used:

- Hobo U12-012 (data logger and sensors) for illuminance (lux), air temperature (°C) and relative humidity (%) range -20 to 70 °C, 0 to 35000 lux, 5 to 95%, accuracy $\pm 0.35^{\circ}\text{C}$, $\pm 2.5\%$,
- KIMO Black Ball + data logger for mean radiant temperature (°C), range 0 to 60 °C, accuracy $\pm 0.5^{\circ}\text{C}$;
- S-LIB M003 Pyranometer + data logger for solar radiation (W/m²), range 0 to 1280 W/m², accuracy $\pm 10\text{ W/m}^2$;
- Onset M-TMB-M006 sensor for air temperature (°C), range -40 to 100 °C, accuracy $\pm 0.2^{\circ}\text{C}$;
- Rs Pro 1340 hotwire anemometer (m/s), range 0.1 to 30 m/s, accuracy $\pm 0.02\text{ m/s}$.

The minimum standard of instruments and measurement methods followed the UNI EN ISO 7726, 'Ergonomics of the thermal environment - Instruments for measuring physical quantities' (UNI EN, 2002). All data collected during the measurement phase was grouped and categorised in Excel files. Afterwards, the indices describing the factors of comfort in the room (such as air temperature in °C, humidity in %, and illuminance in lux) were extracted from the equation and added to the weather file used in the workflow to calibrate the 3D simulation model. Among the collected data measurements, those of two specific days - the sunniest day and the rainiest day - were then

isolated. As per the above description (Section 3.2), the simulation was set up to be as similar as possible to the real conditions in the room, featuring the same thermic and luminous characteristics; here, the measured MRT data is compared to the simulated MRT data (Fig. 6).

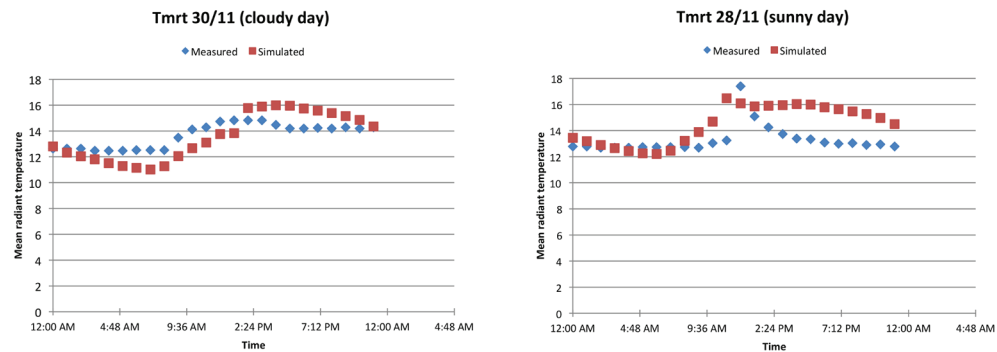


FIG. 6 Comparison between measured and simulated data of the MRT in the room during cloudy day (left) and sunny day (right)

3 ADOPTED FAÇADE TECHNOLOGY

In this section, façade kinetic movements and technology will be examined further. As previously reported, the façade was made using horizontal louvres that shield the sun through an adaptive and intrinsically controlled rotating movement. The geometry of the louvres was shaped using Grasshopper-Honeybee and embedded into the simulation workflow, and its technological aspects were also studied.

In order to shield solar radiation before it impacts on the glass surface and generates an increasing heat load, a façade system has been installed outside the glass surface. The designed solution involves the installation of horizontal louvres of 500 mm depth, with a gap of 500 mm between each one. These horizontal louvres rotate around a pivot and reduce the light permeable surface. To increase the sustainability of the system, a façade moved by a passive control system that could increase thermal and lighting comfort without energy consumption has been assumed as a main objective. Thus, elements of climate adaptive building shell are moved by a thermal actuator that exploits the expansion of a thermo-active resin that melts by absorbing thermal energy (solar radiation). This provides a mechanism that is responsive to passive energy exchanges given by meteorological conditions. A passive movement actuator makes possible the kinetic adaptability. The sun shading subsystem is supported by steel pillars that connect it with the building's structure (Fig.8).

3.1 FAÇADE TECHNOLOGY

Louvres

Horizontals louvres are made from perforated aluminium sheets of dimensions 1200x500mm. They are fixed to the structural steel bracket with bolts and hooked to a pivot that allows rotation (Fig.7). Despite its high-embodied energy, aluminium has been selected for its low weight and high durability for installation in the external environment. The actuator is situated under the shading device because it needs to be sheltered from direct radiation heat gain. A perforated sheet is used to let the air flow for natural ventilation purposes.

Movement actuator

The actuator - designed by an English company (Bayliss Autovents, n. d.) - is usually used for the automatic greenhouse ventilation. It's made up of a hollow aluminium cylinder filled with density-change paraffin. The paraffin increases in volume in relation to the external temperature and allows a piston to move with a straight movement along its longitudinal axis. Furthermore, the rectilinear movement is transformed into a rotational movement by an aluminium support and a hinged joint that is able to rotate and close louvres. The actuator selected for the façade has an operating temperature range between 15 °C (temperature at which the wax starts to melt) and 35 °C (complete melting of the wax). At 35°C, the opening angle reaches 54° of rotation. The pushing force of the resin can bear a weight up to 6 kg (Fig.7).

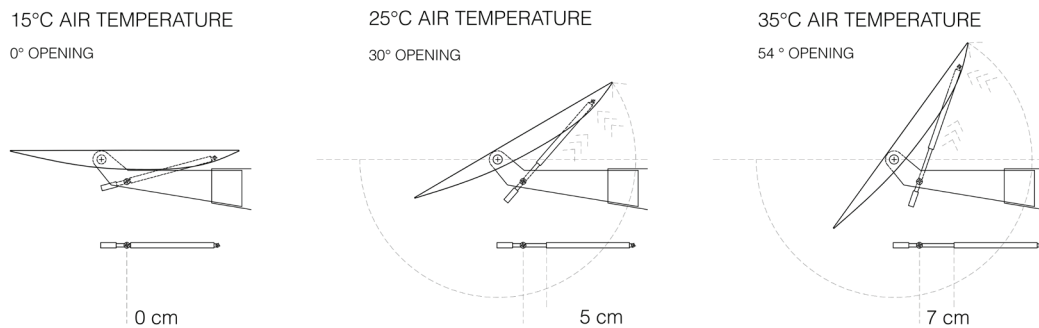


FIG. 7 Mechanical system for implementing the movement of the façade

Structural grid

The sun-blinds are anchored to the building's external walls by a frame made of profiled aluminium. A metal deck acts as a horizontal stiffener, as well as an inspection space for maintenance purposes. Thanks to this system, the ordinary maintenance of each module is allowed without the use of external platforms. Embodied energy issues relating to CABS can be reduced by designing durable and easily maintained components (Boake, 2014).

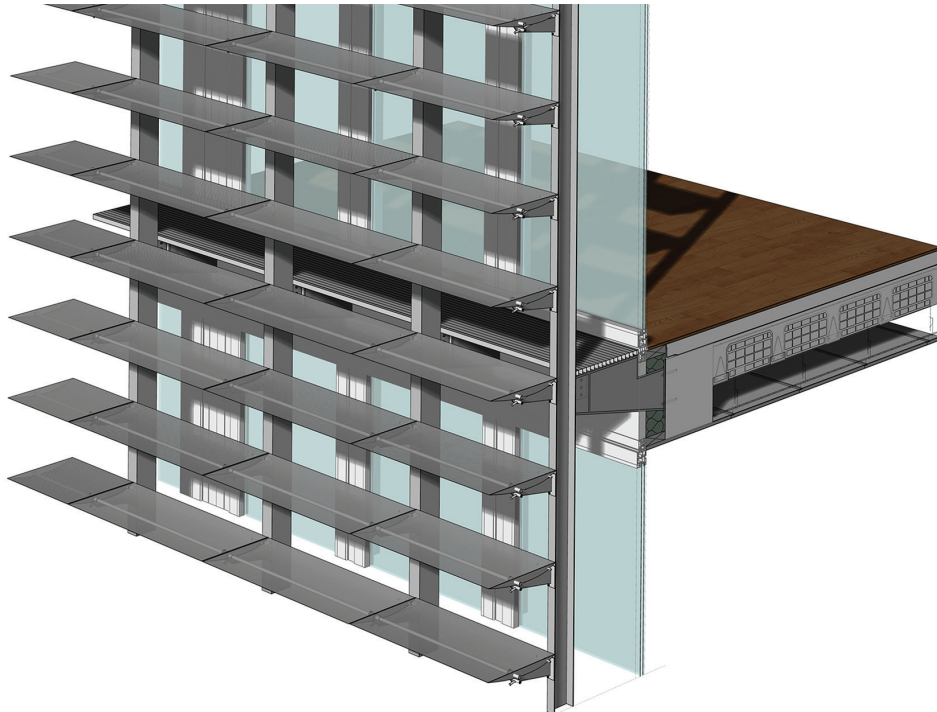


FIG. 8 3D model of façade

4 RESULTS

The outcomes of this testing phase are presented in the following section with the related results of MRT values (°C) in Table 5 and illuminance levels (lux) in Table 6.

4.1 RESULTS OF SIMULATION SCENARIO

Mean radiant temperature (°C)

In Table 5, each configuration's (Fig.3) MRT values at point P2 are presented. The new façade design shows that, in winter-time, the façade stays at Configuration 1 and allows for a slight increase in temperature in the morning (about 0.4 °C), compared to the 'no shells' configuration (Configuration 0), while it's null at noon. Additionally, Configuration 2 isn't obtained because the external temperature of 24°C is not reached. In summer-time, Configuration 2 is obtained. The façade allows the temperature to decrease by 4°C compared to the static configuration (Configuration 1), both at 09.00 a.m. and at noon.

DAY	HOUR	CONFIGURATION 0	CONFIGURATION 1: 0°	CONFIGURATION 2: 45°
21 Dec	9:00	11.4	11.8	-
	12:00	13.8	13.8	-
21 Jun	9:00	32.9	27.0	23.1
	12:00	35.1	28.2	24.3

TABLE 5 Analysis of MRT [°C] values on the measure point P2

Illuminance(lux)

In Table 6, each configuration's (Fig. 3) illuminance values at points P1-P2 are presented. The new façade design shows that in winter-time (Configuration 1), the façade allows values to be obtained that are always higher than 200 lux. As Keller and Rutz (2010) typify in their guidelines for illuminance according to visual task, this threshold is characterised by a 'large visual task, large details, strong contrast. Moreover, in Denmark on 21st December at 09.00 a.m., very low incoming solar radiation is recorded; Configuration 1 doesn't preclude the passage of light.

During summer time, 45° rotated louvres are necessary to lower the level of illuminance below 1500 lux, a threshold characterised by "very difficult visual task, very small details, very low contrast" (Keller & Rutz, 2010).

MRT and illuminance values decrease during summer-time, while solar radiation reaches the core of the room in winter-time. Adaptability allows a substantial gain for thermal performance and therefore increases the system's sustainability.

DAY	HOUR	CONFIGURATION 0	CONFIGURATION 1: 0°	CONFIGURATION 2: 45°
21 Dec	9:00	P1 =3.51 P2 =17.35	P1 =2.56 P2 =8.27	- -
	12:00	P1 =330.4 P2 =1339.9	P1 =257.5 P2 =798.4	- -
21 Jun	9:00	P1 =1744.4 P2 =7462.0	P1 =1145.9 P2 =4044.3	P1 =320.4 P2 =1375.5
	12:00	P1 =1140.9 P2 =5778.8	P1 =856.5 P2 =2879.9	P1 =291.8 P2 =1212.8

TABLE 6 Analysis of illuminance level [lux] on the measuring point P1 and P2

4.2 CASE STUDY APPLICATION

In order to prove the method's replicability, the workflow explained above has been applied to a master's dissertation project within the Sustainable Built Environment graduation laboratory submitted at the School of Engineering and Architecture of Alma Mater Studiorum University of Bologna, on March 22, 2018. The dissertation was concerned with a hostel design located in the city of Bologna, Italy. This city is located in the climatic zone ASHRAE 4A and differs from Copenhagen since it tends to be a warmer climate, especially in summer. This allows us to understand façade behaviours in a different climatic zone from that of Denmark.

Façade technology has been used as shading device on one of the hostel's guest rooms. The room, smaller than the daylight laboratory in Copenhagen, was modelled in the Rhino software and replaced as a new thermal zone. It has an area of 14 m² and a floor to ceiling height of 2.90 m. The external façade to which the adaptive system has been applied, is oriented to the south and has a large glazed surface. The building's construction is made up of a hollow-core concrete structure, similar to that of the test box.

The two measurement points are located in the middle of the room (with respect to the side walls); P2 is located at 1 m from the opening and P1 is located at 2.5 m from P2. Similarly to the test box in Copenhagen, illuminance values were measured at P1 and P2 at a height of 0.8 m from the floor, and MRT values were measured at P2 at 1.1 m.

DAY	HOUR	CONFIGURATION 0	CONFIGURATION 1: 0°	CONFIGURATION 2: 45°
21 Dec	9:00	9.35	9.2	-
	12:00	13.9	13.6	-
21 Jun	9:00	36.4	34.1	33.7
	12:00	41.0	37.9	37.0

TABLE 7 Analysis of MRT values [°C] on the measure point P2

DAY	HOUR	CONFIGURATION 0	CONFIGURATION 1: 0°	CONFIGURATION 2: 45°
21 Dec	9:00	P1= 537.64 P2=1150.3	P1= 443.9 P2=967.8	- -
	12:00	P1= 8998.9 P2=10642.8	P1= 8074.0 P2= 8461.0	- -
21 Jun	9:00	P1= 1425.5 P2= 3690.2	P1= 1076.2 P2= 1927.3	P1=476.8 P2=999.35
	12:00	P1= 2647.1 P2= 7145.0	P1= 1978.3 P2=4147.2	P1= 822.3 P2=1636.8

TABLE 8 Analysis of illuminance level [lux] on the measuring point P1 and P2

As shown in Table 7 and Table 8, results clearly indicate that the façade is effectively efficient with regard to the mitigation of the lux level, while the MRT variation is limited.

5 CONCLUSIONS AND FURTHER DEVELOPMENT

The method explained throughout allows the monitoring of light and temperature within buildings whose parameters are indeed essential to controlling the indoor comfort of the structure, using a completely passive technological adaptive system (David, Donn, Garde, & Lenoir, 2004).

This paper aims to prove that through science and design computation, as well as an empirical research method, design teams are enabled to improve the process involved in managing the simulation and evaluation of daylight and temperature performances over the course of the design process itself.

Some remarks on the results:

- the creation of models has been acknowledged as a useful tool in verifying the design choices relative to the CABS if accompanied by accurate monitoring of the same, as well as data validation;
- CABS have been proven to be an effective choice to improve MRT as well as to balance the illuminance level.

The study leaves room for future developments to be built on its findings, as well as expanded upon exploration of a set of optimisation criteria, which should combine the energy-related indicators with the visual comfort ones, such as glare probability, daylight and illuminance uniformity, and factors of external view.

References

- Ayman, H. A. M., & Yomna, E., (2016). Parametric-based designs for kinetic façades to optimize daylight performance: Comparing rotation and translation kinetic motion for hexagonal façade patterns. *Solar Energy*, vol. 126, pp. 111-127.
- Barozzi, M., Lienhard, J., Zanelli, A., & Monticelli, C. (2016). of the sustainability of adaptive envelopes: developments of kinetic architecture. *Procedia Engineering*, vol. 155, pp. 275-284.
- Bayliss Autovents (n. d.), retrieved September 2017 from www.baylissautovents.co.uk.
- Bluyssen, P.M., Aries, M., & Van Dommelen, P. (2011). Comfort of workers in office buildings: the European HOPE project. *Building Environment*, vol. 46, pp. 280-288.
- Boake, T.M., (2014). Hot climate double façade: avoiding solar gain. *Façades Tectonic*, vol. 14 , pp. 2-24.
- Boerstra, A.C., Beuker, T., Loomans, M.G.L.C., & Hensen, J.L.M. (2013). Impact of available and perceived control on comfort and health in European offices. *Architectural Science Review*, vol. 56, issue 2.
- Cole, R.J., & Brown, Z. (2009). Reconciling human and automated intelligence in the provision of occupant comfort. *Intelligent Buildings International*, vol.1.
- David, M., Donn, M., Garde, F., & Lenoir, A.(2004). Assessment of the thermal and visual efficiency of solar shades. *Building Environment*, vol. 46, pp. 1489-1496.
- Davidson, S. (2013). Grasshopper: Algorithmic Modelling for Rhino, NING/MODE, Brisbane, CA, USA. Retrieved from www.grasshopper3d.com.
- Galasiu, A.D. & Veitch, J.A. (2006). Occupant preferences and satisfaction with the luminous environment and control systems in daylight offices: a literature review. *Energy and Buildings*, vol. 38, pp.728-742.
- Godfried, A., (2011). The role of simulation in performance based building. *Building Performance Simulation for Design and Operation*. Abingdon: Spon Press.
- Jakubiec J. A., & Reinhart C.F.(2011, November). Diva 2.0: Integrating daylight and thermal simulations using Rhinoceros 3D, Daysim, and EnergyPlus, *Proceedings of building simulations: 12th Conference of International Building Performance Simulation Association*, Sydney, 14-16 November.
- Keller, B., & Rutz S. (2010). *Pinpoint: Key Facts + Figures for Sustainable Buildings*. Basel: Birkhäuser.
- Leung, C. (2014). *Passive seasonally responsive thermal actuators for dynamic building envelopes*, (Doctoral dissertation). Retrieved from The Bartlett School of Architecture University College London Database, London.
- Loonen, R. (2010). *Climate Adaptive Building Shells. What can we simulate?* (Master's thesis) University of Technology, Eindhoven.
- Loonen, R.C.G.M., Trčka, M., Cóstola D., & Hensen J.L.M., (2010). Performance simulation of Climate Adaptive Building Shells - Smart Energy Glass as a case study, *Proceedings of the 8th International conference on System Simulation in Buildings*, pp. 1-19.
- McNeel Europe (n. d.) , Food for Rhino, retrieved October, 2017 from www.food4rhino.com/app/ladybug-tools.
- Nielsen, M.V., Svendsen S., & Bjerreg, L., (2011). Quantifying the potential of automated dynamic solar shading in office buildings through integrated simulations of energy and daylight. *Solar Energy*, vol 85, pp. 757-768.
- Paciuk, M. (1989). *The role of personal control of the environment in thermal comfort and satisfaction at the workplace*. (Doctoral Dissertation). University of Wisconsin, Milwaukee.
- Schumacher, M., Schaeffer, O, Vogt, M., (2010). *Move: Architecture in Motion - Dynamic Components and Elements*, Basel: Birkhäuser.
- Shen H., & Tzempelikos, A., (2012). Daylighting and energy analysis of private offices with automated interior roller shades. *Solar Energy*, vol. 86, pp. 681-704.
- UNI EN ISO 7726, (2002). *Ergonomics of the thermal environment - Instruments for measuring physical quantities*.
- U.S. Department of Energy (n. d.), retrieved September 27, 2017 from www.energyplus.net/weatherlocation/europe_wmo_region_6/DNK//DNK_Copenhagen.061800_IWEC.

SMP Prototype Design and Fabrication for Thermo-responsive Façade Elements

Jungwon Yoon¹

¹ Department of Architecture, University of Seoul, Seoul, Republic of Korea, jwoon@uos.ac.kr

Abstract

The aim to attain sustainability in the built environment introduced the innovative application of advanced material technologies for low-energy, but aesthetically intriguing, building design strategies. Adaptive and responsive building skins as embedded and intrinsic control systems can be delivered with smart materials, and thus have the potential to minimise the energy consumption of buildings by maximising the natural and passive adjustment of façade components for shading, air-flow, daylight, and view. The dynamic smart material façade, adaptable to changing outdoor environments, is considered to be a holistic design approach that integrates the behavioural performance effects with the appearance and aesthetics of kinetic ability provided by smart materials acting as actuators, by adjusting their properties according to external stimuli. Of the various environmental inputs sensed by, and actuating, active and dynamic building façade systems, this research focuses on temperature as the stimulus to activate a dynamic shading device with the mechanism of opening and closing, specifically considering Seoul's climate. Among currently available thermo-responsive smart materials, the shape memory polymer (SMP) is investigated as an activator of shading devices to be implemented to adaptive building skin strategies. As the first stage of SMP prototype design and fabrication study toward the thermo-responsive building façade elements, SMP prototypes are proposed in cell types. Among the general thermo-mechanical cycle of thermo-responsive SMP, only programming of the permanent shape via additive manufacturing and recovery at the activation temperature are focused upon in this research. This study proposes a design-to-fabrication workflow integrating computational tools, 3d printing and recalibration of relevant variables in digital design process, G code generation, and manufacturing using commercially available SMP filaments. To verify the 3d printing process, and to demonstrate the shape-changing behaviour of SMP actuators, reproduction of a referenced prototype was conducted, in addition to fabrication experiments of SMP surfaces with various thicknesses and SMP hinges with customised rotating angles. In addition, a base-line prototype combining the static ABS plate and the active SMP hinge is developed to set up the heat test and a digital motion simulation from data of shape changing behaviour acquired from a hands-on model test. After the demonstration of the baseline prototype in design and additive manufacturing process, various SMP prototypes were designed with reference to kinetic prototype researches, but with the consistent 100mm-diameter circular surface, in a scale of 1:3. They were also fabricated with a 3d printer for both open and closed positions to testify to their constructability, and thus to comparatively evaluate the design and fabrication outcomes. Furthermore, after conducting radiation and thermal simulation analysis, shading performance validation is noted for selecting potential prototypes. Lastly, the needs to further develop reversible reiterative shape-changing materials or systems are briefly discussed.

Keywords

thermo-responsive, building skin, shape memory polymer (SMP), 3d printing

DOI 10.7480/jfde.2019.1.2662

1 INTRODUCTION

Smart adaptive, or dynamic skin, façades have been considered a promising and efficient strategy to enhance the internal lighting and thermal comfort in modern buildings, especially in terms of the impact of the target of nearly zero-energy (Boldini, Colangelo, Pilla, Tavanti, & Mariani, 2017). Despite high-tech kinetic and responsive building skin developments, low power consumption through autonomous adjustments has been a dilemma in applying responsive building skins. Among the various concerns involved in the design of high energy-performance buildings, the control of daylight and environmental conditions is of primary importance (Fiorito et al., 2016). The aim to enhance the level of sustainability in the built environment introduced innovative applications of advanced material technologies to achieve low-energy but aesthetically intriguing building design strategies. A concept to integrate the conflicting requirements by superimposing a passive structure with an active structure is proposed and developed by researchers and architects. The passive approach does not consume energy since it adapts in an autonomous way to changes in environmental factors to attain the zero-energy impact. The active system can be actuated to counteract or mitigate the action of the passive system, thus consuming energy only in specific circumstances (Boldini et al., 2017).

Of the various energy efficient state-of-the-art technologies in architecture, adaptive and responsive building skins as embedded and intrinsic control systems can be delivered with smart materials, having huge potential to reduce the energy consumption of buildings by minimising the mechanical system operation and maximising the natural and passive adjustment of façade components for shading, air-flow, daylight, and view. The intrinsic properties of smart materials include the ability to change physical properties or shape without any energy source (Al-Obaidi, Ismail, Hussein, & Rahman, 2017). Addington and Schodek (2005) have classified smart features in terms of immediacy, selectivity, transiency, self-actuation, and directness. The dynamic smart material façade, adaptable to changing outdoor environment, is considered a holistic design approach that integrates the behavioural performance effects with the appearance and aesthetics of kinetic ability provided by smart materials acting as actuators, by adjusting their properties according to external stimuli. Recent work on responsive architecture has capitalised on functional integrity, soft architectural components, and material properties, as opposed to highly mechanistic components, by highlighting kinetic materiality leading to advancements in this domain (Abdelmohsen et al., 2018)

Currently, designers are moving towards a nature-inspired approach in search of the underlying principles of morphogenesis and materialisation inherent to biological entities (Naboni, Kunic, Breseghello, & Paoletti, 2017). Researchers also incorporate the biomimetic approach and research by design method into their projects (Mungenast, 2017), in order to attain façade functions such as thermal separation, natural light control, heat gain control, and natural ventilation through layers, shadings, and openings. Al-Obaidi et al. (2017) list the most common types of materials inspired from nature by categorising, and argue that adaptive dynamic movements derived from plants, with special features such as responding to changing environments, including temperature, making them an inspiration for adaptive movements (López, Rubio, Martín, & Ben Croxford, 2017). Motions and surface structures of plants can be learned in three ways: morphological, physiological, and behavioural. Studies have shown that plants blur mechanism, material, and structural borders, with elastic movement, reversible snapping motion, smart opening-closing, orientation and folding based on temperature sensitivity, and folding inward as a reaction to contact. From biomimicry-based research, the functions of adaptive architectural envelopes have been identified as regulating environmental factors such as temperature, light intensity, humidity, and air quality (López et al., 2017; López, Rubio, Martín, Croxford, & Jackson, 2015).

Above all, smart materials that change and react in response to external stimuli resemble organisms that can change specific characteristics and parameters in response to a series of mechanical, chemical, spatial, and temporal information in different environmental conditions (Al-Obaidi et al., 2017; Lurie-Luke, 2014).

As such, the thermo-responsive building skins can adopt the dynamic mechanisms from plants with material and structure from thermo-responsive Shape Memory Polymer (SMP). The initiative, 'A Study on a Sustainable Energy-efficient Envelope applying Thermo-responsive Smart Materials', of which this research forms a part, seeks to exploit thermo-responsive smart material façade systems. Of the various environmental inputs sensed by, and actuating, active and dynamic building façade systems, the initiative focuses on temperature as the direct stimulus to activate a dynamic shading device to control the indoor climate with the mechanism of opening and closing, from the specific perspective of implementing the consequent study in Seoul. Analysis of the psychrometric chart and adaptive comfort from Climate Consultant software with EnergyPlus climate data demonstrates that sun shading of windows can be adopted as one of key measures to achieve strategic indoor climate control (Yoon, 2018). Also, as shown in Fig.1, the ideal baseline temperature of activation would be between 22°C and 25°C, where the sun shading of windows is demanded.

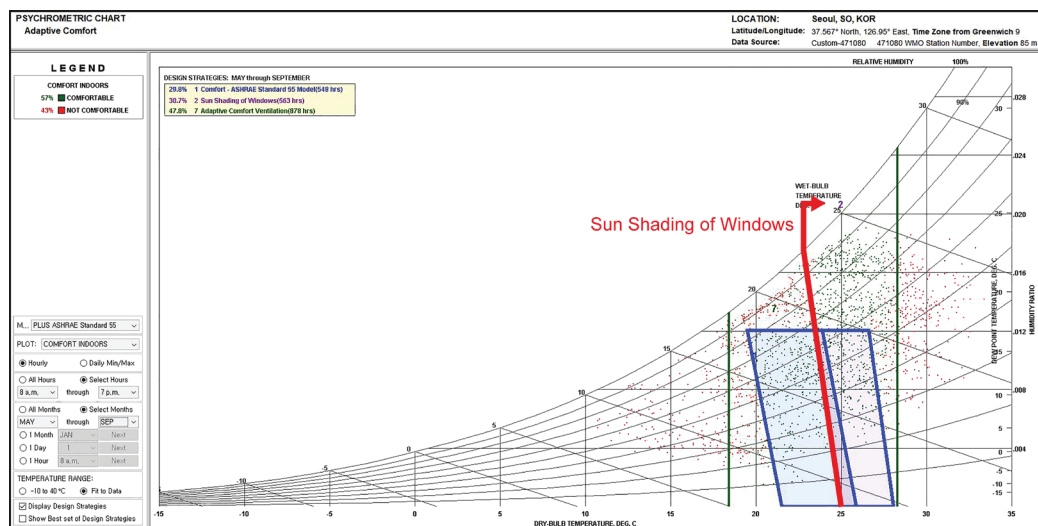


FIG. 1 Psychrometric chart: Adaptive comfort resulted from Climate Consultant with EnergyPlus Data of Seoul

A preceding research (Yoon, 2018) included climate-adaptive building skin typologies and design-driven research process to identify adaptive façade strategies with various thermo-responsive smart materials, specifically focusing on implementation in Seoul. The research summarized four differently categorised adaptive façade strategy types identifying kinetic actuating capabilities of Shape Memory Alloys (SMAs) and SMPs. As part of the aforementioned initiative, SMPs are investigated as façade elements in this research.

Both SMAs and SMPs are common shape memory materials. The main characteristics of shape memory materials in general are that they show a plastic deformation as a temporary shape when an external stimulus is applied and can recover to their original shape from the temporary shape. This is also called 'shape memory effect' (Huang, Ding, Wang, Zhao, & Purnawali, 2010). Shape memory materials possess the unique characteristic of memorising, during appropriate training processes, while also having shapes that can be recovered through the application of external stimuli, such as temperature, light, and moisture (Leng, Lan, Liu, & Du, 2011). However, SMAs have disadvantages among other types of shape memory materials, such as high manufacturing cost,

toxicity, limited recovery, and complicated surgical problems (Ratna, & Karger-Kocsis, 2008; Bengisu, & Ferrara, 2018). SMPs have been preferred in recent times for their advantages compared to SMAs (Arun, Chakravarthy, Arochiakumar, & Santhosh, 2018).

SMPs have particularly useful properties for building technology. Among currently available thermo-responsive smart materials, SMPs offer extensive opportunities of investigation and design interpretation due to their reaction temperatures, deformations and stains, shape-changing behaviours, variety of surface shapes and forms, and possible manufacturing processing (Beites, 2013; Lelieveld, 2013; Ge et al., 2016; Bengisu & Ferrara, 2018). SMPs are programmable, exhibit variable stiffness, undergo extremely large deformation without fatigue damage, and require a minimal actuation force to change shape. In building technology applications, SMPs can morph to several pre-programmed shapes, effectively using smart material to reduce system complexity by lowering reliance on external sensors, wiring, electronics, and digital computation (Clifford et al., 2017). In addition, SMPs have low thermal conductivity in comparison to SMAs, which can be useful for application as insulation materials, with relatively lower cost than SMAs. Therefore, keeping in mind the long-term successive researches and prototype developments, SMPs are targeted as the thermo-responsive materials to be implemented in adaptive building skin strategies. Additionally, in this paper, as the first stage of SMP prototype design and fabrication study of the thermo-responsive building façade elements, SMP is investigated as an activator of shading devices, a climate mediator of thermo-responsive building façades, in a cell type.

The inspiration of the basic form derives from the simple geometry and dynamism implemented in RMIT Design Hub Façade, but with SMP introduction into the system. The initial results of experiments will be presented, concentrating on SMP application for cell components of building skin with rotating movement and bending deformation, inspired from the kinetic façade of RMIT Design Hub having the simple mechanism but elegant look. It investigates the transfer of smart material techniques, low-tech mechanism, and digital 3d printing technologies for applications in building skin elements. The main objective of this research would be the SMP prototype design using 3d parametric design software and scaled-down model fabrication to testify the 3d printing feasibility of different kinetic SMP cell types, and to examine their shape-changing behaviours by heat. In addition, the further research tasks to be carried out for validation of SMP applications and their performances toward the actual implementations are discussed, following the experiment results.

2 METHODOLOGY

The research is conducted in intuitive design propositions and their verifications through experiments of hands-on manufacturing and digital simulation. In experiments, the passive structure is meant to be driven by SMPs according to their activating temperature (Boldini et al., 2017), and changes between open and closed positions of the building skin are assumed to be triggered by a combination of the material behaviour and momentary counteracting of the active mechanism into the reverse condition, but ideally by two-way SMPs. From the similar motivation and objective of the research, Clifford et al. (2017) addressed the challenges of designing adaptive façade systems with dynamic or smart materials. They presented a series of self-shading building tiles that apply the attributes of a class of polymers with shape memory characteristics. The smart material, adaptive, and reconfigurable tiles are designed to wrinkle and reposition themselves in response

to incoming solar radiation to shade building surfaces and lower thermal transmission, with the additional mechanism of pneumatic system.

To design SMP components, the fundamental behavioural properties of SMPs should be understood. The thermo-responsive SMPs have high elastic deformations, and the elastic modulus changes largely at the temperature below and above Glass Transition Temperature (T_g). If SMP is heated with no external force from a low temperature to a temperature higher than T_g , it eliminates the strain, resulting in the recovery of its original shape. SMP allows the maximum strain to be applied up to 400%, which means that SMPs have a shape recovery property of up to 400% of the plastic strain. Between the glassy and rubbery states of SMPs, large reversible changes of elastic modulus can be observed as high as 500 times.

In addition to the behavioural properties, the principle of having the memorised shapes above T_g should be also considered as a progression from the design phase to the manufacturing process. The general thermomechanical cycle of thermo-responsive shape memory polymers consists of three steps at a macroscopic level; (1) programming, (2) storage, and (3) recovery. The shape-shifting behaviour of SMP can be programmed to fix one temporary shape and subsequently recover back to its permanent shape upon heating. The temporary shape is usually defined by applied force during the shape fixing step. Accordingly, this step is also called a programming step (Zhao, Qi, & Xie, 2015). The programming needs the combination of a reversible switching mechanism and a structure. From a design point of view, with materials and morphologies, thermomechanical behaviour should be investigated together with the material properties. As has been realised by many researchers, the shape memory effect is a response of materials under a special set of thermomechanical loading conditions, rather than a material property. Therefore, shape memory effect is determined not only by material properties, but also by complicated thermo-mechanical loading conditions. In many cases, the latter complicates the evaluation of shape memory performance as well as material design (Zhao et al., 2015). In this paper, the entire programming process would not be targeted because it not only needs an extrinsic active mechanism other than by SMP, but also requires a design-driven approach to conceal ancillaries. Rather, this paper focuses on the programming of the permanent shape via manufacturing and recovery at T_g as an activated shape-changing behaviour.

After all, this paper studies a design-to-fabrication workflow for the conception of responsive skin systems that integrates the use of computational tools, 3d printing, and material experiments. As a novel innovative material, the thermo-responsive SMP is known to be easy to process and applicable to moulding or extrusion as a format of pellet or resin. Processing polymers into certain shapes is a necessary step towards their eventual uses. Fabricating SMP components in the relevant and potentially complicated shapes is important given the fact that their functions are much more tightly and uniquely bound to the shapes. In many SMP applications, the involved materials cannot provide the intended functions without being processed into proper 3-dimensional shapes or micro-structured surfaces. In addition to traditional polymer processing methods, such as injection moulding and potting, used to produce relatively simple shapes, several methods that lead to new SMP design, capability, and highly complex shapes have emerged (Zhao et al., 2015). To achieve rapid manufacturing and promote prompt feedback between design and fabrication, experimental 3d printing is undertaken to fabricate SMP components in this research by using an FFF (Fused Filament Fabrication) 3d printer, Cubicon Single Plus. The maximum nozzle temperature reaches 260 °C and the maximum heating bed temperature reaches 120 °C.

From the research on current states of commercially available smart material products and manufacturers, it was found that a widely-used polyurethane (PU)-based SMP was developed by

Mitsubishi Heavy Industries (Erkeçoglu, Sezer, & Bucak, 2016), and the SMP used in this research was acquired from SMP Technologies, led by Dr. Shunichi Hayashi, formerly of Mitsubishi Heavy Industries. Following an inquiry to SMP Technologies, SMP filaments, jointly developed by SMP Technologies and Filament KO-BO, were employed with the 3d printer.

To verify the 3d printing processing in SMP fabrication, the SMP prototype developed by Beites (2013) was reproduced as in Fig.2. While Beites manufactured the prototype with injection-moulded SMP actuator and Polypropylene (PP) panels, the tested model (Fig.2) was created with 3d printed SMP actuator and ABS panels, to demonstrate the shape-changing behaviour of the same prototype with different processing methods. The rotating movement and bending deformation pattern of SMP hinges can be interpreted as mechanisms of opening-closing shading devices, which are the main principles of shape-changing behaviours.

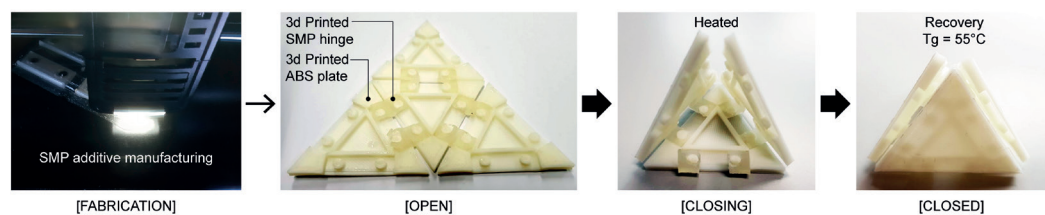


FIG. 2 Shape-changing behaviour demonstration of 3d Printed SMP hinges by reproducing Beites' prototype (Beites, 2013)

As previously mentioned, to focus on simple behavioural principles in the first stage of prototype design and fabrication, this paper limits the scope of the skin morphology into circular components. In the field of architecture, cellular solids are constructions based on assembly of cells with solid edges or faces packed together to fill a space (Gibson & Ashby, 1997). In the manufacturing process, the infill density of 3d printed cells should be defined appropriately to maintain the structure, shape, and behaviour (Naboni et al., 2017). This study starts from homogeneous cells with a solid state of high density based upon the stability of fabrication, material behaviour, and expected movement outcomes. To implement experimental building skin systems based on SMP application, the computational design tools, hands-on scale-down model, and 3d printing manufacturing are used in parallel.

This research provides a foundation for kinetic SMP applications in cell-type shading devices of building skins with a focus on the prototype design and 3d printing fabrication to demonstrate adaptability with activation temperature, cell morphology, scale, cell material behaviour, controlling mechanism, movement and deformation pattern, subsequent opening and closing effect, and reversible reiteration pattern. Within the field of architecture, the shift from prototyping to direct manufacturing is mainly connected to material improvement, which, in comparison to product design, is more complicated to achieve. Material characteristics and behaviour, mechanical properties, and dimensional requirements are key elements in evaluating the use of digital fabrication. Therefore, the exploration of a material system should be held to understand the way it can be exploited, with a rigorous multi-scalar analysis of the material coupled with the fabrication system that will be used. This process starts with analysing the materialisation process through fabrication experiments and the observation of their geometrical and mechanical characteristics (Naboni et al., 2017). The research starts with applying SMP as an activator to input heat and output movement or deformation in very simple circular cells.

This study introduces novel materialisation processes of SMP additive manufacturing. Logics of sustainability and efficiency that are typical of mass-production are no longer applicable. Taking inspiration from the multiple references, a design methodology which adapts to the thermal environmental changes with various surface shapes and structures, hinges as activators, and opening-closing mechanisms is developed. The outcome of this process is an impetus for the thermo-responsive building envelope system, which allows for the creation of adaptive façades with smart materials. This experimental approach challenges current design paradigms of mechanically active architecture. The research develops a system for responsive building envelopes based on SMP properties and behavioural design concepts. The design process is inspired by the external shielding formation in autonomous response to temperature conditions. The opening-closing mechanism, which allows visual permeability as well as light transmission by exhibiting the constructive geometry of cell surfaces or actuating components, is a required performance in SMP building skin applications.

SMPs have wide range of T_g from -70°C to $+100^{\circ}\text{C}$. Since they have a wide range of glass transition temperatures, their stiffness can be tailored. For example, SMP Technologies provides 7 different glass transition temperatures (T_g) of 25, 35, 45, 55, 65, 75 and 90°C , in four different types of pellet, resin & hardener, solution, and filament. Pellets are processed by injection moulding, and resin should be cured in specific conditions with a vacuum oven. Therefore, for the rapid production and testing, the 3d printing filament was selected for the fabrication method. The 3d printing filament is only available with T_g at 55°C , made of MM5520, although 25°C would be the optimal activation temperature to examine the climate-adaptability of SMP façade elements in Seoul. MM 5520 shows almost no definite property difference from MM2520, which is the target to be applied in the long-term research, as shown in Table 1. In the future experimentation, SMP pellets with activation temperature at 25°C , MM 2520 would be examined for 3d printing, as Yang used MM 4520 pellets from SMP Technologies (Yang, Chen, Wei, & Li, 2016), but probably with different settings for the 3d printer and the controlled experiment environment.

ITEM	UNIT	SMP TECHNOLOGIES MM 2520		SMP TECHNOLOGIES MM 5520	
		Glass Region	Rubber Region	Glass Region	Rubber Region
Hardness	H _D	78	26	77	27
100% Modulus	MPa	-	3	-	2.1
TS (Tensile Strength)	MPa	45	12	48	13
Elongation	%	30-50	>600	30-50	>600
B M (Bending Modulus)	MPa	2450	-	2150	-
B S (Bending Strength)	MPa	90	-	80	-
T_g (Glass Transition Temperature)	$^{\circ}\text{C}$	25		55	

TABLE 1 SMP Material Properties (SMP Technologies)

The main hypothesis is that defined cell types from deductive and analogical interpretation and design process, using Rhinoceros and Grasshopper, are fabricated and tested using achievable materials – ABS for non-activating parts and SMP for activating parts, and simplified details to verify the design-to-manufacturing workflow from 3d design process to 3d printing for the further study of a full-scale prototype of the dynamic cell skin typology in the near future, to analyse performative possibilities and the aesthetic behavioural properties of actual building skin designs. Specific logics pertaining to rotating activators and bending deformation of SMP, such as thicknesses, hinge angles, activating directions, and stretchable textures are tested to examine the material, morphological,

and mechanical behaviour patterns. This experiment involves the iterative workflow to generate and materialise cell components combined with proper activators and surfaces. Fig.3 indicates the overall research workflow scheme involving computational tools, 3d printing fabrication, and simulation for performance validation, focusing on SMP cell components composed of simple activators and surfaces with rotating movement and/or bending deformation.

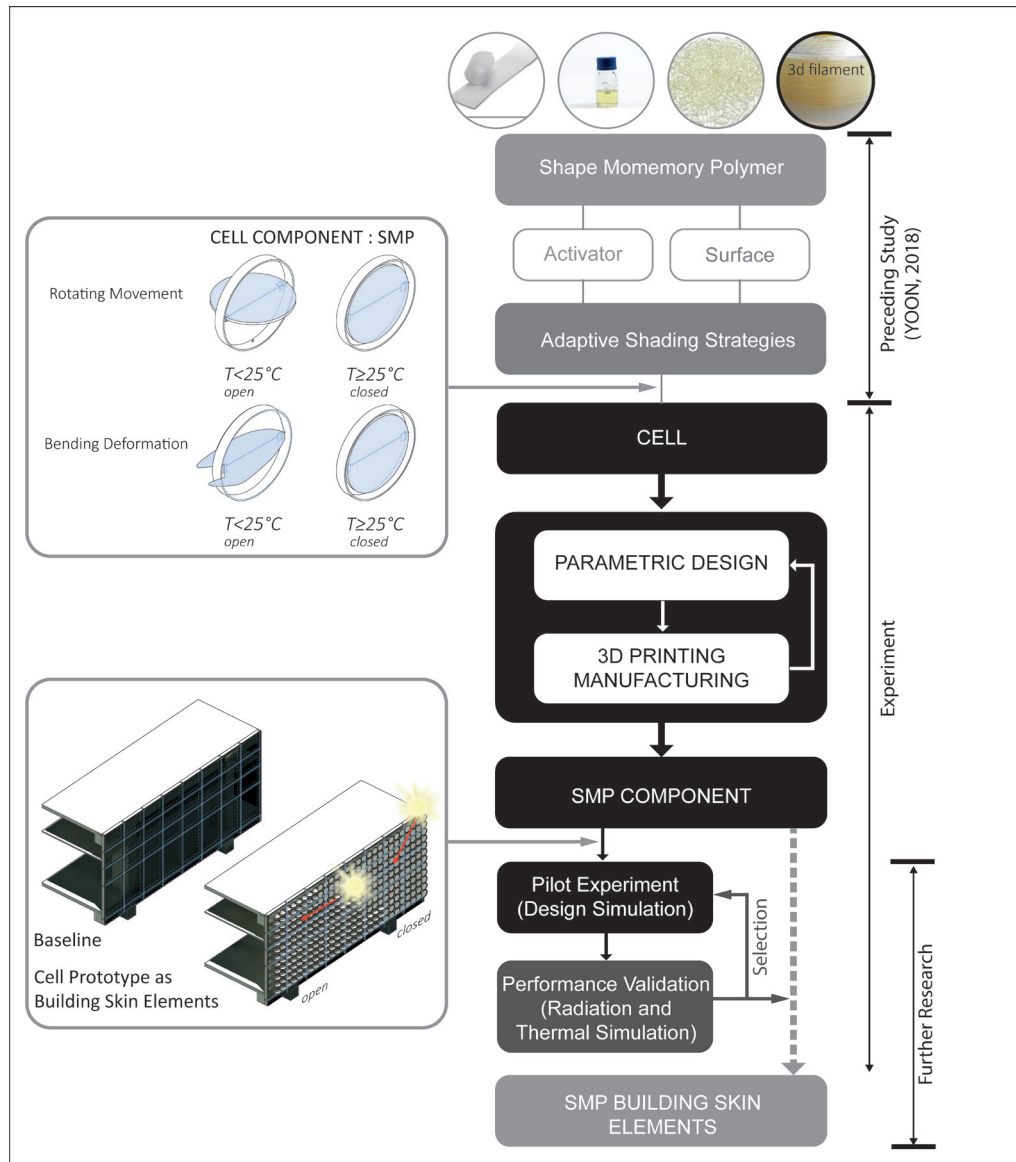


FIG. 3 Overall Research Workflow Scheme, involving computational tools, fabrication, and performance validation

The computational design and 3d printing fabrication experiments were carried out to tackle the prototype design and fabrication feasibility. Through the fabrication experiments, difficulties and opportunities to develop the initially proposed SMP cell components into the kinetic façade elements can be evaluated in consideration of structural and performative optimisations.

Furthermore, performance simulations of building skins with tested SMP prototypes were conducted to validate the performance as shading devices and climate-adaptive building skins after applying

SMP prototypes to a pilot project, located in Seoul, in design simulations. As the beginning stage of performance validation setup, solar radiation and thermal simulations using Rhinoceros and Grasshopper with plug-ins such as Honeybee and Ladybug were conducted to analyse the results to verify the possibility of energy performance evaluation to select the optimal prototypes. From the performance simulations, prototypes demonstrating more efficacy in solar radiation reduction and thermal impact can be sorted out for further development in the next stage of the research. The complex and elaborate workflow including parametric design and energy simulation would allow feeding productive information into the workflow as proposed in Fig.3. Therefore, this paper discusses the opportunities of such procedures as well as the limit of current experiment and further fabrication issues to be studied.

3 RESULTS

3.1 FABRICATION EXPERIMENTS OF SURFACES AND ACTIVATORS

To determine the design parameters, including the minimum surface thickness, perforation, and programmed shape angles, a series of experiments were set up. First, SMP components based on the selected cell morphologies and movement mechanisms were fabricated and tested, starting from circular disc samples of 100mm diameter, at a scale of 1:3, with a variety of thicknesses – 0.15, 0.2, 0.3, 0.5, 0.75, 1.0, 3.0mm, as shown in Fig.4. To compare the surface finishes and stability, ABS surfaces were 3d printed as control groups. These samples contributed to the definition of an optimal fabrication thickness. The thicknesses less than 1.0mm had issues with printing quality and bending in a neutral state. In addition, this test is intended to ensure the best compromise between production precision and printing speed, with an average production time of 3 to 5 hours.

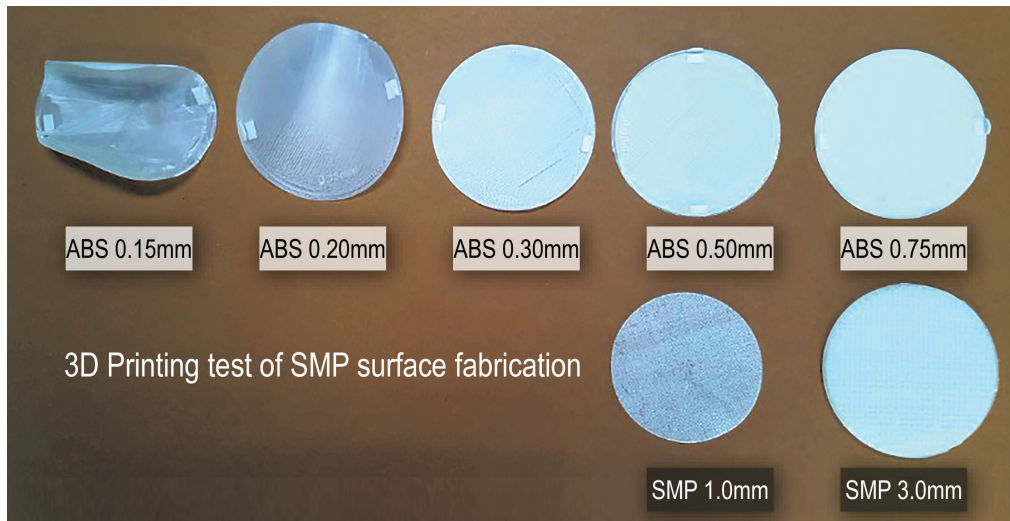


FIG. 4 Fabrication experiments of SMP surfaces in comparison with ABS surfaces

Second, in the process of manufacturing, SMP hinged activators for the prototype in Fig.2, the quality of finishing, and creating perforations in vertically printed plates used as joinery holes,

created difficulty in additive manufacturing. To adjust the primary parameters in 3d printing by focusing only the completeness of the construction, perforations were omitted. As the extruder temperature (T_e) was set higher than T_e for ABS 3d printing, the quality improved as shown in the second pictures of Fig.5. However, at T_e higher than 250°C, SMP outputs are burnt brown when extruded. After a series of errors and tunings, and adopting references (Yang, Chen, Wei, & Li, 2016) and correspondence from Clifford (Clifford et al, 2017), the 3d printer setting was finalised as shown in Table 2. Consequently, the final 3d printed outcome could be generated, even with perforations on both horizontal and vertical surfaces.

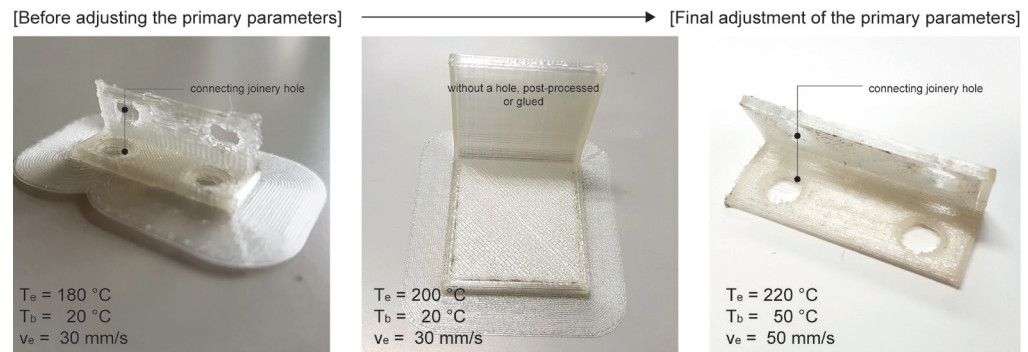


FIG. 5 Fabrication experiments of SMP hinges as joints and activators with various 3d printing parameters

PARAMETERS	VALUES			
	Yang (2016)	Clifford (2017)		Yoon (2018)
Extruder Temperature T_e (°C)	220	210		215 ~ 220
Bed plate temperature T_b (°C)	45	48		50
Speed while extruding v_e (mm/s)	30 < v_e < 60	25 (Perimeter)	30 (Infill & Support)	50
Speed without extruding v_f (mm/s)	150	30		150
Gap between nozzle tip & build layer d (mm)	0.3	(No information)		0.3
Retraction Distance (mm)	-	-		3~10
Printing Infill percent (%)	100 (vibration issue)	Custom 0.3 (Triangles) Infill overlap 0.06mm		30 ~ 100

TABLE 2 Comparison of primary parameters of 3D printing machine by Yang and Clifford with the finalized parameters

Yang et al. (2016) note that there is no previous report about process studies on the 3d printing of SMP materials. The FDM (Fused Deposition Modelling) 3D printing process is similar to a moulding process, as they both include melting and reshaping of material. 3D printing quality is managed by controlling the quality of SMP filament and the bubble content in the filament extrusion process, and by setting up the process parameters related to the FDM printing process, such as nozzle temperature, scanning speed, and part cooling. Yang et al. (2016) used the MM-4520 pellets with a Makerbot Replicator 2X. However, Clifford (2017) used MM-5520 Filament, i.e. the same as used in this research, with a Creator Pro machine, and the fabrication setup parameters are acquired by inquiry.

Table 2 shows a set of 3d printing parameter values for SMP material. In addition, several matters require attention, including the extruding flow amount adjustment, transfer from the printed SMP

to the ambient air, surface roughness, and the retraction distance calibration. Furthermore, from continued studies, additional parameters including layer height at 0.3mm, quantity of wall line at 3, flow ratio at 50%, retraction speed at 100mm/s, support structure type as raft, and infill type as zigzag were additionally set up for better printing quality. However, in the 3d printing process, the unexpectedly high ambient temperature of the work environment caused many troubles in producing good-quality outcomes, resulting in air bubbles in the extruded SMP and the obstruction of the extruders with SMP lumps.

The design of shading systems can be developed to meet adaptivity principles based on two approaches of activators and surfaces. SMP activators allow the kinetic behaviours through intrinsic material properties directly affected by changes of temperature. SMP surfaces are actuator-embedded envelopes which show surface deformations and configuration changes through the dynamic motion mechanisms. The SMP layer of shading devices will react to different input of heat, opening and closing accordingly in an autonomous way. A critical phase in the development of cell type building skin is the definition of the baseline cell. This implies that the geometry constraints of SMP are first to be taken into account in this evaluation. For example, to figure out the restorative behaviour and force with the marginal angles in recovery of hinge rotation, hinges can be differently shaped and programmed to result in customised rotating movements, as in Fig.6. To programme rotating angles other than 90°, the support structures between plates should be adequately set for 3d printability to stably acquire the outcome without falling down in the fabrication process and detachability to obtain clean final products. However, the rotating behaviours tend to be degraded after the first recovery in multiple reiterative operations (Bae, Choi, & Yoon, 2018), by 20 to 40%. In this research, the recovery fatigue was not considered in design process, but later in developing the installation design with a certain expectation of kinetic movements, the recovery fatigue should be counted.



FIG. 6 Programming of rotating angles by 3d printing the customised angled hinges

3.2 BASELINE CELL PROTOTYPE FABRICATION AND KINETIC SIMULATION

As the baseline cell prototype, a prototype in an ABS circular plate with a SMP hinge is considered (Fig.7). The idea is simply to rotate the ABS plate with forces caused by SMP hinges. However, the pulling force by the SMP hinge folding is insufficient to rotate the ABS plate and the position after rotating is not sustained. By repositioning the SMP hinges to the ABS tester, it was discovered that the centre of gravity can be translated by rotating SMP hinges and the fixed shape of SMP activator can hold the ABS plate position. To testify shape-changing behaviour activated at 55°C, five different devices were devised and examined: (1) hot plate, (2) warm water basin, (3) insulated box with electric heating cable and thermostat, (4) insulated box with higher-temperature electric heating cable and thermostat, and (5) heating cabinet. Direct wiring with heat cables was avoided,

considering the heat would be transferred to SMP components through the ambient temperature. At the beginning, using a warm water basin was enough to observe the thermal behaviour of SMP, but SMP shows weak moisture-resistance and after several handlings of SMP in the basin, the original shape was deformed too much. In other test settings with a hot plate and electric heating cables, the ambient temperature didn't reach 55°C. After all, the heating cabinet provides the best testing environment in more stable conditions. Therefore, the following experiments at 55°C are conducted using the heating cabinet.



FIG. 7 Baseline prototype and heat test setup

With the baseline prototype combining the ABS plate and the SMP hinge, the digital motion simulation was studied. Grasshopper with Kangaroo Plug-in is selected as a live physics engine for kinetic simulation directly within Grasshopper and Rhinoceros. The purpose of kinetic simulation is to demonstrate the dynamic movement of prototypes and to find an aesthetically pleasing prototype design. Furthermore, it is assumed that the kinetic adaptability to the specific temperature can be modelled and imported to the energy simulation software. However, the physics and the relation between SMP elasticity, gravity centre translation, and rotational movement of the prototype could not be achieved, due to the unknown value of each variable. Also, from the research (Bae et al., 2018), it was found that the recovery pattern is not maintained at an equal level at all times. Therefore, the simulation setup was determined to follow the empirical results.

From the hands-on model test, the shape-changing behaviour is examined to measure the bending angle of the hinge, the rotation angle of the plate, and the time taken for hinge bending and plate rotation. The acquired movement data is input to Grasshopper with a simplified control of parameters to simulate the motion mechanism of rotating and bending. As the relative effects by the bending hinge, the rotation of plate occurs, and the shading device is closed. The demonstration of the SMP activator with the ABS circular cell disk is provided in Fig.8. The activation by temperature is programmed as Boolean logic at this stage. The simulation setup should be further developed to include the activation by temperature with climate data to demonstrate the actual performance of a prototype as well as more precise relations among all kinds of influence factors after collecting their values from measurement experiments. To exemplify the model-driven programmable matter design approach in the future and to tailor the thermo-responsive behaviour of SMP for the design and construction of a shape-changing façade element, physical parameters controlling the morphing behaviour and response time (Abdelmohsen et al., 2018) of SMP to T_g should be explored.

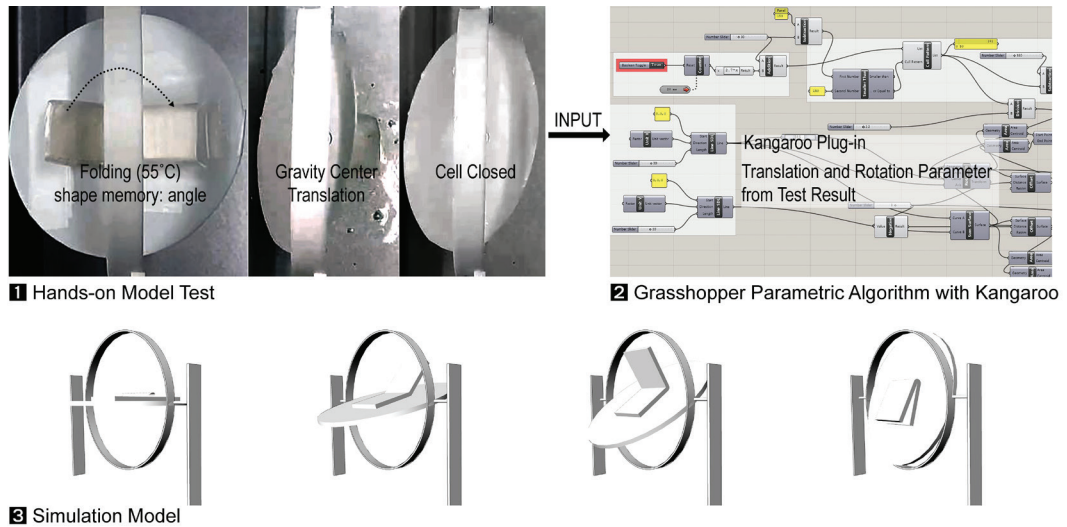


FIG. 8 Baseline model test and motion simulation

3.3 DESIGN AND FABRICATION OF CELL PROTOTYPES

After the demonstration of the baseline prototype in the design and additive manufacturing process, various SMP prototypes were designed with reference to kinetic prototype researches using SMA, biomimetic design approaches, and 4d printing from disciplines other than architecture (Al-Obaidi et al., 2017; Coelho & Zigelbaum, 2011; Ning, Wang, Zhang, Yu, Choi, Zheng, & Rogers, 2018), but with the form and size restrained to the circular cell of 100mm diameter, at a scale of 1:3. In the prototype design process, each cell was intended to be manufactured entirely with SMP as the activator-embedded surface, and to reduce the additional complexities by joints and connections for further applications involving installation details. The challenge in designing thermo-responsive building skins with SMP is to evaluate and expect transformation behaviours between two different pliability statuses before and after reaching T_g . Both rigid and elastic bodies are able to perform mechanical movements (Fiorito et al., 2016) but in dissimilar ways. With the combined mechanism of rotating and bending in addition to connections and joints, movement patterns can become more complicated and broken down to swivel, revolve, swing, flap, lever, and slide, which should be further explored in continued study. In case of the baseline prototype, the SMP activator and the ABS plate were attached with Cyanoacrylate-based glue.

The design of thermo-responsive building skin cells involves the design of programming SMP to determine the permanent shape above 25°C activated by heat and to control heat gain and natural light. Based upon the opening-closing mechanism given the circular cell types, by borrowing the surface structure from references (Coelho & Zigelbaum, 2011; Ning et al., 2018), five cell component types are proposed for experiment. To conduct morphology study, 3d geometry production and G code generation for 3d printing, Rhinoceros with Grasshopper and Cubicreator were used. Five cell components were designed by programming the closed surface, shown in Fig.9. The big difference between it and other kinetic structures is that the activated phase of mechanism is closing, while most kinetic façade installations have the opening condition as the activated phase. However, to compare the effects of kinetic movement from opening to closing, open surface models were also additively manufactured. This process includes creating both open and closed models in Rhinoceros, exporting to STL files, importing STL files in Cubicreator to finally acquiring G codes ready for 3d printing.










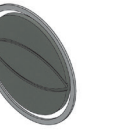
TYPE	A BASELINE	B HINGED PORES	C KIRIGAMI	D RADIAL FOLDING	E FLAPPING
open < T_g					
closed > T_g					
Ref.	RMIT Design Hub Facade	Hinged Surface (Coelho, 2011)	Kirigami (Ning, 2018)	Origami (Ning, 2018)	Venus Flytrap

FIG. 9 Five cell component types and their morphologies

To define an optimal configuration, two main parameters of formability and responsive outcome are considered. The employed material, thermo-responsive SMP, demonstrated compatibility with 3d printing fabrication for actuators and bending surface components by setting up the optimised printing parameters such as nozzle temperature, bed temperature, nozzle speed, extrusion amount etc. as previously discussed, which enables various morphology studies.


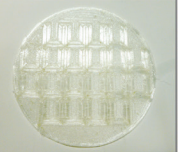
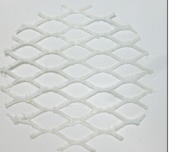



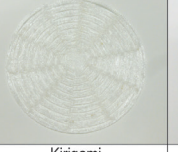
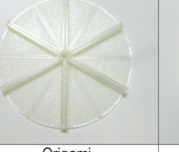

TYPE	A BASELINE	B HINGED PORES	C KIRIGAMI	D RADIAL FOLDING	E FLAPPING
open ↕ closed	No separate test (Hinge or Bending) 			Unprintable	Fail: Unprintable 
closed					
Ref.	RMIT Design Hub Facade	Hinged Surface (Coelho, 2011)	Kirigami (Ning, 2018)	Origami (Ning, 2018)	Venus Flytrap

FIG. 10 Cell component 3d printing results

SMP prototype components were 3d printed and, iteratively, the designs and G codes were revised to control the outcomes. The best final outcomes after several tests are shown in Fig.10. For Type B, the sizes of hinged pore, the minimum spacing between pores, and openings between the hinged surface and spacings were variables tested for design decisions. For Type C, the minimum thickness and width of structure, and spacing between structures, were edited for 3d printing feasibility and quality control. For Type D and E, the design process and G code acquisition proceeded smoothly, but the open position models could not be printed. In case of Type D, the spacings between folded surface and structure are not achievable with the precision of the used 3d printer. In addition, to hold the angled surface stacking, supports are required under the folded surface, but they are too small to be printed. In the case of Type E, the open flap could not be supported in vertical stacking. While the angled SMP hinges were produced as in Fig.6 with multiple tests, the bended curvature with bigger sizes are obstacles to successfully fabrication in 3d printing. Additionally, pliability of SMP in extruding moment makes it very difficult to sustain the vertically built-up surfaces and complicated surfaces. Through the 3d printing process, SMP filament softens when it heats after printing, thus

memorising the customised shapes. This unique process and material property provide not only the opportunities of kinetic elements but also the major barriers to manufacturing SMP components. The 3d printing process and the observed result of thermo-responsive behaviour would affect the next step of integrating geometries, functions, and reversing programming.

Regarding the responsive outcomes, all of the fabricated prototypes showed prompt responses at the activation temperature with good performances, as shown in Fig.11. The response lead time varies depending on the morphology, the thickness of surface, the scale of a transformed part, and rotating or bending angles, but the general response lead time with the tested prototypes are within a maximum of 4 minutes.

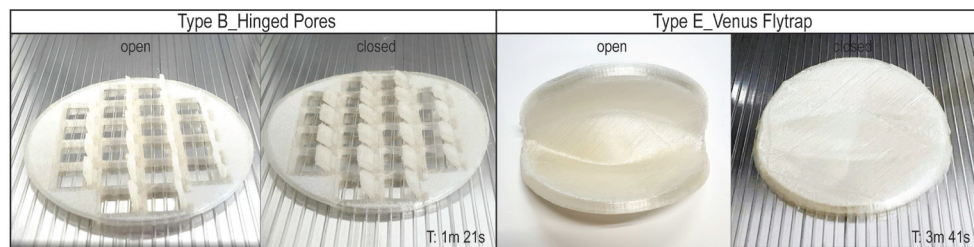


FIG. 11 Heat test result of Type B and Type E

However, after recovering to the permanent shape, the pliability of SMP yields its shape to other external forces, or simply to gravity, depending on SMP shell thickness. Thus, the strain fatigue becomes an obstacle to implementing the SMP component on a building skin that should resist various external loads. In addition, the sensitivity of the mechanical properties of SMPs to humidity is pointed out and it requires a covering structure that protects them from possible harsh environmental conditions (Boldini et al., 2017). This research excludes integrated solutions for solving these issues at this stage and assumes that the temperature in the building is mainly controlled by using a double skin façade.

The evaluation of design and fabrication test results is made by a matrix, as in Table 3, to find out which prototypes and which combination of mechanisms will be further developed in more detail in future studies. The evaluation index includes structural optimisation, performative optimisation, material dependency, morphological dependency, autonomous activation, and reversibility friendliness in the process of closed positions to open positions of the five tested prototypes. Structural optimisation means compatibility with the fixing framework. In case of type A and B, the circular surface forms and the central axis are maintained in spite of shape-changing, gravity translation, bending deformation, and rotation movement. Therefore, these types can be easily installed with a simple framework. Type C is difficult to hold within a consolidated framework due to the stretching of its entire surface and its perimeter deformation. Types D and E can be structurally optimised to the framework with points. Performative optimisation indicates the shading effects by closed and open positions of prototypes. Except for Type C, which has permeability in both closed and open positions, four other prototypes show obvious surface closings reducing light and heat transmission. Material dependency is the index evaluating the inherent materialisation of SMP, which is not substituted by SMA. Morphological dependency is the shape-changing behaviour determined by SMP surface geometries and structural shapes. Each type can be autonomously activated by the proper temperature. The reversibility friendliness means the shape programming from the closed position to the open position. Types A and E can be easily reverted to their permanent

shapes with one-directional force. Types B and D need multiple forces to be reverted. Type C needs delicate operations of forces to be programmed in order for it to be returned to its original and consistent position and shape. From this evaluation, Types B and E are considered to be the most effective for their design, fabrication, and operation.

TYPE	EVALUATION INDEX					
	Structural Optimisation	Performative Optimisation	Material Dependency	Morphological Dependency	Autonomous Activation	Reversibility Friendliness
A	+	+	0	-	+	+
B	+	+	+	0	+	0
C	-	-	+	+	+	-
D	0	+	0	+	+	0
E	0	+	+	+	+	+

TABLE 3 Evaluation matrix of the results

+: Good/High | 0: Average/None | -: Bad/Low

However, in this experiment, the heat tests with prototype models were tested in a laboratory setup using a heat cabinet. Thus, their implementations in operative conditions of buildings would require further development of the consistent and stable material behaviours and optimised additive-manufacturing techniques with SMP activated at 25°C, as previously mentioned. Additionally, further development of SMP with T_g at 25°C would require mock-up tests in the adequately controlled environment through a full-scale architectural demonstrator, where a wider set of evaluative criteria are to be measured and assessed.

3.4 PILOT SIMULATIONS AND SHADING PERFORMANCE VALIDATION

For pilot simulations and shading performance validation, the façades with studied prototypes were modelled with Rhinoceros and Grasshopper. The façades are assumed to face south in an office building located in Seoul, integrating a glass curtain wall façade and SMP shading devices. In the pilot studies, required criteria of energy use set points and average heat coefficients of the total building envelope should be employed. The average thermal transmission coefficient requirement shall be set at 1,500 W/m²·K for glazing as a baseline.

To evaluate and validate the system, energy simulation shall be incorporated into the design process. Merla, Diaferia, & Dibari (2016) discussed a comparison of several integrated software suites. Combined use of Ladybug and Honeybee would demonstrate the pros by performing very detailed and reliable parametric analyses. As presented in Fig.12 and Fig.13, the radiation simulation and thermal simulation were conducted for all the prototypes in order to verify the effectiveness of SMP shading mechanisms and to discuss further agendas to be studied in the next stage of the research in relation to holistic analysis of SMP building skins. In order to proceed and acquire simulations within a reasonable rendering time, as well as to identify the effect of SMP in activating, the simulations were done between May 1st and September 30th (Lim & Yun, 2017), when the average high temperature ranged from 23°C to 30°C (Yun, Kong, & Kim, 2012) with the pilot project facing south.

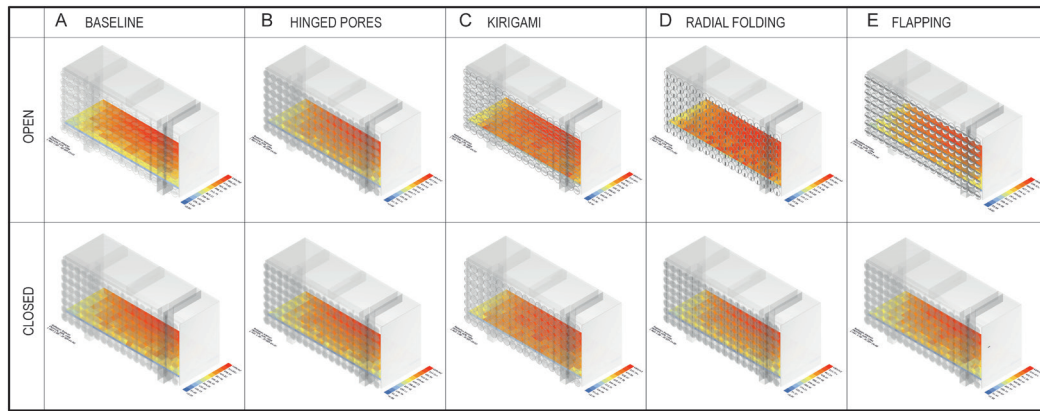


FIG. 12 Radiation simulation results of SMP cell building skins

To achieve the precise radiation simulation results and deduce the quantitative effects of direct solar radiation reduction, the dynamic kinetic transformation of SMP building skin elements, depending on the ambient temperature, should be input into the algorithm. However, in this research, to roughly estimate the effects of radiation reduction, two radiation simulations of each type at both open and closed positions were undertaken, and the big radiation difference between open and closed positions is interpreted as the most evident radiation reduction effect of SMP building skins. However, as shown in Fig.13, with the generally applied thermal simulations, the analysis results failed to verify the thermal impacts by shading devices between closed and open positions of designed prototypes. Further energy simulation algorithms with more detailed information should be developed to validate the performance by SMP kinetic shading façades.

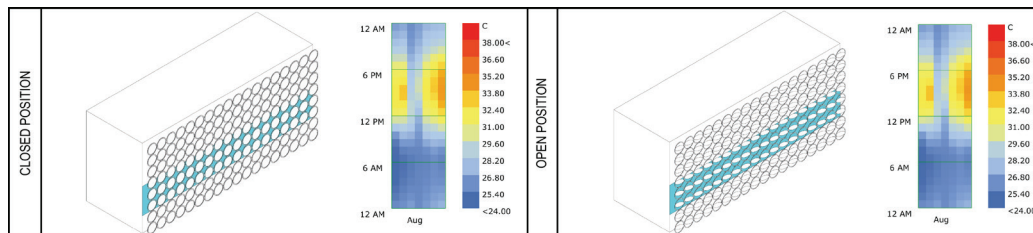


FIG. 13 Thermal simulation results of SMP cell building skin type A (baseline)

Nevertheless, to roughly evaluate the effects of reducing direct radiation by SMP cell mechanisms, differentials between the radiation simulations at open and closed positions are visualised in Fig.14. The differentials are represented in colour, and a colour with a higher hue and saturation indicates a wider radiation difference, which means more distinct radiation reduction effects. From the figure, Type D and Type E show more apparent colours than the other types. From radiation simulations, the radiation levels between May 1st and September 30th are estimated approximately between 371.39 to 530.56 kWh/m² at the open position of Type D, which has the lowest façade coverage at the open position among five types and their positions. When it is closed, the perimeter area has a radiation between 256.85 and 308.23 kWh/m². In the case of Type E, the radiation ranges between 320.65 and 534.42 kWh/m² at open position, and the radiation reduces to between 257.21 and 514.43 kWh/m² at closed position. Regarding Type C, the radiation ranges between 320.18 and 533.64 kWh/m² at open position while it ranges between 319.97 and 533.29 kWh/m². Although the radiation reduction effect of Type C is more evident than Types A and B, the effect is not distinctly advantageous in considering

the complexity of cell structure accompanying the perimeter deformation. If the framework to hold the dynamic kirigami structure and the activator system to provide the distributed forces to contract the cell structure into the closed position are devised, Type C can be explored, but in this research, to strategically search for simpler application methods, Type C is excluded from the further development.

However, Type B shows distinctive solar radiation effects. From Fig.14, and based on the fundamental assumption of radiation reduction by closing the cell with the SMP actuating, it can be concluded that Type B does not verify the radiation reduction so as to reduce energy load. Due to its porous surface condition, Type B has a radiation level from 258.77 to 517.54 kWh/m² when it is open, which is as low as solar radiation amounts of other prototypes at their closed positions, while the radiation level of closed Type B is between 256.85 and 513.71 kWh/m². Therefore, it would be difficult to state that Type B doesn't have an environmental impact from this analysis. In addition, other factors such as thermal comfort, daylight, and natural ventilation, which should be measured to discuss about energy performance, have not been reviewed in this research.

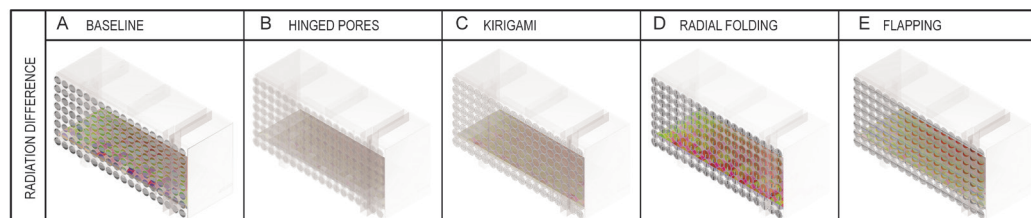


FIG. 14 Differentials of radiation simulation results between open and closed positions

4 DISCUSSIONS

4.1 REVERSIBLE REITERATION OF SHAPE-CHANGING

Besides securing the recovery strength, and scaling up the prototype production, the critical issue is acquiring the reversible reiteration of shape-changing. Within a one-way shape-memory cycle, the shape recovery step can only go from the temporary shape to the permanent shape. Unless the SMP is mechanically deformed again via a re-programming process, the recovered permanent shape cannot revert back to the temporary shape by altering the external stimulus only (Zhao et al., 2015). By now, there are no commercial two-way SMPs, which have instead been produced in a laboratory for research reasons. Therefore, previous researches (Boldini et al., 2017) selected other materials as alternatives to two-way SMPs for the actuation of the passive system in the prototype, since it presents other promising features such as a multi-way shape memory effect, and an electrical triggering. Additionally, in many cases, the actuation mechanism was obtained with two counterposed one-way SMA springs. This solution allows an enhanced movement control of the actuator, but considerably increases the complexity of the feedback design, easily resulting in a wired and distracted unattractive system. Therefore, a considerate design approach that minimises the counteracting mechanism parts, and incorporates it into a simple system, should be steadily studied.

Therefore, two-way reversible SMP is desirable for building skin applications, as such for actuators, artificial muscle, sensors, and self-locomotion robotics (Li, Liu, & Leng, 2014). Such polymers may vary between two distinct shapes when they are exposed to stimuli creating the opposing conditions, such as heating and cooling. But two-way SMPs are harder to achieve and have become the most desired shape memory materials due to their unique properties (Wang, Jia, & Zhu, 2017). The future developments of two-way SMPs will permit a more practical functioning of the system. The reduction of the cost of SMPs is then supposed to promote a real implementation of the proposed concept (Boldini et al., 2017). Ideally the interdisciplinary and collaborative research between engineers developing two-way SMPs and architects would shift the paradigm and territory of thermo-responsive adaptive façades.

4.2 FURTHER SMP PROTOTYPE DEVELOPMENT

Beyond this research, advanced foreseen versions of responsive systems exhibit further surpassing conventional and mechanistic dynamic motion by generating reactions according to responses from the environment (Abdelmohsen et al., 2018). As presented in the experiment result and discussed with shading performance validation, Types B, D, and E, among proposed prototypes, are sought to be exploited for further prototype development.

As visualised in Fig. 15 with simple 3d modelling, there are wide ranges of issues to be tackled through the prototype development with Types B, D, and E. From the economic and efficient use of SMP, the active and responsive parts, and the static and passive parts of prototypes can be separated in materials such as SMP and ABS but shall be integrated into one cell to preserve the dynamic and kinetic effects as experimented in this research. Also, to further develop the prototypes into façade elements, the optimum size of each cell should be defined in terms of its behaviour, performance, and beauty. Lastly, the attachment and framework details, in addition to controlled SMP behaviour in reiterative and reversible pattern, should be tailored.

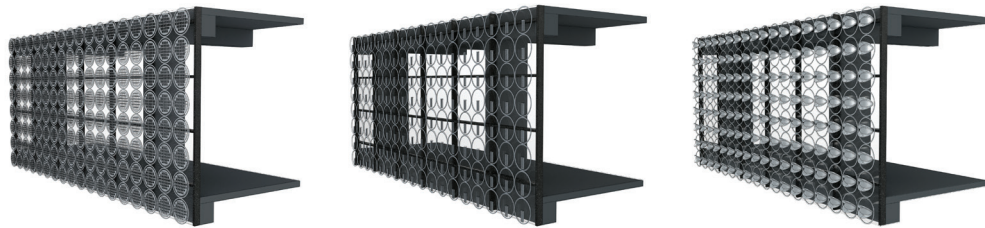


FIG. 15 Further research direction: Prototype development with Type B, D, and E at open positions

5 CONCLUSION

The paper aims to summarise the coordination process of SMP material programming, design, and fabrication, focusing on simple circular cells, and their opening and closing mechanism resulting from SMP bending deformation and/or rotating movement. The design and G code generation was conducted with a process combining Rhinoceros, Grasshopper, and Cubicreator. The kinetic movement of a tested prototype could be simulated using Rhinoceros, and Grasshopper with

Kangaroo plugin, but with the simplified interpretation and algorithms of data obtained from the hands-on model test. The iterative process of additive manufacturing with reference reviews led to the optimal parameter setting for 3d printing. The further SMP prototype design studies, which borrowed morphologies from precedent references, were fabricated to review their constructability in 3d printing. Within the constrained surface geometry and size of circle, the 3d printing feasibility is related to thickness, required finishing precision, vertical additivity with proper supports, and geometric complexity. Manufactured outcomes were reviewed with a focus on material morphing behaviour, structural and performative optimisation, material and morphological dependency, autonomous activation, and reversibility friendliness. The results of this research project developing SMP prototype design and fabrication show a great opportunity for the goal of applying novel smart materials in adaptive and responsive building skins by user-friendly manufacturing methods with easily accessible materials. However, the use of SMP, which shows instabilities depending on the manufacturing and operating environments, is still a challenge.

Moreover, performance analysis of the proposed prototypes was briefly conducted with Ladybug and Honeybee. Radiation simulation led to the ruling out inefficient prototypes. However, more detailed material information of SMP and behavioural relations of variables should be acquired from experiments in order to have more precise and adequate simulations and validations of kinetics and performances of SMP applications. The morphology, kinetic mechanism, and fabrication method of proposed SMP prototypes can be considered to be simple if undertaken with optimal design and 3d printing parameter settings. However, reiterative reversible movement designs and performance validations, with numerous material and behavioural property studies, should be developed in the direction of thermo-responsive SMP façade implementation, as well as material improvements to achieve reiterative shape-changing and stability by scientists and engineers in other disciplines.

Acknowledgements

This research was supported by Basic Science Research Program through the National Research Foundation of Korea (NRF) funded by the Ministry of Science, ICT and Future Planning (NRF-2017R1C1B5015080). The author would like to thank Sanghyun Bae and Seokwon Choi for their assistance in developing samples of the SMP components by 3d printing.

References

- Abdelmohsen, S., Adraenssens, S., El-Dabaa, R., Gabriele, S., Olivieri, L., & Teresi, L. (2018). A multi-physics approach for modeling hygroscopic behavior in wood low-tech architectural adaptive systems. *Computer-Aided Design*, 106, 43-53. <https://doi.org/10.1016/j.cad.2018.07.005>
- Addington, M., & Schodek, D. (2005). *Smart Materials and New Technologies - For architecture and design professions*. New York, USA: Routledge.
- Al-Obaidi, K. M., Azzam Ismail, M., Hussein, H., & Abdul Rahman, A. M. (2017). Biomimetic building skins: An adaptive approach. *Renewable and Sustainable Energy Reviews*, 79(June), 1472-1491. <https://doi.org/10.1016/j.rser.2017.05.028>
- Arun, D. I., Chakravarthy, P., Arochiakumar, R., & Santhosh, B. (2018). *5.5 Comparison of SMPs and SMAs. Shape Memory Materials*. Boca Raton, USA: CRC Press, 50.
- Bae, S., Choi, S., & Yoon, J. (2018). *A Study of the Influence of 3D Printing Infill Densities on SMP Shape Recovery Behaviors*. Submitted for Autumn Annual Conference of AIK(Architectural Institute of Korea), 2018.
- Beites, S. (2013). Morphological Behavior of Shape Memory Polymers toward a deployable, adaptive architecture. *ACADIA 2013 Adaptive Architecture*, 121-128.
- Bengisu, M., & Ferrara, M. (2018). *Materials that Move, PoliMI Springer Briefs*. https://doi.org/10.1007/978-3-319-76889-2_5
- Boldini, A., Colangelo, M., Pilla, A., Tavanti, M., & Mariani, S. (2017). Metereosensitive user-controllable skin for dynamic façades. In *12th Conference on Advanced Building Skins* (pp. 740-832). Bern: Advanced Building Skins GmbH.
- Clifford, D., Zupan, R., Brigham, J., Beblo, R., Whittock, M., & Davis, N. (2017). Application of the dynamic characteristics of shape-memory polymers to climate adaptive building façades. In *12th Conference of Advanced Building Skins* (pp. 171-178). Bern: Advanced Building Skins GmbH.
- Coelho, M., & Zigelbaum, J. (2011). Shape-changing interfaces. *Personal and Ubiquitous Computing*, 15(2), 161-173. <https://doi.org/10.1007/s00779-010-0311-y>

- Erkeçoglu, S., Sezer, A. D., & Bucak, S. (2016). Smart Delivery Systems with Shape Memory and Self-Folding Polymers. In *Smart Drug Delivery System*. InTech. <https://doi.org/10.5772/62199>
- Fiorito, F., Sauchelli, M., Arroyo, D., Pesenti, M., Imperadori, M., Masera, G., & Ranzi, G. (2016). Shape morphing solar shadings: A review. *Renewable and Sustainable Energy Reviews*, 55, 863–884. <https://doi.org/10.1016/j.rser.2015.10.086>
- Ge, Q., Sakhaei, A.H., Lee, H., Dunn, C.K., Fang, N.X., & Dunn, M.L. (2016). Multimaterial 4D printing with tailorable shape memory polymers. *Scientific Reports* 6: 31110. <https://doi.org/10.1038/srep31110>
- Gibson, L. J., & Ashby, M. F. (1997). *Cellular Solids: Structure and Properties (2nd edition)*. Cambridge: Cambridge University Press.
- Huang, W., Ding, Z., Wang, C., Zhao, Y., & Purnawali, H. (2010). Shape Memory Materials. *Materials Today*, 13(7–8), 54–61.
- Lelieveld, C.M.J.L. (2013). Smart materials for the realization of an adaptive building component. (Doctoral Thesis). Delft: Delft University of Technology.
- Leng, J., Lan, X., Liu, Y., & Du, S. (2011). Shape-memory polymers and their composites: Stimulus methods and applications. *Progress in Materials Science*, 56(7), 1077–1135. <https://doi.org/10.1016/j.pmatsci.2011.03.001>
- Li, W., Liu, Y., & Leng, J. (2014). Shape memory polymer nanocomposite with multi-stimuli response and two-way reversible shape memory behavior. *RSC Advances*, 4(106), 61847–61854. <https://doi.org/10.1039/c4ra10716k>
- Lim, J.H., & Yun, G.Y. (2017). Cooling energy implications of occupant factor in buildings under climate change. *Sustainability* 2017, 9, 2039. <https://doi.org/10.3390/su9112039>
- López, M., Rubio, R., Martín, S., & Ben Croxford. (2017). How plants inspire façades. From plants to architecture: Biomimetic principles for the development of adaptive architectural envelopes. *Renewable and Sustainable Energy Reviews*, 67, 692–703. <https://doi.org/10.1016/j.rser.2016.09.018>
- López, M., Rubio, R., Martín, S., Croxford, B., & Jackson, R. (2015). Active materials for adaptive architectural envelopes based on plant adaptation principles. *Journal of Façade Design and Engineering*, 3(1), 27–38. <https://doi.org/10.3233/FDE-150026>
- Lurie-Luke, E. (2014). Product and technology innovation: What can biomimicry inspire? *Biotechnology Advances*, 32(8), 1494–1505. <https://doi.org/10.1016/j.biotechadv.2014.10.002>
- Merla, M., Diaferia, R., & Dibari, G. (2016). Application of parametric study and generative algorithms to optimize building physics analyses. In P. LaRoche & M. Schiler (Eds.), *PLEA 2016 32nd International Conference on Passive and Low Energy Architecture* (Vol. I, pp. 23–28). Los Angeles, California.
- Mungenast, M. (2017). Future Façades – Development of 3d-printed Functional-Geometries for Building Envelopes, January 19th 2017-Munich Powerskin Conference Proceedings, 307–317.
- Naboni, R., Kunic, A., Breseghello, L., & Paoletti, I. (2017). Load-responsive cellular envelopes with additive manufacturing. *Journal of Façade Design and Engineering*, 5(1), 37–49. <https://doi.org/10.7480/jfde.2017.1.1427>
- Ning, X., Wang, X., Zhang, Y., Yu, X., Choi, D., Zheng, N., & Rogers, J. A. (2018). Assembly of Advanced Materials into 3D Functional Structures by Methods Inspired by Origami and Kirigami: A Review. *Advanced Materials Interfaces*, (February). <https://doi.org/10.1002/admi.201800284>
- Ratna, D., & Karger-Kocsis, J. (2008). Recent advances in shape memory polymers and composites: a review. *Journal of Material Science*, 43, 254–269. <https://doi.org/10.1007/s10853-007-2176-7>
- SMP Technologies (n.d). *Shape Memory Polymer Product Info*. Retrieved June 26, 2018, from <http://www2.smp techno.com/en/smp/>
- Wang, K., Jia, Y. G., & Zhu, X. X. (2017). Two-Way Reversible Shape Memory Polymers Made of Cross-Linked Cocrystallizable Random Copolymers with Tunable Actuation Temperatures. *Macromolecules*, 50(21), 8570–8579. <https://doi.org/10.1021/acs.macromol.7b01815>
- Yang, Y., Chen, Y., Wei, Y., & Li, Y. (2016). 3D printing of shape memory polymer for functional part fabrication. *International Journal of Advanced Manufacturing Technology*, 84(9–12), 2079–2095. <https://doi.org/10.1007/s00170-015-7843-2>
- Yoon, J. (2018). Climate-adaptive Façade Design with Smart Materials: evaluation and strategies of thermo-responsive smart material applications for building skins in Seoul. Submitted for *PLEA 2018 HONG KONG: smart and healthy within the 2-degree limit* (unpublished).
- Yun, G.Y., Kong, H.J., & Kim, J.T.(2012). The effect of seasons and prevailing environments on adaptive comfort temperatures in open plan offices. *Indoor and built environment*, 2(1), 41–27
- Zhao, Q., Qi, H. J., & Xie, T. (2015). Recent progress in shape memory polymer: New behavior, enabling materials, and mechanistic understanding. *Progress in Polymer Science*, 49–50, 79–120. <https://doi.org/10.1016/j.progpolymsci.2015.04.001>

Auxetic Structures and Advanced Daylight Control Systems

Yun Kyu Yi¹, Ryan Sharston², Dua Barakat³

- 1 School of Architecture, University of Illinois at Urbana-Champaign, Illinois, USA, email: ykyi@illinois.edu
- 2 Florida Institute for Built Environment Resilience, University of Florida, USA
- 3 School of Architecture, University of Illinois at Urbana-Champaign, Illinois, USA

Abstract

Building envelopes in general and, in particular, fenestrations are the places in which most interactions between indoor and outdoor environment take place. As a result, an effective shading structure for windows, which can provide sufficient illuminance levels and at the same time ensure acceptable visual comfort by controlling the glare is highly desirable.

Static daylight control systems are mostly designed to either completely shade the façade from sunlight or admit and re-direct it to the indoor spaces. Dynamic control systems adjust the amount of intake sunlight with assistance from users or mechanical devices. Studies to date have not thoroughly and comprehensively developed an alternative system in which a self-morphing structure that is responsive to outdoor environmental conditions can function as an "adaptive daylight control system".

This paper has investigated the effects of the adaptable auxetic shading structure with varying geometries to optimise illuminance levels and reduce probability of glare. The paper developed a model to be tested in various locations in the U.S., to evaluate the illuminance and glare performance. The results suggest that the auxetic shading structure can effectively block sunlight from entering the space by adjusting its geometry in response to varying outdoor and sky conditions. In addition, a strong correlation can be concluded among daylight availability, sun exposure, and glare probability. Additionally, the optimisation of daylighting parameters such as illuminance and glare show a clear correlation between the location of the case study and its corresponding sun angles, and the performance of the shading structure. Future studies may explore the effect of auxetic shading structures on energy consumption and thermal comfort parameters. In addition, the relation between auxetic shading devices and the health and well-being of building occupants may be another factor to be considered in the evaluation of effectiveness of this new generation of shading devices.

Keywords

adaptable shading system, auxetic structures, optimisation, illuminance, glare

DOI 10.7480/jfde.2019.1.2620

1 INTRODUCTION

The impact of building envelopes on indoor environmental quality (IEQ) and energy consumption in built environments is well documented. The building industry in the United States accounts for nearly 40% of total U.S. energy consumption (Ge et al., 2015). The concept of net-zero energy buildings, where the building makes no energy demands on the grid and is 'energy self-sufficient' has recently been gaining significant attention.

The interactions between built and natural environments mostly occur at the building envelope, which makes any improvements in its performance critical in terms of achieving energy self-sufficiency. The design and use of new energy efficient materials and technologies is also crucial to meeting net-zero energy goals. Due to their significant interactions with the ambient conditions, there has been tremendous interest in harnessing roofs, skylights, and fenestrations such as windows (Debije, 2010; Gutierrez & Lee, 2013; Gutierrez & Zohdi, 2014) in the push for energy self-sufficiency.

In addition to impacting energy use, building fenestrations also have undeniable impacts on daylight admission and consequently indoor environmental conditions. Among all contributions that building envelopes can have on IEQ, the control of incoming daylight is particularly important given the extensive effects that daylighting can have on occupants' health and well-being. To capitalise on these effects, designers and engineers have developed 'intelligent' building envelope systems in which the building envelope components, such as shading systems, are responsive to changing outdoor environmental conditions.

This research addresses the subject of adaptable daylight control systems and their contributions to illuminance levels and glare in indoor spaces. Through the use of an auxetic shading structure, this study explores the effects of varying geometries of shading structure on illuminance availability, as well as glare probability, in multiple locations representing different latitudes. The main research question is - for each location - what are the specifications of auxetic structure, particularly in terms of geometry and pattern, that produce maximum acceptable illuminance while reducing lighting energy requirements?

2 GEOMETRY OF AUXETIC STRUCTURES

Fig. 1 shows a process in which an auxetic structure can be formed. The definition of auxetic structure in this paper is a structure that can be expanded and contracted with a simple force, which can provide a great opportunity for daylight control. It is worth noting that the geometric patterns of auxetic structures can be seen around the world, e.g. in decorations and finishing in ancient Islamic architecture, which has intriguing patterns that interest many audiences (Fig. 2). For these reasons, this paper aims to develop a shading structure in which the geometric patterns and symbols are based on Islamic architecture.

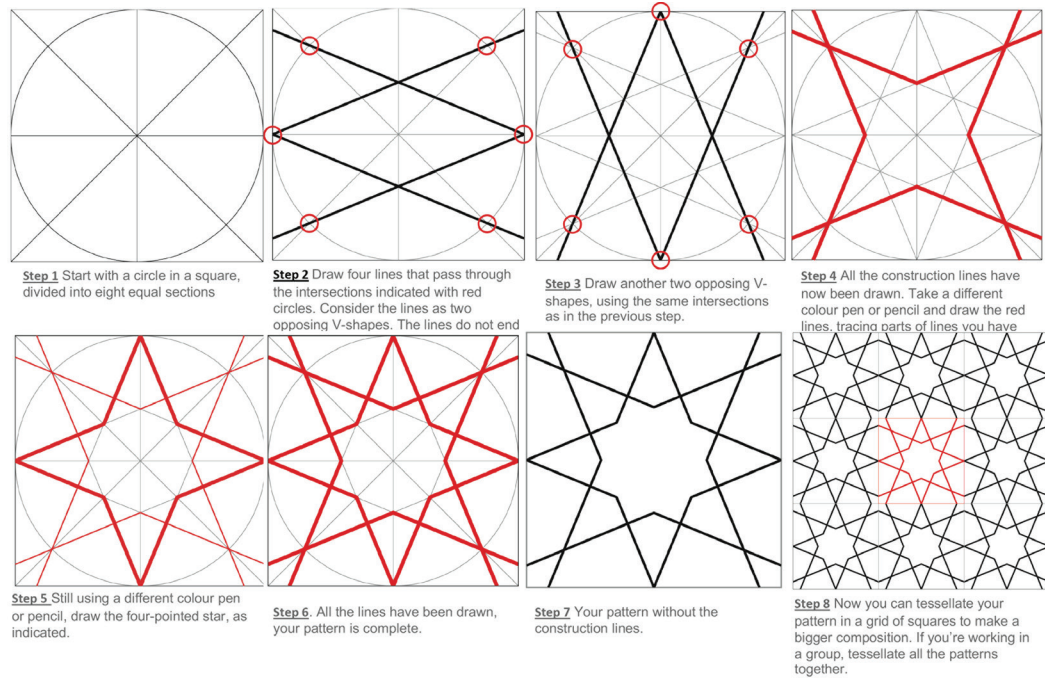


FIG. 1 Process of forming an auxetic structure (School of Islamic Geometric Design, 2018)

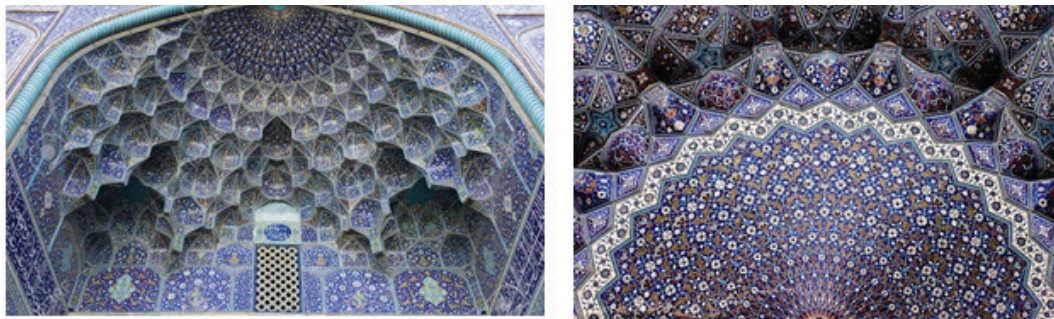


FIG. 2 Imam Mosque, Isfahan, Iran (Shah Mosque, 2018)

Fig. 3 (top) shows one of the typical auxetic patterns, which can be relatively easily drafted by following the steps described. As shown, the basic element of 'Step A' is hinged at the midpoint, and then when connected to another hinged element, creates the 'Step B' geometry, which in turn creates the 'Step C' geometry. 'Step C' connects two other basic elements to the geometry created in 'Step B'. At the end of 'Step D', two more basis elements are added to the geometry leading to the first semi-complete auxetic 'cell'. 'Step E' is a demonstration of how this newly-built geometry responds to the tensile forces to which it has been subjected. By continuing to add more elements to the geometry, one can create a complete set of elements as shown in the figure. As previously indicated, this 'system' can now expand and contract in response to applied tensile or compressive forces, which can be used as a 'shading device' for the purposes of daylight control. However, this pattern covers a relatively small area, which can reduce its effectiveness in terms of providing adequate shading. To address this problem, the geometry was advanced through changing the shape of basic element to a triangle and thereby increasing the coverage area provided by the element (Fig.3 (bottom)). Although the initial geometries of each have a similar construction process, with additional surface areas the new geometry can provide greater shading and, subsequently, greater daylight control.

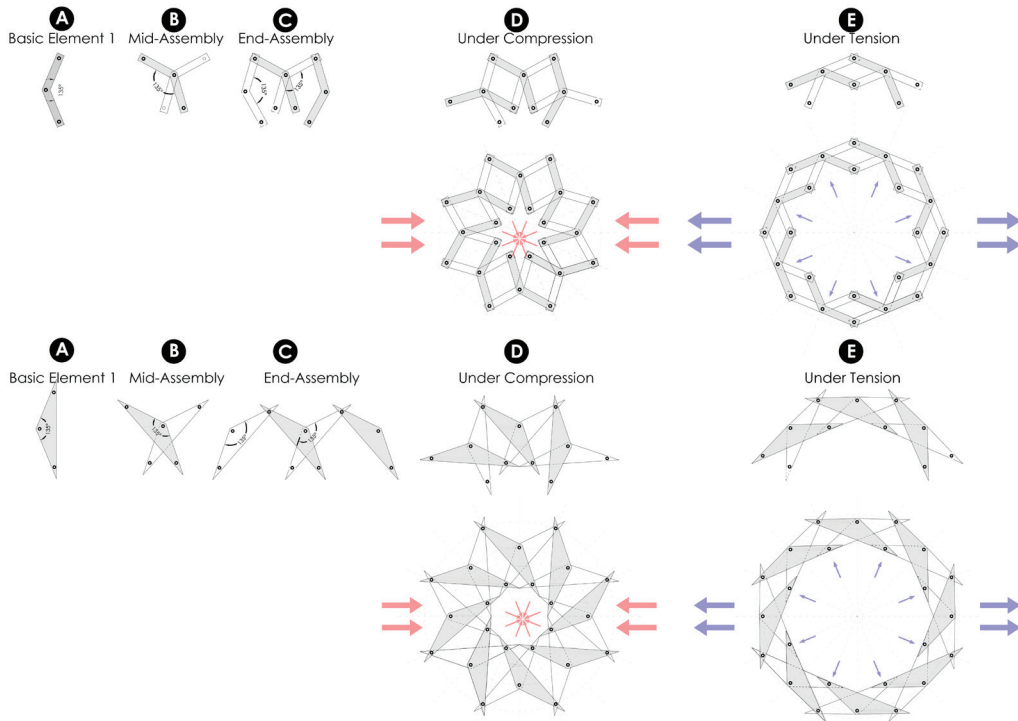


FIG. 3 Process of developing auxetic geometry

Additionally, the pattern can be created by using following equation to find the number of angles. The number of vertices is determined by the following equation:

$$\text{No. of vertices} = 360^\circ / (180^\circ - \text{Angle}) \quad (1)$$

$$= 360^\circ / (180^\circ - 135^\circ) = 8^\circ$$

Table 1 shows the efficiency comparison between both patterns. 'Area closed' represents the area of fenestration that has been covered by the shading structure. 'Area open' indicates what amount of window area is admitting daylight and not shaded. 'Window length' and 'Area % Decrease' demonstrate the overall dimension of the fenestration and the percentage of fenestration coverage, respectively. As shown, Pattern II (2nd geometry) provides 3% more efficiency than Pattern I (1st geometry), however, the second pattern leads to an even higher efficiency as four modules of it cover a large fenestration area and create a greater degree of shading. Therefore, Pattern II was selected as the final shading geometry.

	ANGLE (°)	NUMBER OF VERTICES	AREA CLOSED(M2)	AREA OPEN(M2)	WINDOW LENGTH (M)	AREA % DECREASED
Patten I	135	8	0.032	0.044	1.62	23.03
Patten II	135	8	0.045	0.065	2.05	30.00

TABLE 1 Efficiency comparison between auxetic geometry patterns

3 OPTIMISATION

The proposed auxetic structure in this paper is sufficiently flexible that it can deform when subjected to even small forces. This characteristic makes this geometry a suitable candidate as a shading system that can be either adjusted manually or integrated with a mechanical system that would change the geometry through motors. However, both methods have significant limitations, which can hinder their capability to improve daylight control. The manual control system can remain irresponsive to changing outdoor conditions as it would require constant attention by building users to adjust the shading blinds. The mechanically controlled system can also underperform as easily, due to potential malfunctioning of light sensors. Another option would be to utilise 'smart materials' that automatically respond to varying outdoor conditions. Yi (2018) showed a promising outcome for this method. However, these new materials are still in development stage and further research is needed before they can be implemented in building applications.

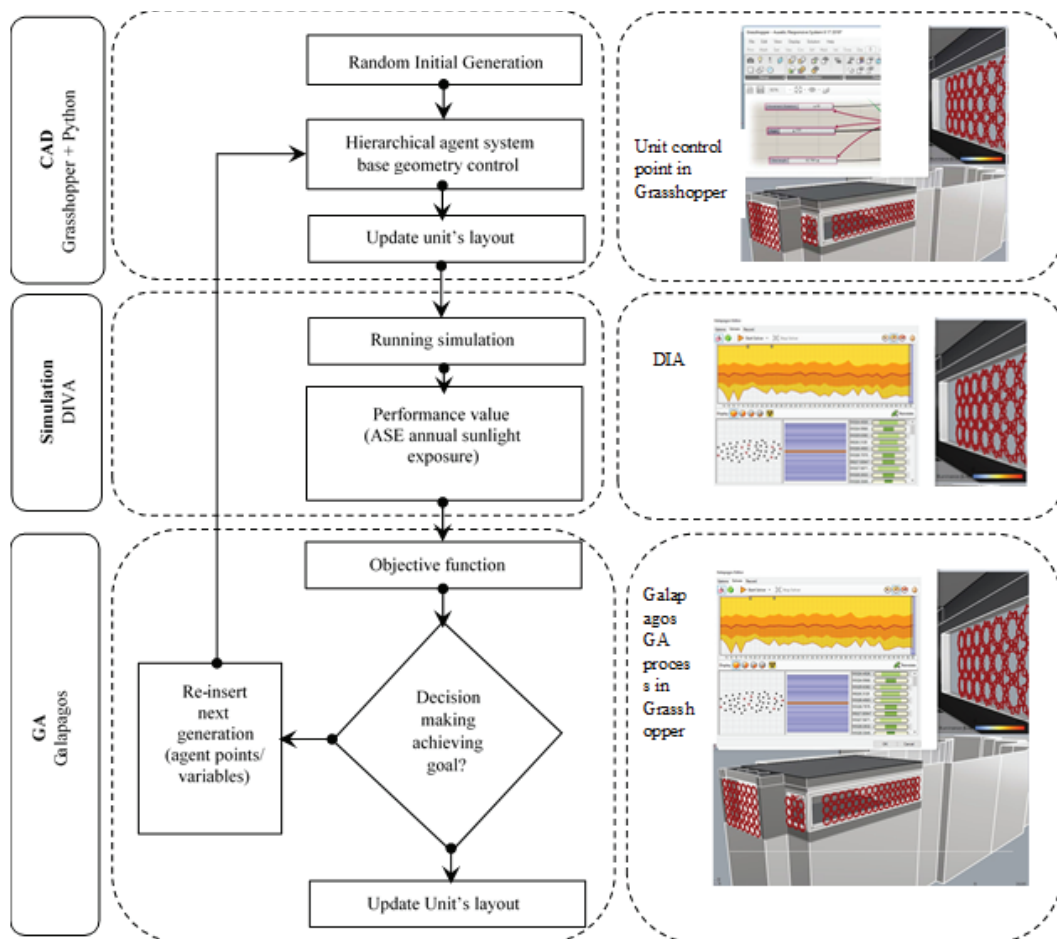


FIG. 4 Summary of research methodology

In this paper, authors chose a different approach to introduce a greater and more efficient responsiveness into the shading system. The chosen method is to find an optimum configuration of shading geometry for a given location, which has been customised for that location and is able to

reduce manual and/or mechanical interferences. To find optimal configuration, the paper follows a process to find optimal shapes for different locations as shown in Fig. 4.

Initially, random agent point values are generated and passed to a hierarchical agent point system in a CAD model, which updates the auxetic system configuration. Once the shape is changed by the agent point's values, a simulation tool calculates the annual daylight accessibility received by each measuring node. Next, these performance values (sDA, ASE, DGP) are passed to the evaluation process to check where the objective values satisfy the goal. If the performance value is not satisfied, the reproduction process starts. The reproduced 'offspring', containing new agent point values, are passed to a CAD model that updates the auxetic system and simulation program to generate the next generation's (iteration) performance values. These values are then used in the evaluation process and will continue until either the objective function value is satisfied, or the maximum generation has been reached.

For implementation, this paper uses Grasshopper, a plugin for a CAD tool called Rhinoceros (Robert McNeel & Associates, 2017) as CAD tool to control geometry. It should be noted that Grasshopper contains several plugins that allow users to utilise various functions without leaving the tool itself. This feature allows users to easily and seamlessly integrate different functions by eliminating the need to share information between different software tools, specifically, geometric information.

The performance measure for daylight is Spatial Daylight Autonomy (sDA). sDA measures how much of a space receives sufficient daylight. Specifically, it describes the percentage of floor area that receives at least 300 lux for at least 50% of the annual occupied hours, which indicates how much daylight an indoor space can receive overall, annually. To calculate the sDA of each measuring point, this paper uses a tool called DIVA (Solemma, 2017) which utilises a Radiance tool to predict several measures of daylight based on sky conditions acquired from location-specific meteorological data. In addition to sDA, this study also uses Annual Sun Exposure (ASE) and Daylight Glare Probability (DGP). The ASE represents a percentage of area which has had an illuminance level higher than 1000 lux for more than 250 hours a year, and the DGP indicates the percentage probability of glare occurrence. Wienold (2009) defines $DGP \leq 35\%$ as the 'class A', meaning that it is the best class and one in which 95% of office-time glare is weaker than 'imperceptible'. Therefore, in this study, a DGP value of 35% was chosen as the criterion for glare. For optimisation purposes, the paper uses another grasshopper tool called Galapagos. Galapagos is the built-in optimisation application for Grasshopper and is used widely by designers.

4 METHODOLOGY / SIMULATION SET-UP

The test case study was an office space on the 3rd floor of Temple Buell Hall (TBH) located on the campus of University of Illinois at Urbana-Champaign (UIUC). The room, which currently serves as an architectural design studio, is 12m x 10m with a height of 5m, and has openings towards the south, west, and east orientations. Fig. 5 shows the location of TBH on the UIUC campus, and the exterior and interior of the test study room.



Interior view
 FIG. 5 Site map and test case exterior and interior view

The auxetic shading structure was added to south, east, and west oriented façades using the Grasshopper plug-in. This model was controlled to expand or contract to find the appropriate form of the auxetic shading structure, based on annual sun exposure, daylight autonomy (DA300 lux), and glare probability given specific locations and times of the year. Three U.S. cities including Miami, Florida (latitude: 25.7617° N), Champaign, Illinois (latitude: 40.1164° N), and Sitka, Alaska (latitude: 57.0531° N) were chosen as the locations based on their various climate zones, which, in turn, have effects on sun altitude, and consequently illuminance levels and glare conditions. For glare analysis, three times of the day were selected: 8 a.m., 12 p.m., and 4 p.m. on December 21st. The reason to choose this particular date was due to the sun altitude being expectedly low at this time, and therefore the chance of glare occurrence (to be overcome by the shading structure) would be high. 8 a.m. and 4 p.m. were the times at which the sunrise and sunset would occur for the studied locations, except for Sitka, AK, where these times had to be adjusted for this location to 9 a.m. and 3 p.m., respectively, to accommodate low sun altitude.

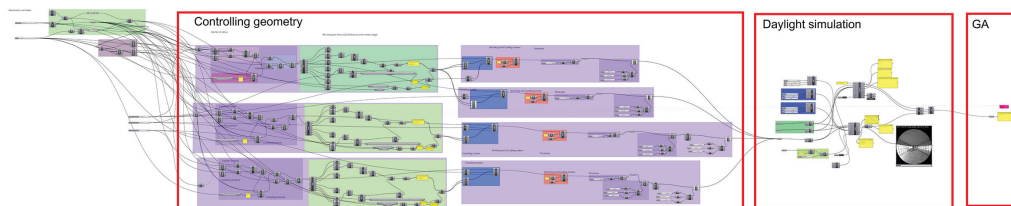


FIG. 6 Screenshot of Grasshopper file

Fig. 6 shows a screenshot of the Grasshopper file that conducted simulation. The optimisation process was carried out by Galapagos, which is one of the Grasshopper's commands, providing 'evolutionary computing' for the geometric variables of the shading structure. Galapagos is GA optimisation that is used for single objective optimisation. However, in order to optimise the shape and geometry of the auxetic shading structure, the following three performance standards were focused on to evaluate the extent to which, simultaneously: 1) annual sun exposure (ASE) would be minimised; 2) spatial daylight autonomy (sDA) would be maximised, and; 3) daylight glare probability (DGP) would be minimised. In order to test a case that contains three objectives to optimise, it requires that three objectives be combined into a single objective in order to utilise Galapagos.

The governing equation for the objective function can be written as:

$$\min_{x \in X} f(x) = \sum_{i=1}^n (r_{ASE})_n + (r_{sDA})_n + (r_{DGP})_n = -1 \quad (2)$$

where:

$$r_{ASE} = \frac{(r_{ASE})_n - 10}{100} = 0 \quad (3)$$

$$r_{sDA} = -\left(\frac{(r_{sDA})_n}{100}\right) = -1 \quad (4)$$

$$r_{DGP} = \frac{(r_{DGP})_n - 0.35}{0.35} = 0 \quad (5)$$

The objective is to maintain an ASE less than 10%, therefore, given equation 3, the minimum ASE must be 0. As for sDA, the greater the area percentage, the greater the sDA. Therefore, according to equation 4, the minimum sDA must be -1. As mentioned before, 'class A' DGP requires a value less than or equal to 35%. By using equation 5, the minimum DGP is determined to be 0.

Therefore, the overall minimum value to be assigned to Galapagos, as indicated in equation 2, is

$$(\text{minimum ASE} + \text{minimum sDA} + \text{minimum DGP}) = -1 \quad (6)$$

5 RESULTS

Fig. 7 shows the best-case scenario for each location with respect to optimised solution. In other words, the geometry of the auxetic shading structure shown in the images has produced the closest objective goal.

As shown in Fig. 7, the auxetic shading structures demonstrate different geometry patterns in response to different sky conditions in various locations. While in Champaign the shading structure opens up to the sunlight, in Miami, and particularly in Sitka, the degree of 'openness' is considerably lower. In fact, in Sitka, the shading structure almost completely blocks the sunlight from entering the space. This variety can be attributed to the simulation requirement to limit the sun exposure in Miami, where the sun altitude is high (40.6° at noon on 12/21/2018), and glare probability in Sitka, where the sun altitude is low (9° at a similar time). Table 2 shows the best-case scenario for optimised variables at each location.

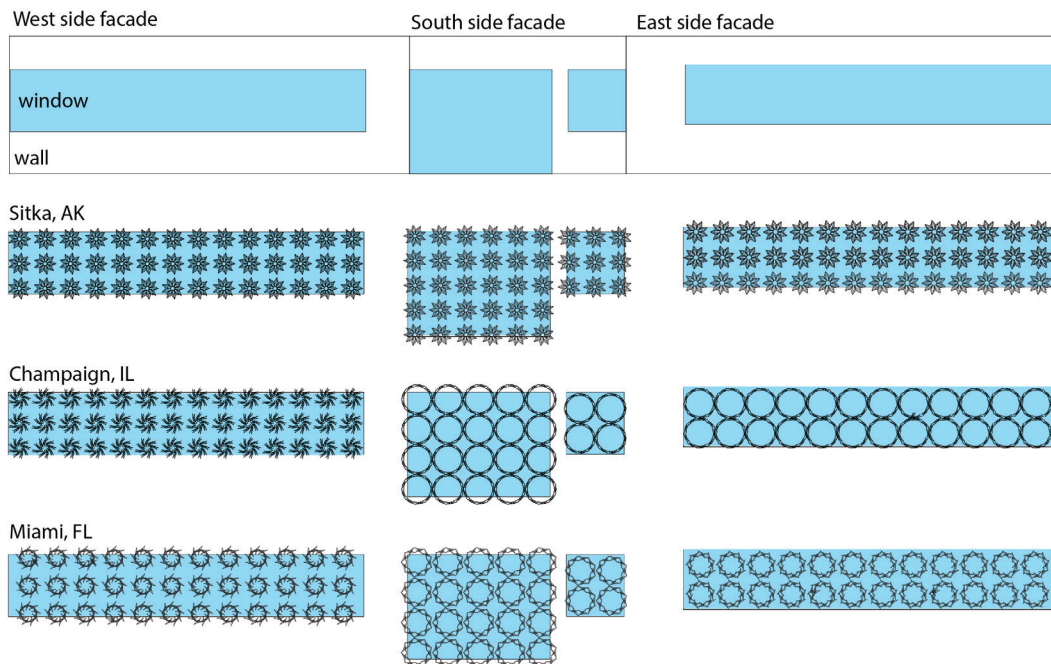


FIG. 7 Optimised shading structure in three different locations

As shown in Table 2, Sitka has the closest Galapagos value to the target value of -1, followed by Champaign, and then Miami. This phenomenon can be correlated with the lowest and highest sun altitudes in this study represented by Sitka and Miami, respectively. In Champaign, the shading structure in the south and east façades have a greater degree of 'openness', while the west façade is significantly more shaded. Higher temperature and lower sun angle in the afternoon are primary reasons for this outcome. In Miami, south and east façades call for greater shading, which is expected given Miami's considerably higher sun altitude (40.6° compared to 26.5° in Champaign). However, similar to Champaign, the west façade requires more shading in the afternoon. Sitka shows the greatest degree of shading in all three façades, compared to the other two locations. The main reason is the significantly lower sun altitudes that create glare. Therefore, the shading structure

ought to be further congested to provide adequate visual comfort for occupants. The next section will discuss the effects of auxetic shading structures on DGP in more detail.

LOCATION	MOVEMENT (VARIABLES VALUE)			OBJECTIVE VALUE
	South facade	East facade	West facade	
Miami, FL	60	78	110	-0.715
Champaign, IL	24	17	128	-0.825
Sitka, AK	128	123	128	-0.982

TABLE 2 Optimised Galapagos values in various locations

5.1 GLARE

Figs. 8-10 demonstrate the level of glare in each location for December 21st, 2018, at 8 a.m., 12 p.m. and 4 p.m. These are the approximate times for sunrise, noon, and sunset, respectively. However, due to the high latitude in Sitka, sunrise and sunset do not take place around 8 a.m. and 4 p.m. so, for the sake of consistency, the times were adjusted to 9 a.m. and 3 p.m., respectively. The images below are the outcome of DIVA/Radiance simulations in which the inside camera is facing the south façade.

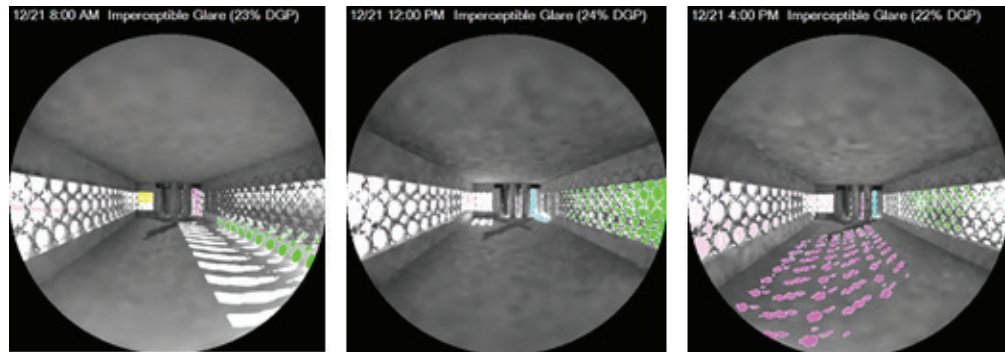


FIG. 8 Glare occurrence and DGP results in Miami at 8 a.m. (left), 12 p.m. (middle), and 4 p.m. (right)

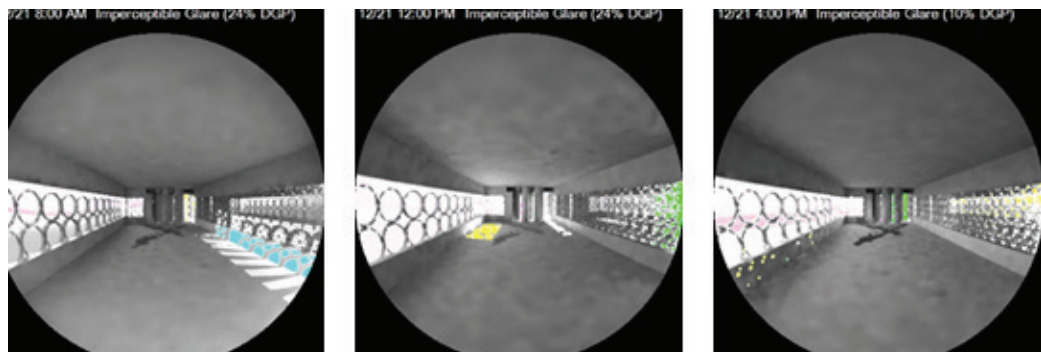


FIG. 9 Glare occurrence and DGP results in Champaign at 8 a.m. (left), 12 p.m. (middle), and 4 p.m. (right)

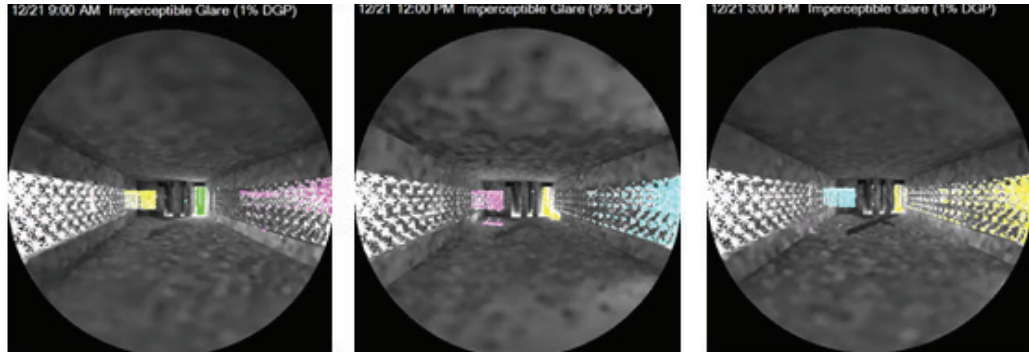


FIG. 10 Glare occurrence and DGP results in Sitka at 9 a.m. (left), 12 p.m. (middle), and 3 p.m (right)

In Miami, for all three times of day, the DGP is less than 35%. It is also interesting to observe that all three DGPs are fairly close, which suggests that the high sun altitude, and likely a more uniform sun exposure compared to other the two locations, can reduce the presence of glare in indoor environments.

In Champaign, the DGP values resulting from east and south sun exposures are similar, while it is much lower in the west façade suggesting that the lower sun altitude in the month of December causes significantly less glare in the afternoon in comparison with other times in the same location, and comparable times in locations with lower latitudes such as Miami.

Although one would expect to observe the largest degree of glare in Sitka due to its higher latitude, glare results show the lowest degree of probability among all case studies. It appears that in response to the simulation requirements, the auxetic shading structure has blocked the sunlight so effectively that a location with a comparatively high latitude demonstrates the lowest DGP. In addition, the minimal sun exposure in Sitka as shown in Table 3 can also be a major contributor to this phenomenon. Table 2 summarises the results for sDA, ASE, and DGP for each location.

As shown in this table, Miami and Champaign have fairly similar sDAs, ASEs, and DGPs, however, the value of these parameters are significantly lower in Sitka. It can be concluded that there is a strong correlation between daylight availability, sun exposure, and glare occurrence.

LOCATION	SDA (%)	ASE (%)	DGP (%)		
			8:00 am	12:00 pm	4:00 pm
Miami, FL	73.3	46.5	23	24	22
Champaign, IL	79.4	51.4	24	24	10
Sitka, AK	0.2	1.4	1 (9 am)	9	1 (3 pm)

TABLE 3 sDA, ASE, and DGP values in various locations

CONCLUSIONS

This study has investigated the effects of an auxetic shading structure with varying geometries on illuminance levels and glare probability. The simulation research methodology using Grasshopper, DIVA, and Rhino (interface) carried out the assessment for three U.S. cities including Miami,

Champaign, and Sitka. The case study office space was an architectural design studio located on the third floor of TBH on the UIUC campus. The optimisation of the following parameters was conducted to evaluate the performance of the shading structure: sDA, ASE, and DGP, where the optimisation objective for the Galapagos parameter was to simultaneously maximise sDA and minimise ASE and DGP.

The results suggest that the auxetic shading structure can effectively block the sunlight from entering the room by adjusting its geometry in response to varying outdoor and sky conditions. Furthermore, a strong correlation can also be drawn between sDA, ASE, and DGP in each location. In other words, the greater the illuminance level and sun exposure, the higher the probability of glare occurrence. In addition, the optimised Galapagos value shows a clear correlation between the location of case study and the optimisation performance of auxetic structures meaning the higher the latitude, the better the optimisation.

The main purpose of this paper is utilising an auxetic structure to easily customise shading for a specific location. To maximise the daylight control system, each location requires a specific configuration to design such a daylight control system. However, the proposed system can change its shape to satisfy the performance goal without specifically configuring its daylight control system.

This paper is the initial investigation of utilising an auxetic structure at building scale. The auxetic structure proposed in this paper can be operated with a simple force to expand and contract. It can be further coupled with Shape-Memory Alloys (SMA) to develop an alternative system whereby a system responds to constantly changing outdoor environmental conditions. It is a self-morphing structure that can function as a 'Self-response daylight control system'

In addition, one may want to investigate the effect of varying auxetic shading structures on energy use (lighting, heating, and cooling), and thermal comfort performance of the case studies. In addition, the relationship between adaptable shading structures, of which the auxetic structure is one, and the health and well-being of building occupants is another opportunity to thoroughly evaluate the effects of this new generation of shading devices.

Acknowledgements

This work was supported by Design Research Initiative fund from the College of Fine and Applied Art at the University of Illinois.

References

- Debije, M. G., (2010). Solar Energy Collectors with Tunable Transmission, *Advanced Functional Materials*, Vol. 20,1498
- Ge, D., Lee, E., Yang, L., Cho, Y., Li, M., Gianola, D., & Yang, S. (2015). A Robust Smart Window: Reversibly Switching from High Transparency to Angle-Independent Structural Color Display. *Advanced Materials*, Vol. 27, 2489–2495
- Gutierrez, M. P., & Lee, L. P., (2013). Engineering. Multiscale design and integration of sustainable building functions. *Science*, Vol. 341, 247
- Gutierrez, M. P., & Zohdi, T. I. (2014). Effective reflectivity and heat generation in sucrose and PMMA mixtures. *Energy and Buildings*, Vol. 71, 95
- Robert McNeel & Associates (2017). Rhinoceros 5 [software program]. Seattle, WA, USA: Robert McNeel & Associates.
- School of Islamic Geometric Design. (2018). Islamic pattern. Retrieved from http://www.sigd.org/resources/pattern/pattern-1/Shah_Mosque.
- (n.d.) In *Wikipedia*. Retrieved September 27, 2018 from https://en.wikipedia.org/wiki/Shah_Mosque
- Solemnia, LLC. (2017). DIVA-FOR-RHINO 4 [software program]. Cambridge, MA, USA: Solemnia, LLC.
- Wienold, J. (2009, July). Dynamic Daylight Glare Evaluation, *Eleventh International IBPSA Conference*. Glasgow, Scotland July 27-30
- Yi, Y K. (2018). Developing an advanced daylight model for building energy tool to simulate dynamic shading device. *Solar Energy*, Vol. 163, 140-149

Impacts on the Embodied Energy of Rammed Earth Façades During Production and Construction Stages

Lisa Nanz¹, Martin Rauch², Thomas Honermann², Thomas Auer¹

1 Chair of Building Technology and Climate Responsive Design, Technical University of Munich, Munich, Germany, lehrstuhl.klima@ar.tum.de

2 Lehm Ton Erde Baukunst, Schlins, Austria

Abstract

Rammed earth is a technique for constructing sustainable buildings, with a low energy demand encompassing the whole life cycle of buildings. Soil from the excavation can be compressed on-site to build a façade. Due to its hygroscopic and thermal properties, rammed earth façades stabilise indoor comfort, which potentially supports the minimisation of use of mechanical systems. In order to reduce the energy demand for the entire life cycle of buildings, the embodied energy must be taken into account. Databases, such as the German Ökobaudat, provide data for a life cycle assessment (LCA). For rammed earth, aggregated data at product stages A1-A3 are provided, but transport, which is included in stages A2 and A4, and construction processes at stage A5 are barely documented. Thus, the energy demand for transport, production, and construction of two rammed earth façades was measured. The results are documented in this paper, which provides a more thorough understanding of the entire building process and helps to expand the database. One can conclude that transportation has the largest impact on the embodied energy of rammed earth façades, so it's essential to use local material. Furthermore, the results illustrate the implication of transport on a life cycle assessment, as well as for other constructions.

Keywords

embodied energy, Life Cycle Assessment, stages A1-A5, transport, rammed earth façade

DOI 10.7480/jfde.2019.1.2786

1 INTRODUCTION

Since 1977 (WSchVO, 1977), German policies have supported the decrease of the energy demand of buildings in order to reach national and international climate targets. National regulations, like EnEV, are still enforcing the reduction of the operational energy of buildings. However, the embodied energy of buildings has barely been considered. In order to minimise the energy demand over the entire life cycle of a building, current research (Auer, Santucci, Knaack, & Hildebrand, 2015; Meex, Knapen, Hildebrand & Verbeeck, 2018; Markus, Jensch & Lang, 2014) and practice, such as DGNB certifications since 2009, are now also focusing on the embodied energy.

In this regard, rammed earth façades provide a sustainable approach because of their thermal and hygroscopic properties, their low embodied energy, and their high recycling potential. The material has a high thermal mass due to its fairly high heat capacity ($c_p \approx 850 \text{ J/kgK}$), high thermal conductivity ($\lambda \approx 1.1 \text{ W/mK}$), and high density ($\rho \approx 2300 \text{ kg/m}^3$). Thermal mass stabilises the indoor climate by buffering fluctuating heat loads related to the outdoor temperature, solar gains, and internal loads. A passive building design activates thermal mass by natural night-time ventilation during hot summer periods. In addition, rammed earth also buffers moisture peaks due to its hygroscopic properties. The adsorption of moisture is four times higher than that of mineral building materials, e.g. gypsum plaster (Klinge et al., 2016). The adsorption and desorption of moisture is self-regulating. Thus, rammed earth façades promote a healthy and comfortable indoor climate. Respiratory diseases caused by a dry climate or mould formation caused by a humid climate can be reduced. Furthermore, Osanyitola & Simonson (2006) showed that 2% of the total heating energy and 11% of the total cooling energy in the continental climate region of Germany can be reduced by combining hygroscopic materials with a well-controlled HVAC system. Another phenomenon results from the heat of adsorption, which is released by the adsorption of moisture and heats up the material (and vice versa). This hygrothermal potential is reversible and decreases the surface temperature during desorption.

As seen, the properties of building materials can significantly reduce energy demand for building operations. Furthermore, literature data based on the German database ÖkobaDat show that the energy demand of the raw material supply, the transport to the production site, and the manufacturing of rammed earth is about 70% lower than that of conventional façades, e.g. brick façades. As the production and construction process of rammed earth differs to conventional façades and has not yet been fully explored, this study analyses the impacts on the embodied energy of rammed earth façades in production and construction including transportation.

2 THEORETICAL BACKGROUND: THE EMBODIED ENERGY OF RAMMED EARTH FAÇADES

2.1 ACTUAL STATE OF SCIENCE

The German database ÖkobaDat is based on DIN EN 15804. This standard describes the life cycle of buildings from the production and construction stage to the end of life by dividing it into different stages:

- A1-A3 product stages
- A4-A5 construction process stages
- B1-B7 use stages
- C1-C4 end-of-life stages
- D reuse, recovery, recycling potential

The database provides data to calculate the embodied energy for thousands of building materials, though many data sets are not complete. Stages A1-A3 are usually provided as aggregated data, including the raw material supply (A1), the transport to the production site (A2), and the production (A3). Aggregated data sets cannot be divided into stages due to a lack of information. In general, stages A4 and A5 are insufficiently documented. Values for stage B are given by standard calculation of energy certificates or thermal simulation. However, data for the end of life and the recycling potential of building materials is incomplete. For rammed earth, aggregated data for stages A1-A3 only is available (see Fig. 1).

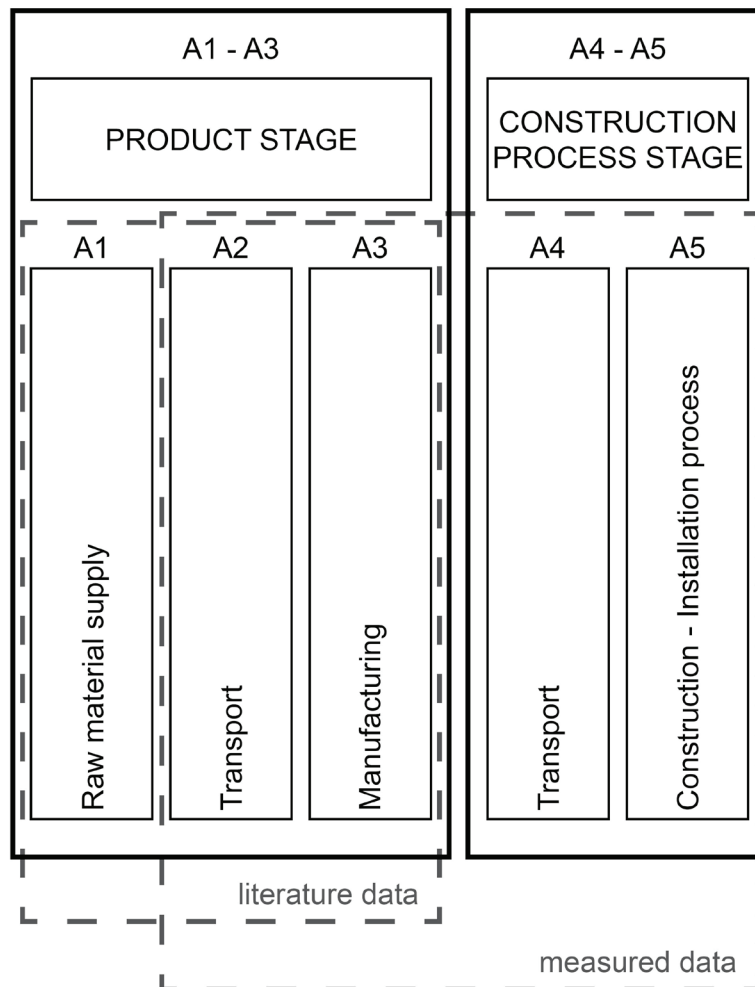


FIG. 1 For rammed earth, aggregated literature data at stage A1-A3 is available. Stages A2-A5 are measured in this paper. Figure based on DIN EN 15804

2.2 METHODOLOGY, FUNCTIONAL UNIT, SYSTEM BOUNDARIES

This paper focuses on the primary energy demand at stages A1-A5 of rammed earth façades (see Fig. 1). Two case studies (Variant A and B, see Chapter 2.3) are selected because of their different production (on-site vs. off-site) and construction processes (monolithic and double-shelled), as well as the origin of the excavated earth (local vs. non-local). At first, the embodied energy for stages A1-A3 is calculated based on literature data representing the status quo. In order to reference these results to conventional façades, stages A1-A3 are also calculated for theoretical brick façades (Reference A and B, Chapter 2.3) with similar thermal performance. Subsequently, the primary energy demands of stages A2-A5 are measured for Variant A and Variant B. Stage A1 could not be measured because of a lack of data due to external material supply. However, the primary energy demand for stage A1 was found in previous literature research. Finally, the results for stages A1-A5 are referenced against their References A and B.

The data for the conventional brick façades is provided by an Austrian brick association Initiative Ziegel (2015) and is based on ÖNORM EN 771-1 (2005) and ÖNORM EN 15037-3 (2001). Data that was found to be missing in Ökobaudat (2017) are completed with comparable data sets of other building materials and data to complete missing transport distances are based on Kellenberger & Althau (2008) and Binz, Erb & Lehmann (2000). The primary energy demand listed in (Initiative Ziegel, 2015) is about 40% lower than other literature data, e.g. (AG Mauerziegel, 2015). Thus, the comparison between the references and variants represent a worst-case scenario for rammed earth façades.

The total primary energy demand (PE) is measured and calculated, including renewable (PERT) and non-renewable (PENRT) primary energy ($PE = PERT + PENRT$). Primary energy factors f_{PE} are given in Table 1. In order to facilitate the comparison of the results with different façade systems, the functional unit is 1m^2 of an opaque façade component. The density and mass are taken into account. No other properties, e.g. heat capacity, U-Value, or hygroscopic performance are taken into account. Specific construction processes related to outdoor climate conditions, e.g. protection against freezing, are excluded. The PE for transportation ($PE_{transport}$) is calculated as a product of the mass, m , in kg, which is transported over a distance of x in km multiplied by the energy factor of the vehicle. A truck with an average load of 24 tons (Ökobaudat 2017, data set 9.3.01) is assumed.

$$PE_{transport} = x \cdot m \cdot f_{vehicle} \quad (1)$$

ENERGY CARRIER	F_{PE} [-]	REFERENCE
German electricity mix	2.80	(DIN18599-1, 2016)
Diesel	1.22	(Frischknecht, Et. Al, 2012)
Transport vehicle	f_{PE} [MJ/1000kgkm]	
Truck (average load 24 t)	0.74	(Ökobaudat 2017, data set 9.3.01)

TABLE 1 Primary Energy Factors

2.3 DESCRIPTION OF VARIANT AND B AND THEIR REFERENCES

Variant A (see Fig. 2) is the world's largest contemporary rammed earth façade, with a total area of 2790 m², a thickness of 45 cm, and consists of 667 pre-fabricated rammed earth units. It is the façade of a Swiss industrial production and storage unit for a herbal confectionery company. To store herbs, the indoor temperatures can vary between 5 °C and 28 °C, while relative humidity has to be kept at 50%. Due to the temperature range of 23 K, a U-Value of 1.7 W/m²K is acceptable to comply with Swiss code requirements for energy conservation. The rammed earth façade guarantees a fairly constant indoor climate with 50% relative humidity (Herzog de Meuron, 2015). The hygroscopic, self-regulation effect of rammed earth supports the design of a smaller HVAC system and still provides the required conditions. The production of rammed earth façade elements is located close to the building site (3 km).

In order to compare the results of Variant A with a conventional façade of similar thermal performance, a brick façade with a thickness of two bricks is considered (see Fig. 2, Reference A). As bricks are fabricated in standard widths of 24 cm, the thickness of the wall is 48 cm. Due to this and the material characteristics of the bricks, the wall has a U-Value of 1.5 W/m²K, which is comparable with Variant A. The bricks have a density of 2000 kg/m³ and a specific heat capacity of 1.00 kJ/kgK (see Table 2).

Variant B (see Fig. 2) is the largest rammed earth façade in an office building, with a total area of 1417 m² and a thickness of 68 cm. It consists of 384 pre-fabricated rammed earth units. The self-supporting façade is three floors high and is fixed to the floor plate every 4 m in order to avoid folding. The plasticity of rammed earth enables a monolithic and jointless façade. In order to improve thermal performance, the U-Value has to be at 0.35 W/m²K. This has been achieved using a double-shelled construction with foam glass granulates in the centre. The inner shell contains a capillary conditioning system, which activates the thermal mass of the façade. The capillary conditioning system is neglected in this study. The massive walls ensure a relatively constant indoor climate due to the thermal mass. The production of the pre-fabricated rammed earth façade units is done on-site.

As it follows, Reference B (see Fig. 2) is a theoretical conventional façade with a similar U-Value of 0.34 W/m²K. It is a brick wall of 24 cm with an expanded polystyrene (EPS) insulation of 10 cm. Consequently, the thermal mass is less than that of Variant B. The impact on the embodied energy due to different thermal mass will be discussed in Chapter 3.

	VARIANT A	REFERENCE A	VARIANT B	REFERENCE B
Density ρ [kg/m ³]	2350	2000	2150	2000
Specific heat capacity c_p [kJ/kgK]	0.85	1.00	0.85	1.00
Mass per m ² façade [t/m ²]	1.06	1.04	1.28	0.57
U-Value [W/m ² K]	1.70	1.50	0.35	0.34

References A and B are calculated based on literature for density (Ökobaudat, 2017) and heat capacity (ÖNORM B 8119-7, 2013)

TABLE 2 Physical properties of Variant A and B and References A and B. Data for rammed earth is based on measurements (ZAE Bayern, 2011)

2.4 DESCRIPTION OF PROCESSES IN STAGES A1-A5

The production and construction of rammed earth façades are different to a conventional brick façade. To point out the differences, the two process chains are described in the following:

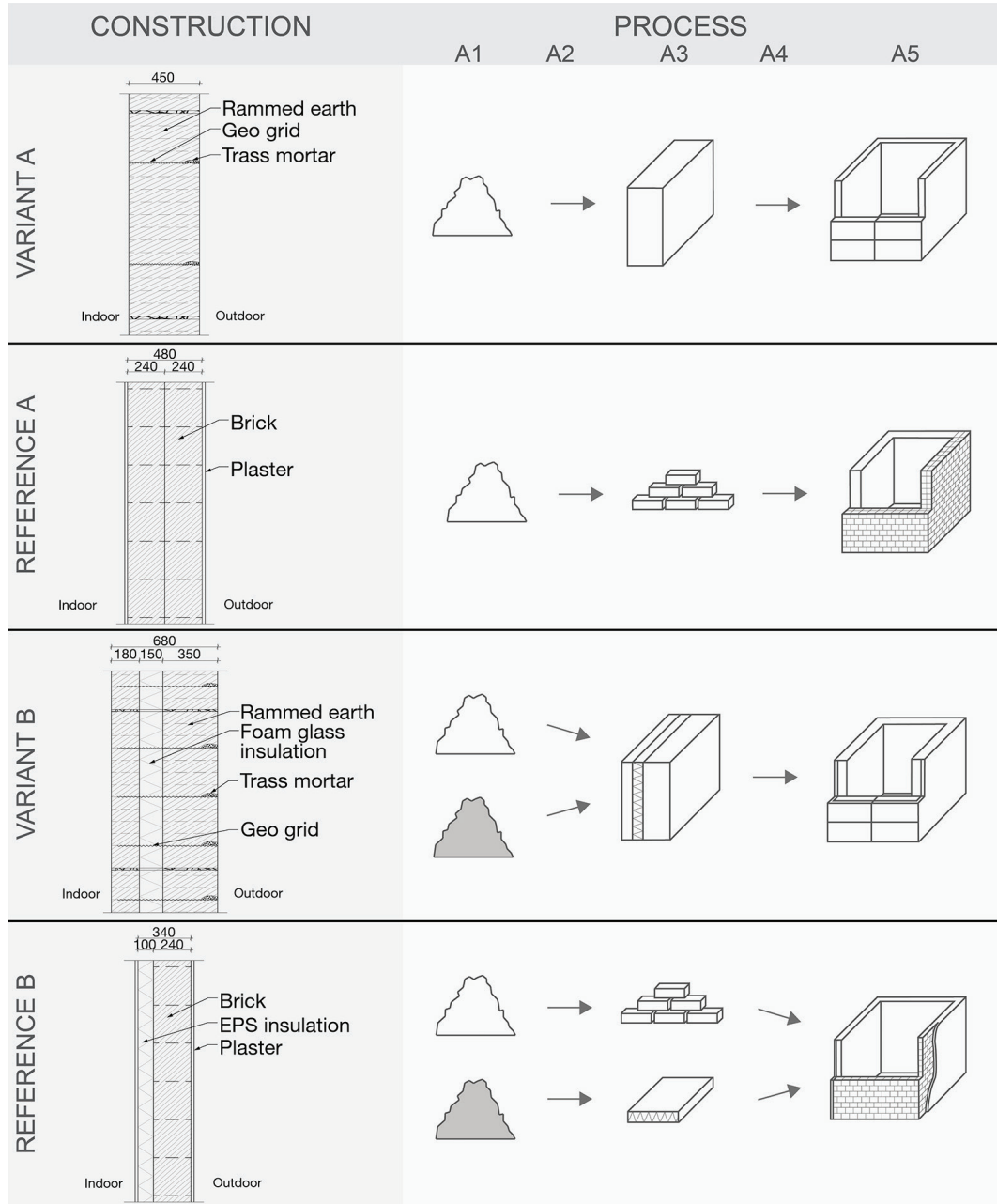


FIG. 2 Construction of Variant A, Variant B, and their references A and B, and their production and construction processes

The first step to build a brick façade is to excavate the raw materials (A1) to produce a brick. Bricks are based on similar raw materials as rammed earth: clay, sand, lime etc., which have to be extracted from a mine. In contrast to rammed earth, the other materials must be screened and packed at

the mine and transported to a factory, where they are baked (A2) at around 1000 °C. After the production of the brick (A3), it is transported to the construction zone (A4) to build the façade (A5). In stage A5 all building materials (bricks, mortar, insulation, and plaster) are brought together to build the entire façade.

The process of rammed earth façades is less complex; excavated soil, e.g. from the building pit, can be used to produce a rammed earth façade. The excavated soil consists of raw materials such as clay and gravel. Even earth mixtures that cannot be used for the fabrication of bricks (based on processed clay) or concrete (based on processed gravel) are usable. Depending on the quality of soil, some additional materials have to be supplemented. Thus, the composition of each rammed earth façade is individual. Geo grids stabilise the entire façade and trass mortar lines are set every 40-50 cm to protect the façade from erosion. In the pre-fabrication process, single façade units with weights of up to 5 tons and lengths of 3.5 m are produced in three steps:

- mixing process
- ramming process
- drying process

As the production site can be installed flexibly, the transport distance to the building site (A4) can even be reduced to zero if it is on-site. At stage (A5) the façade units are piled up into an entire façade.

2.5 MEASUREMENT CONCEPT

Fig. 3 and Table 3 describe the measurement concept of Variant B. For stage A2, the total transport distance is measured based on delivery notes. Stage A3 considers the whole production process, including mixing, ramming, and drying. Due to installation issues, the mixing plant and the compressor are measured by electric meter 1, and the material turner, the material feeder with ramming robot, and cutting unit are measured by electric meter 2. The diesel consumption of the telescope loader and the fork lift is measured and scaled by the number of operating hours. To calculate the total distance of stage A4, the distance between the production and building site is multiplied by the amount of trips that a truck has to make to transport all façade units to the construction site. The embodied energy for the construction is measured by the diesel consumption of the mobile crane and scissor lift.

The measurement concept of Variant A is less complex: Transport stages A2 and A4 are measured like stage A4 of Variant B. The mixing, ramming and drying process of stage A3 are not measured separately. Stage A5 follows the methodology of Variant B.

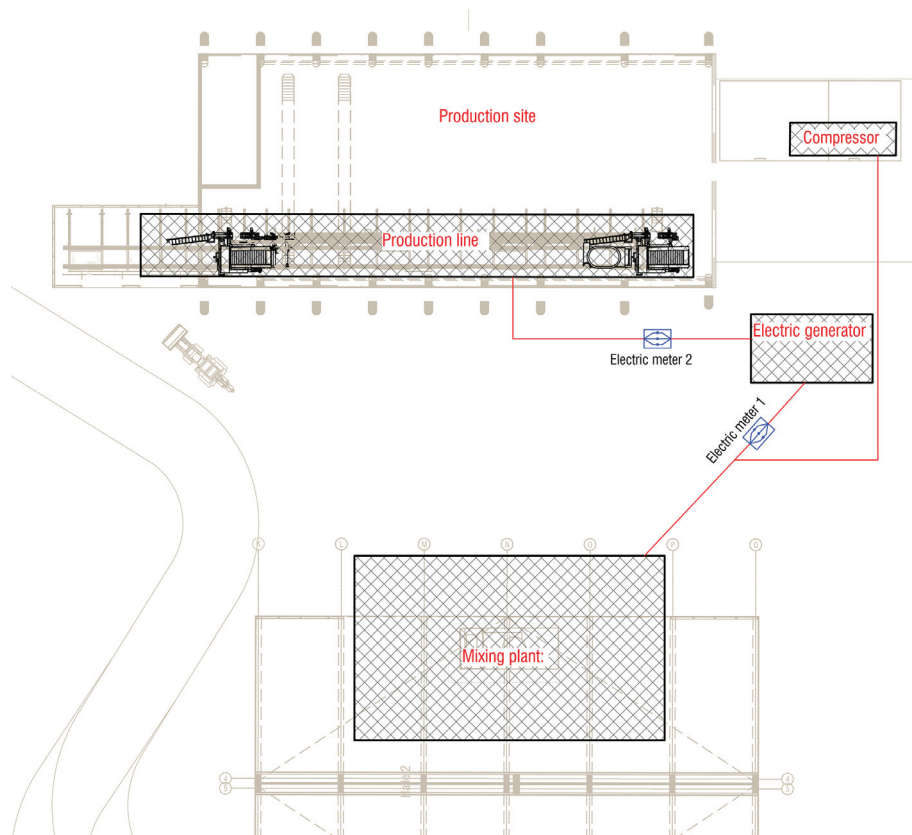


FIG. 3 Installation of electric meter at the production site of Variant B

	STAGE	DATA RECORDING
A2	Transport to production site	
	Material transports	Delivery notes
A3	Mixing process	
	Mixing plant	Electric meter 1
	Material turner	Electric meter 2
A3	Ramming process	
	Material feeder with ramming robot and cutting unit	Electric meter 2
	Compressor	Electric meter 1
A3	Drying process	
	Fork lift	Diesel consumption and operating hour meter
	Heating in winter	Excluded
A4	Transport to building site	
	Distance of journey	Geodata
	Amount of truck trips	Counting
A5	Construction	
	Mobile crane	Diesel consumption and operating hour meter
	Scissor lift	Diesel consumption and operating hour meter

TABLE 3 Measurement concept, documentation of data recording for stage A2-A5 for Variant B

3 RESULTS

3.1 LITERATURE STUDY AT STAGES A1-A3 FOR RAMMED EARTH AND BRICK FAÇADES

The embodied energy for Variant A and B and their References at stages A1-A3 is calculated based on literature (Ökobaudat, 2017). The results are shown in Fig 4. Variant A (150 MJ/m^2) requires 70 % less PE than Reference A (498 MJ/m^2). The main reason for the lower primary energy demand is that rammed earth façades are not baked. Bricks are baked at temperatures of around $1000 \text{ }^\circ\text{C}$, which requires a huge amount of energy. Variant B (395 MJ/m^2) requires only 21% less than Reference B (500 MJ/m^2) because of the massive construction of Variant B (1.28 t/m^2) compared to Reference B (0.57 t/m^2).

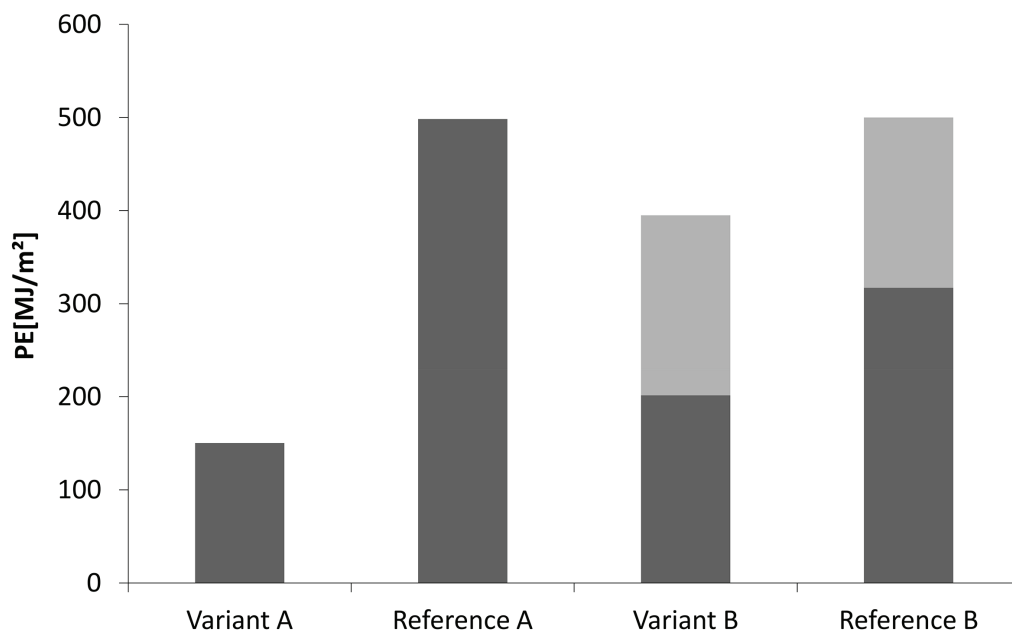


FIG. 4 Results of literature study on the primary energy demand at stage A1-A3 based on (Ökobaudat, 2017). The light coloured part represents the impact of the insulation

Another reason for the higher PE of Variant B compared to A is the extra energy demand for the production of the foam glass insulation. The results show that the impact of the insulation material is significant. Almost half of the total embodied energy of Variant B is due to the insulation material.

3.2 LITERATURE STUDY ON PRIMARY ENERGY AT STAGE A1

Due to external material supply the energy demand at stage A1 could not be measured. Hence, a literature study on the raw material supply is done to quantify stage A1. The entire primary energy demand, which is needed to excavate soil or to prefabricate additional materials, e.g. geo grids or foam glass, is taken into account. The total primary energy demand of Variant A is 167 MJ/m^2 and for Variant B is 435 MJ/m^2 . In Table 4, the impact of each material on the PE at

stage A1 is documented. As seen, pre-fabricated materials, e.g. for clay powder or foam glass, have a crucial impact on the PE even with small mass fractions. In comparison to section 3.1, it becomes apparent that the aggregated data set assumes an energy efficient production and construction process and potentially excludes pre-fabricated materials.

Building material	VARIANT A		VARIANT B		Data
	Mass fraction [%]	PE [%]	Mass fraction [%]	PE [%]	
Excavated earth	30.30	0.00	58.51	0.00	N/A, assumption recycling material
Excavated raw clay	22.97	5.93	8.70	1.04	Excavation (Ökobaumat, 2017), preparation (supplier information)
Clay powder	0.98	41.17	2.59	11.25	(Ökobaumat, 2017) 1.1.04 clay powder
Gravel/marl	43.50	27.89	14.55	2.09	(Ökobaumat, 2017), 1.2.01 gravel 2/32
Sand	1.69	0.20	2.76	0.40	(Ökobaumat, 2017), 1.2.01 sand 0/2
Trass mortar	0.54	16.36	0.45	1.90	EPD-RHT-20111111-D
Geo grid	0.01	8.45	0.10	30.72	(Ökobaumat, 2017), 6.6.07 Fortrac® T
Crashed lava stone	-	-	9.55	8.09	(Ökobaumat, 2017), 1.2.02 crashed stone 2/15
Foam glass	-	-	2.80	44.51	EPD-MIS-20150019-IAA1-DE
Total PE [MJ/m²]		166.69		434.62	

TABLE 4 Results of literature study on primary energy demand at stage A1 for Variant A and B

3.3 MEASUREMENT OF THE PRIMARY ENERGY AT STAGES A2-A5

Fig. 5 shows the results of the measurements for stages A2 to A5. As seen, transport has the highest impact on the embodied energy, especially for Variant B at stage A2. The reason for this is that 1061 tons of excavated soil are transported over a total distance of 9143 km, which involves about 5200 MJ/m². The excavated soil is taken from a tunnel construction (223 km away) as recycling material instead of being transported to a landfill. In a holistic view, it has to be taken into account that the transport to a landfill also demands energy, which is considered in the form of a credit. In this case, the credit is about 25% due to the distance to the landfill of about 60 km (supplier information). In this regard, the primary energy demand of stage A2 is about 3833 MJ/m². For Variant A, more than 98% of the materials are transported for distances of less than 10 km to the production site (see Table 6). Only some additional components (<1% of mass fraction) such as trass mortar and geo grids are transported over longer distances (>100 km). Thus, the primary energy demand of stage A2 is lower than that of Variant B (209 MJ/m²).

The transport from the production to the building site (stage A4) for Variant A requires almost 291 MJ/m². The reason for this is that 667 façade units with a total mass of more than 2956 tons are transported for a distance of only 3 km. In this context, the mass and not the distance is the crucial point. The primary energy demand of Variant B is zero due to its production on-site.

Considering both transport stages, A2 and A4, the impact of transport is more than 55% of the total embodied energy (A1-A5) for Variant A and more than 84% for Variant B. In Table 5, the total distance of all materials and all journeys is specified on a 1 m² façade surface in order to compare the measurement results. The values consider the total mass of each façade (Variant A: 2956 tons, Variant B: 1813 tons) due to the number of journeys taken by a truck with an average load of 24 tons. Depending on its production process, the PE required by the transport can be shifted from stage A4 to A2 (see Fig. 5). Thus, an aggregation of stages A1-A3, can hide transport energy by obtaining further information about transport distances at stage A2. The aggregation can limit the clarity of data.

For stage A3, the primary energy for Variant A is 151 MJ/m² and for Variant B 174 MJ/m². The values are about the same as calculated literature values for stage A1-A3 (see section 3.1). Thus, literature data assumes less primary energy demand as is measured in reality. This leads to the conclusion that the aggregated data set of ÖBD is based on a building, where the excavated soil for the building foundation is rammed directly on-site without processing the soil and using additional material. Thus, the energy demand at stages A1 and A2 can be neglected. This assumption is valid for a smaller family house, such as 'Wohnhaus Rauch' (Mattli, Klauz, Plüss, & Menti, 2010).

The foam glass granulates of Variant B are rammed during the production process of the façade units. Thus, there is no further energy demand for installing the insulation (A5). The PE at stage A5 of Variant A (84 MJ/m²) is slightly lower than that for Variant B (95 MJ/m²) because of the lighter façade units. About 80% of the PE is consumed by the use of a crane to pile up the units and about 20% is due to the transport of the façade units to the crane.

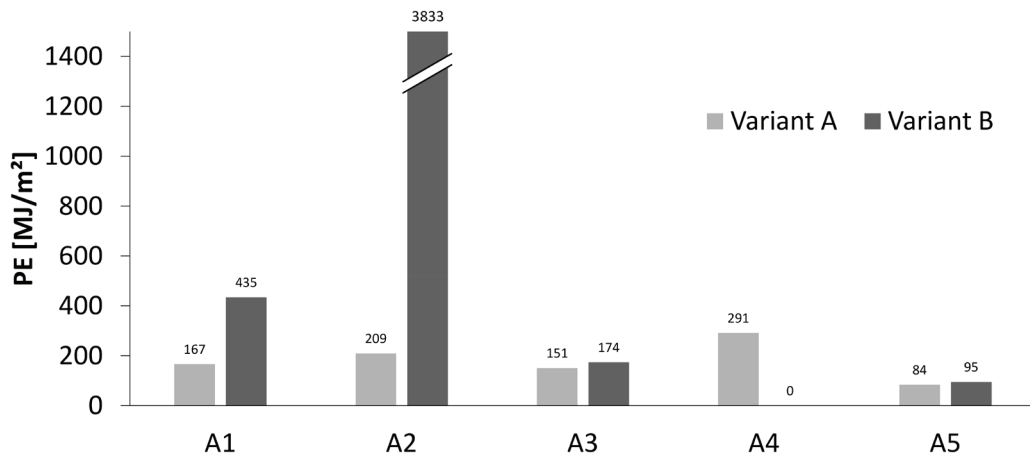


FIG. 5 Results for primary energy demand at stage A1-A5. Stage A1 is based on assumptions and literature data, stages A2-A5 are measured.

	A2 [km/m ²]	A4 [km/m ²]
Variant A	0.61	0.13
Variant B	7.93	0.00

TABLE 5 Transport distance referenced on 1 m² of an opaque façade component. Measured data for Variant A and Variant B.

BUILDING MATERIAL	VARIANT A			VARIANT B		
	Mass fraction [%]	Transport distance A2 [km]	PE fraction [%]	Mass fraction [%]	Transport distance A2 [km]	PE fraction [%]
Excavated earth	30.30	8	33.50	58.51	223	97.35
Excavated raw clay	22.97	3	7.21	8.70	93	1.18
Clay powder	0.98	426	1.56	2.59	125	0.18
Gravel/marl	43.50	8	56.75	14.55	6	0.17
Sand	1.69	8	0.10	2.76	29	0.03
Trass mortar	0.54	436	0.88	0.45	142	0.01
Geo grid	0.01	19	0.00	0.10	321	0.02
Crashed lava stone	-	-		9.55	12	0.15
Crushed foam glass	-	-		2.80	361	0.92
Total PE [MJ/m ²]			209			3833

TABLE 6 Mass fraction, transport distance (one way) and primary energy (PE) fraction for stage A2 for Variant A and Variant B

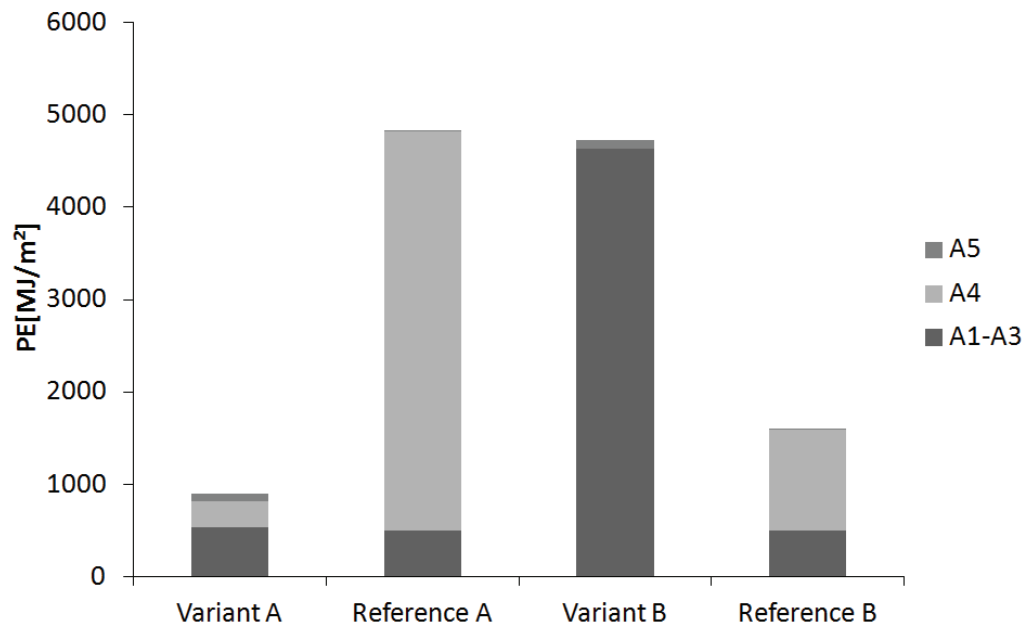


FIG. 6 Total results for PE in MJ/m² at stages A1-A5 for Variant A and B (A1 based on literature study, A2-A5 based on measurement data) and their conventional brick references Reference A and B (based on literature data, worst case scenario for rammed earth)

3.4 SUMMARY FOR STAGES A1-A5 FOR RAMMED EARTH AND BRICK FAÇADES

In Fig. 6, the results of Chapter 3.2 and Chapter 3.3 are summarised and compared with literature data for Reference A and B. As described in Chapter 3.3, the literature data assumes less primary energy demand than that measured in reality. Referring to the proportions of Fig. 4, and the more complex production process of brick façades (see Chapter 2.4), it is expected that the PE at stages A1-A3 for Reference A and B is higher. However, this uncertainty does not change the conclusion of this study that transport has a huge influence on the embodied energy of rammed earth façades.

The embodied energy of the rammed earth façade A is more than 80 % less than its conventional reference. Compared to literature study at stage A1-A3 (see Chapter 3.1) the potential at stages A1-A5 is even higher. However, this conclusion is only valid for local material, as the case study B shows: The transportation requires almost three times more energy than its conventional reference at stage A1-A5. This long transportation of heavy material has a significant impact on the embodied energy. The impact is even higher than the production energy of the insulation (see Fig. 4). This effect is also represented in the comparison of Reference A and B at stage A4: As Reference A is a double brick wall, double the amount of bricks (2m) have to be transported over double the distance (2x) which causes four times PE of Reference B (see equation (1)).

4 CONCLUSIONS

In general, rammed earth façades provide sustainable solutions with a low embodied energy demand. In the considered projects, the production requires only about 151-174 MJ/m². As case study A shows, the embodied energy at stages A1-A5 is more than 80% less compared to its conventional brick reference. However, this conclusion is only valid when using local material, as case study B shows. The impact of transportation is significant, especially for massive constructions in low tech designs with a high thermal mass. Considering both transport stages, A2 and A4, the impact of transport is more than 84% of the total embodied energy (A1-A5) for Variant B.

Furthermore, the comparison of the aggregated literature data with the measurement results shows that aggregation can hide the impact of transportation (A2) in a life cycle assessment. It is critical to obtain information about transport distances at stage A2, when aggregating the PE at stages A1-A3. The study also identifies the need to quantify stages A2 and A4, at least for all materials that contribute to the superstructure of buildings.

References

- AG Mauerziegel. (2015). *Owner of dataset in Ökobaudat Arbeitsgemeinschaft Mauerziegel im Bundesverband der Deutschen Ziegelindustrie e.V.* Retrieved from http://www.oekobaudat.de/OEKOBAU.DAT/datasetdetail/process.xhtml?uuiid=-f98eea66-671c-4014-bfbb-2db1ffb8331&stock=OBD_2017_I&lang=de
- Auer, T., Santucci, D., Knaack, U., & Hildebrand, L. (2015). *Abschlussbericht des Forschungsprojektes Az: 32312/01-25 Entwicklung von Strategien zur Implementierung des grauen Energieaufwandes in den interaktiven integrierten Entwurfsprozess von Gebäuden.* (Development of strategies for considering embodied energy demand in the iterative holistic design process of buildings using the example of the Alnatura Campus in Darmstadt). Deutsche Bundesstiftung .
- Binz, A., Erb, M., & Lehmann, G. (2000). *Ökologische Nachhaltigkeit im Wohnungsbau; eine Bewertung von Erneuerungsstrategien.* (Ecological sustainability in housing construction, an evaluation of refurbishment strategies) Muttenz: Fachhochschule Basel.
- DIN18599-1. (2016). *Energetische Bewertung von Gebäuden - Berechnung des Nutz-, End- und Primärenergiebedarfs für Heizung, Kühlung, Lüftung, Trinkwarmwasser und Beleuchtung - Teil 1: Allgemeine Bilanzierungsverfahren, Begriffe, Zonierung und Bewertung der Energieträger.* (Calculation of the net, final and primary energy demand for heating, cooling, ventilation, domestic hot water and lighting - Part 1: General balancing procedures, terms and definitions, zoning and evaluation of energy sources).
- Herzog de Meuron, J. (2015). Ricola Kräuterzentrum in Laufen. (Ricola herbal centre in Laufen). *DETAIL* (03), p. 210.
- Initiative Ziegel. (2015). *Initiative Ziegel im Fachverband der Stein- und keramischen Industrie Österreich.* Wiedner Hauptstraße 63, 1045 Wien. Retrieved from www.ziegel.at .
- Kellenberger, D., & Althaus, H.-J. (2008). Relevance of simplifications in LCA of building components. *Building and Environment* 44(2009) 818-825.
- Klinge, A., Roswag-Klinge, E., Fontana, P., Hoppe, J., Richter, M., & Sjöström, C. (2016). *Reduktion von Lüftungstechnik durch den Einsatz klimasteuernder Naturbaustoffe-Ergebnisse aus dem EU Forschungsvorhaben H-House und der Baupraxis.*(Reduction of ventilation by using clima regulating natural materials- Results of the EU research project H-House and building experiences).
- Markus, W., Jensch, W., & Lang, W. (2014). The convergence of life cycle assessment and nearly zero-energy buildings: The case of Germany. *Energy and Buildings*, p. 551-557.

- Mattli, S., Klauz, S., Plüss, I., & Menti, U.-P. (2010). *Wohnhaus Rauch - Lehmhaus - Studie bezüglich Grauer Energie, Heizenergie und Komfort bei einem Lehmhaus*. (Residential building Rauch - rammed earth building - study about embodied energy, heating energy and comfort in a building made of rammed earth) Lucerne University of Applied Science and Arts.
- Meex, E., Hollberg, A., Knapen, E., Hildebrand, L., & Verbeeck, G. (2018). Requirements for applying LCA-based environmental impact assessment tools in the early stages of building design. *Building and Environment*, pp. p. 228-236.
- Ökobaudat. (2017). *Bundesministerium des Inneren, für Bau und Heimat (BMI)*. Retrieved from <http://www.oekobaudat.de/>
- ÖNORM B 8119-7. (2013). *Wärmeschutz im Hochbau - Teil 7: Tabelierte wärmeschutztechnische Bemessungssysteme*. (Thermal insulation in building construction - Part 7: Default values for energy benchmark systems).
- ÖNORM EN 15037-3. (2001). *Betonfertigeteile-Balkendecken mit Zwischenbauteilen-Teil 3: Keramische Zwischenbauteile*. (Precast concrete joist ceiling with connecting materials - Part 3 ceramics).
- ÖNORM EN 771-1. (2005). *Festlegung von Mauersteinen*. (regulation of brick stones).
- Osanyintola, O., & Simonson, C. (2006). Moisture buffering capacity of hygroscopic building materials: Experimental facilities and energy impact. *Energy and Buildings* 38:1270-82.
- WSchVO. (1977). *Verordnung über einen energiesparenden Wärmeschutz bei Gebäuden (Wärmeschutzverordnung - WärmeschutzV)*. (Thermal Insulation Ordinance of Buildings for Energy Savings).
- ZAE Bayern. (2011). *Bestimmung von Kenngrößen für Stampflehmproben*. (Analysis of physical properties of rammed earth samples).

Bio-inspired Transparent Microfluidic Platform as Transformable Networks for Solar Modulation

Mark E Alston¹, Uta Pottgiesser², Ulrich Knaack³

1 School of Engineering, Architecture and the Built Environment, University of Nottingham, mark.alston@nottingham.ac.uk

2 Professor of Interior Architecture – Faculty of Design Sciences, University of Antwerp

3 Professor of Design of Construction - Department of Architectural Engineering + Technology, TU Delft

Abstract

The glazed envelopes on buildings play a major role in operational energy consumption as they define the boundary conditions between climate and thermal comfort. Such a façade is viewed as an uncontrolled load that sets the operational performance requirements for artificial lighting and air-cooling mechanical systems. This is in contrast to nature, which has evolved materials with the ability to learn and adapt to a micro-environment through self-regulation using materials that are multifunctional, formed by chemical composition in response to solar load. Leaf vasculature formations are of particular interest to this paper. Through leaf maximisation of daylight capture, the total leaf area density and angular distribution of leaf surfaces define the tree structure.

This paper will define an approach to simulate nature to advance a microfluidic platform as a dynamic NIR absorber for solar modulation: a transformable network of multi-microchannel geometry matrix structures for autonomous transparent surfaces, for real time flow management of conductivity. This is realised through active volumetric flows within a capillary network of circulation fluidics within it, through it, and out of it for energy capture and storage, the cycle of which is determined through precise management of heat flow transport within a material. This advances transparent façades into an energy system for heat load modulation nested to climate and solar exposure, which is demonstrated in this paper.

Keywords

microfluidic, thermal transport, absorber, solar, geometry matrix, bio-ins

DOI 10.7480/jfde.2019.1.2785

1 INTRODUCTION

Transparent glass façades play a major role in operational energy consumption, as they define the boundary between climate and human comfort. This determines operational performance requirements in setting mechanical systems (air-conditioning, artificial lighting demands) in the consumption of primary energy. The conductance of opaque materials for solar modulation is well researched and advanced analytically, and such materials are well established as energy collectors. These materials outperform optic materials and there is nothing of note to add in terms of this research. Optic materials' performances, however, are energetically weak in terms of visible transmittance, and have limited solar energy modulation efficiency and high transmission temperature. As these façades suffer from long-wave solar radiation inputs leading to the overheating of internal spaces and increased cooling demand loads, façades are viewed in terms of transmission loss. This is due to a resulting inflow heat load that is dependent on the overall solar transmittance 'g', including any solar shading. The technical challenges in providing thermal and visual comfort in buildings with large expanses of floor to ceiling glazing are significant. Large areas of glazed façades orientated to the east, west, or south (or north if in the southern hemisphere) (Hens, 2011) will experience the thermal impact of overheating due to sunlight and harsh solar glare. Energy demands in buildings bring together a range of complex relationships between the climate, individuals, and their perception of comfort.

The glazed boundary layer has been determined to date by impact energetic flows focused on high energy consumption, lighting lumens/watts, HVAC, and plug-in end-use loads. Passive systems of Low Zero Carbon (LZC) technologies have been employed as active responses to solar radiation and these measures have been determined by: ventilated, double-skin, kinematic shading system, hybrid, nanocoating thin film reflective, PCM membranes, vacuum insulation, electrochromic, and transparent insulation materials. The minimisation of operational energy building use and maximisation of generated energy in order to reduce greenhouse gas emissions is an aim of the European Directive 2010/31/EU (2010). However, this strategy requires material component elements to respond in real time to yearly, seasonal, and hourly changes in climatic and microclimatic conditions. This multiscale design approach would enable materials to react to external influences and change their thermal behaviour and functionality accordingly (Knaack, Klein, Bilow, & Auer, 2014). LZC technologies do not currently adopt such characteristics of integrated material functionality. The challenge is to progress from the static boundary conditions of steady state theory to the characterisation of non-steady states, and this is determined by thermal (energy) flow. Government targets are making considerable demands on energy reduction targets within an increasingly uncertain climate. These facts all converge on a clear need for a solution that is more compliant than the current state of the art. There is a greater need to measure and understand the nature of thermal transfer effects at the material level for real time responsive conductance measures.

Nature's use of matter and energy is a dynamic relationship that is achieved at differing scales through material diversity (species) and material connectivity (chemical compounds). Nature assembles materials at a formation level to actively manage the composition of a microenvironment that obeys the rules of minimum energy loss and minimum effective power output. Leaves are of particular interest to this research proposal, in terms of management of fluidics through absorption (photosynthesis). This research uses a leaf-like model to progress experimental absorption testing to establish proof of concept.

This paper demonstrates this as an early assessment prototype that could be established at a larger scale for greater comprehensive performance evaluation.

This absorption approach is not used in the current state of the art for fully glazed buildings, in which directly transmitted natural light often needs to be controlled by shading or reflection in order to avoid glare problems and unfavourable distribution of light within a room. Various coatings and pigments are available for glazing to reduce the transmission of solar radiation near infrared irradiation in buildings. Reflecting metal oxide layers are most frequently used for this purpose. By reflecting solar infrared irradiation, heat gains inside the building are avoided, but incident energy is also lost when heat gains would be favourable. Furthermore, this reflective solution will be absorbed by other structures around the building and thus would contribute to urban heat island effects. Research has been undertaken to introduce fluidics into windows, using the FluidGlass technology (Stopper, Boeing, & Gstoehl, 2013) as an absorption solution rather than a reflective one. This work used a triple glazed unit with two fluidic chambers acting as absorption layers by fluid depths of 2mm. The glazing panes that formed this assembly to create the overall unit is composed of 6mm (3 in total) clear glass and two low-E coated 6mm panes.

This study utilised the cavity void between glass panes by filling the void with water for conductivity absorption of solar radiation. The research demonstrated optimised results in a dyed metal particle anti-freeze fluid, demonstrating a reduction in cooling demand energy of 39%. This was achieved through the fluid volume in active flow within the two chambers absorbing solar radiation.

The introduction of anti-freeze eliminates the possibilities of freezing at low night-time temperatures. Further research highlighted a similar approach however the fluidic window generated warm water that was used for heating applications (Chow, Chunying, & Zhang, 2011). The use of water gave higher conductivity for effective window cooling designs in warm climates (Chow & Chunying, 2013).

Water flow in the experiments was set at 200 ml/min with the greater efficiency gained in higher incidence of solar radiation for working efficient conditions. However, the lack of fluidic flow management within the free-flowing volume resulted in flow turbulence and water movement uncontrolled by gravity. This also impacted on water thermal fluidic expansion through solar radiation heat transfer and glazing deflection of the water under gravity. This presents challenging issues for full volume chamber fluidics, which remain unresolved.

It was observed that the water chamber reduced the indoor temperature to 26.14°C in comparison to convection double glazed air-filled unit of 37.72°C on the summer solstice (Lopez & Gimenez-Molina, 2012). However, the difference in temperature, through natural heating buoyancy, created a temperature variation in the liquid volume. This variation in temperature heating and decay increased the thermal expansion issues and diminished control of the liquid volume for solar absorption optimisation. The volumetric weight of the liquid within the assembly is also significant when applied to floor-to-ceiling glazed façade engineering, which further reduces the effectiveness of the application. The research presents a microfluidic-based platform as a method to advance solar modulation, not through a reflective approach of current practice but through an absorption solution, as a leaf-like model. This experimental work is exploratory in nature, as it is established within a laboratory environment to make an early assessment for proof of concept. The paper presents possible methods of integration within an envelope fabric that can possibly be scaled up for advances in envelope design. However, this manuscript does not set out to demonstrate a

comprehensive performance evaluation, but rather presents the next stage in which the process is scaled up for manufacturing.

This introduced method uses an IR absorbing fabrication process and characterisation method with a vascular heat transport system. Using fluidics in capillary channels as heat sinks within a material, we can modulate volumetric flows rates in the material to manipulate the material and fluid thermal transfer. Using active fluids in flow within a material will enable the removal of material thermal stresses, as a material absorbs solar radiation.

2 LEAF-LIKE MODEL

Leaves sync in real-time with the pattern changes of solar radiation (Feugier, Mochizuki, & Iwasa, 2005; Blonder, Violle, Bentley, & Enquist, 2011). Each leaf reacts and responds to variations in wind direction and orientation, and they adjust their surface exposure to harvest solar gain (Fig. 1).

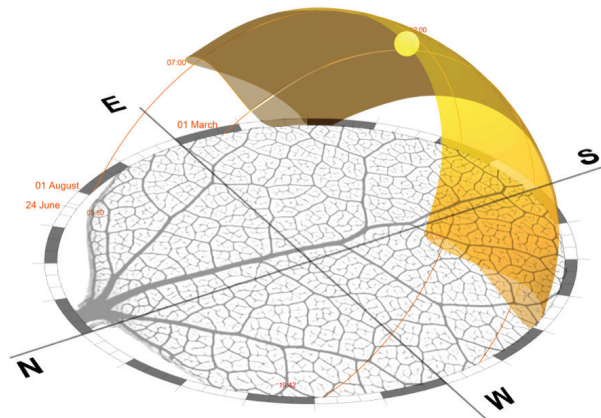


FIG. 1 Leaf Solar Model



FIG. 2 Illustrates how the network can continue to supply fluid flow even when the main central leaf fluid structure has been damaged (denoted by the central punched hole, (Katifori, Szollosi, & Magnasco, 2010).

This single leaf unit acts within a transformable daylight capture system: the tree canopy— through distribution of the leaf surfaces for daylight capture. This is determined by canopy volume, total leaf area density, and the angular distribution of leaf surfaces, to form the tree structure.

This approach to solar orientation and absorption of light energy by biochemical processes are responsive measures and a dynamic system of solar radiation.

Leaves use embedded microfluidic channels as a means to harvest solar energy through fluidic volume filled networks . This formation of capillaries is determined through precise control of channels' geometries set within a material determined by a rule-based hierarchical pattern for the transportation of active liquids. This approach of a leaf-like model could advance materials that are thermally functional to act as a NIR stop band through an absorption approach.

These networks of micro-channels are called vascularisation patterns. This is a highly refined energy reaction system for enhanced material properties of chemical energy flow.

Vasculature patterns are linked to material scale, leaf size, and species in the formation of the channel network (Dengler & Kang, 2001). These closed loop exothermic networks are subject to flow resistance and flow rate, thus enabling significant regulatory roles with tolerances given to damage and water stress conditions (Fig. 2).

The leaf fluid network structure (illustrated by the yellow colour, Fig. 3) exhibits a diminishing order of vein size, as all classes of veins contract in size distally from the main fluidic (central) stem vasculature channel (Turing, 1952). This distribution network is defined by hierarchical scaling that conforms to rules of minimum energy loss, minimum effective fluidic power flow rates, and minimum pressure drop, determined through pressure equalisation by diminishing flow pressure variation across the network. This can be simulated through resistance circuit theory (Oh, Lee, Ahn, & Furlani, 2010), by the regulation of fluidics that is achieved by unified flow rate regulation and thermal dynamics of the fluid within the capillaries.

An experimental device was fabricated to assess and validate the concept within a laboratory environment. Sensors and actuators connected to the device gave active measures in regulating flow rate and absorptivity in setting steady state energy capture and storage. A thermal transport system was determined by energy load – unload processes to maintain a steady state liquid temperature for solar modulation.

2.1 EXPERIMENTAL MULTI MICROCHANNEL DEVICE

A plant closed loop vasculature can be analysed through simulation to generate optimum succession sequencing of a multi microchannel network, such as a leaf-like model. A device demonstrated this iterative approach to obtain a flow parabolic profile for a fully developed flow rate, to advance a multiple channels' network defined by hydrodynamic control of fluids. This optimisation work of capillary succession of channels achieved an accuracy of 1 micron in the capillary geometry formation.

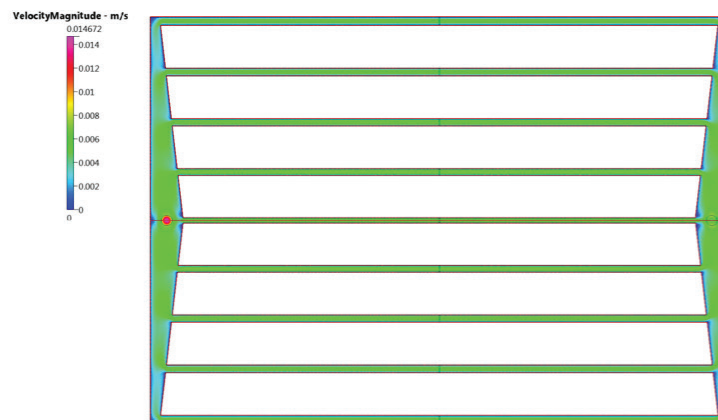


FIG. 3 CFD illustrates a unified flow rate to enhance uniform absorption of solar radiation at high temperature.

The device demonstrated this functionality by IR absorption that is dependent on solar radiation at high temperature (Alston & Barber, 2016). CFD illustrates the optimisation of flow rate within the multi microchannel network to achieve unified planar extensional flow across a planar device (Fig. 3).

NIR absorption is characterised by heat flow determined through the temperature difference between input and extract liquid, coming from the flow circuit (Alston, 2017). The fluid in this network circuit increases in temperature in a non-linear way as a result of solar radiation hitting the surface of the polymer (Fig. 4).

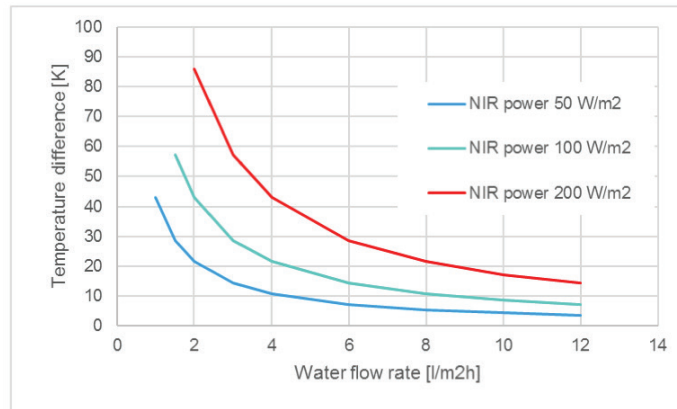


FIG. 4 Temperature gain in K for absorption rates as a function of flow rate (Nestle, Pulbere, & Alston, 2018)

Fig. 4 illustrates the temperature difference between fluidic feed-in to the network and the extract temperature of the fluid coming from the microchannel flow circuit. The NIR power (W/m^2) determines the thermal profile of liquid temperature rise (Δt) by passage through the microfluidic network. By changing the flow rate, we change the temperature increase of the fluid in steady state flows. This contribution proposes that a microfluidic-based platform will advance NIR control by low transition temperature polymer using an absorption fluid approach. The geometry of the channels is determined by systematic resistance networking of multi micro-channel succession, inspired from biology, specifically a bifurcated leaf formation. The input and extract microchannels (manifolds) play a primary role for feed-in fluidics for the network's longitudinal channels. Simulation (CFD) have been undertaken to focus on successive channel widths, and to develop a hierarchy that emulates leaf vascular principles as a closed loop network. Flow input and export channels to accommodate and distribute incoming fluidic flow into the network define this optimised sequence of channel widths. Successive channel widths will increase in relation to increasing flow path length that is determined roughly by the square root of flow to channel path length. The optimised channel sequence in the polymer device was set at longitudinal channels at an equal spacing pattern formation of 15.575mm, with channel widths of:

R0-2.0mm, R1-2.3mm, R3-2.6mm, R4-2.8mm, and the outermost channel R4-3.0mm.

This channel geometry sequence is a hierarchical pattern defined by setting the value of resistance that is emulated by all channels. This was determined by the central channel R0 (target channel) to evaluate all others. This is a leaf-like absorption model which reflects the control of fluidics within capillary channels for unified flows across a network at low-pressure drop. This method follows

the leaf vein formations by the principle of all veins diminishing in size distally from the fluidic input supply. This approach does not use or try to emulate leaf photosynthesis chemical solution fluidics due to formulation fluid complexity. Analysis of leaf-like model advances laminar non-turbulence flows at low flow rate for heat transfer. To optimize heat transfer by volumetric fluidic flow through uniform distribution across the network, the external face of the device, as a scale up, would comprise: 6mm Low-E coated glass Planitherm One to act as a weather facing material and fire protection to form the initial solar control layer. Bonding of this pane to the polymer-based material allowed direct lateral heat flow transfer into a liquid, which was observed by experimental testing as indicated in Fig. 4 results. The synthetic polymer material overall depth is 10mm (formed by two panes). Channel depth within a network composite material (2mm) reduces the associated weight that is currently associated with volume chamber fluidic windows. Thermal functionality is determined through optimum lateral heat transport flow with a minimum amount of fluid volume in network channels at a low flow rate of 1ml/min. Results indicated that water temperature rise occurred through the passage of a fluid within the network by absorbed solar heat gain from a heated polymer surface.

Experimental results demonstrated that input distilled water temperature at 10 °C was heated to an output temperature of 14°C by the polymer heating up through the passage within the capillary network. The solar load applied to the device was 1000 W/m². This energy gain was distributed within the device through the top polymer pane absorbing 210W/m², the fluid absorbing 707W/m² and the lower polymer pane 83W/m². If this device was to be scaled up to a façade area of 10m², 200 litres of water would be obtained at this temperature. Increased solar loading would amplify water temperature rise in the network and associated water output storage temperatures. In principle, polymer microfluidics act as IR stop bands through absorption that is modulated by fluidics to manage the thermal stress that would occur if heat storage was not removed within the material. This is achieved by a reactive response to changing solar intensity environments that is managed by flow rate ml/min and temperature rise, delta t, measurements.

Flow rate sensors and temperature sensors, thermocouples, are established practices within the automotive and aerospace industries, and measure the above parameters. These sensors were used in the experimental device set-up, to actively modulate temperature by fluidics to regulate high temperature thermal issues. This contribution, however, does not address the visible part of the electromagnetic spectrum. Static solar shading or translucent materials would have to be incorporated within the façade design to avoid unwanted glare. The encouraging proof of concept determined a polymer acting as an infrared IR stop-band block at high temperatures through a material ability to lower its phase transition temperature. The functionality of the device is defined by heat flow transport within a composite polymer for enhanced thermal conductance. Application to the real world of the experimental device would need to consider others factors that cannot be replicated within a laboratory setting, which depends on building scale and geometry orientation connected to fluidic management.

3 SYNCHRONIZING MODULAR SOLAR GEOMETRY

Current transparent façade technology considers a glass building to be one surface, notwithstanding that this one surface is comprised of a number of assembly components, frames, mullions, waterproofing gaskets, and drainage channels. The entire glass envelope in a capillary composite glass material could not be treated as one entity, as the vascular network will have a significant

resistance to flow. Pumping pressures need to be controlled for solar modulation, as this function would be outweighed by the pumping energy demands within the network. If the façade was broken into segments per floor level to work collectively to form the emergent façade, this would enhance fluidic flow regulation that is contained within a floor layer, (Fig. 5).



FIG. 5 Building Level Layering Approach

Each level acts as a photoactive layer to create the planar surface. This layer-by-layer approach, using gravitational pull to influence and manage fluidic flow, will reduce energy power demand, by avoiding the pumping of fluids through continuous vertical surfaces over multiple floors. This approach contains the fluid to a zonal (floor) level to manage energy load shift in segments for re-circulation. This load shift moves the active fluids in a flowing circuit into thermal storage tanks. By using the structural floor zone, the reservoir feed in and extract flows will be determined through fluidic temperature rise in relationship to time, T. Extract reservoirs, at the structural floor zone, will remove fluid at higher temperature (Fig.6), from the network for energy download heat exchange. This energy removal cycle is determined by heat transport flow within the network system that is regulated by hydrodynamic and thermal sensors in connection to a defined material datum temperature. By modulating volumetric flow rate ml/min in the networks, we are able to manipulate heat gain at fluid / polymer interfaces, using energy transfer (thermal storage, and electrical – energy conversion from Peltier devices) to monitor temperature. This process would advance energy syncing to user energy demands for consumption profiling to each and every floor (Fig. 6).

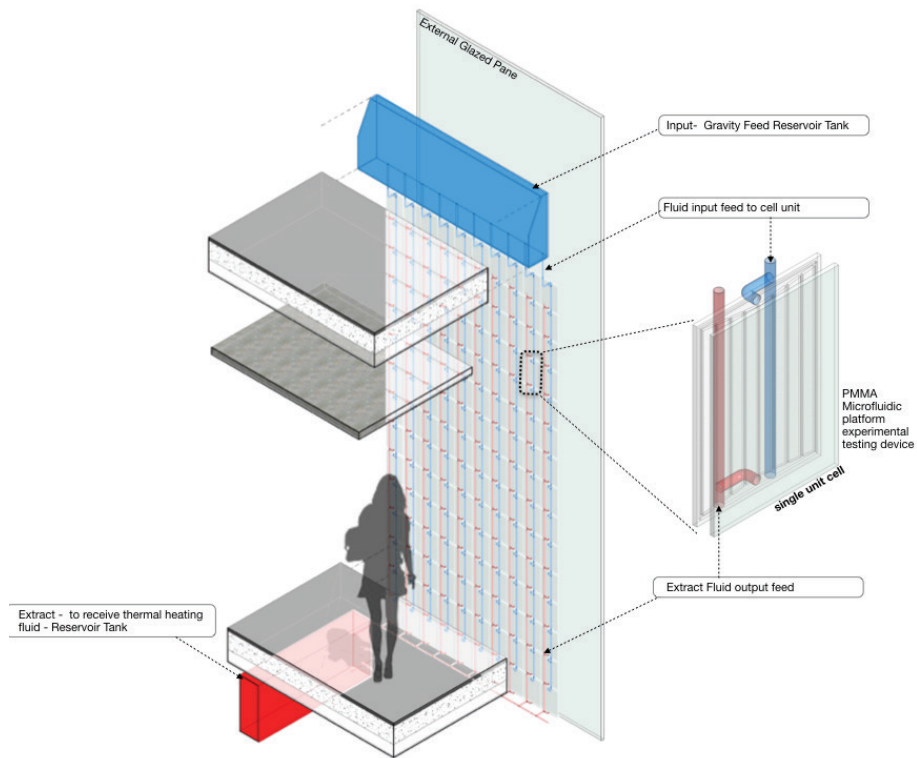


FIG. 6 Section through a building layer with a Capillary Glazed System

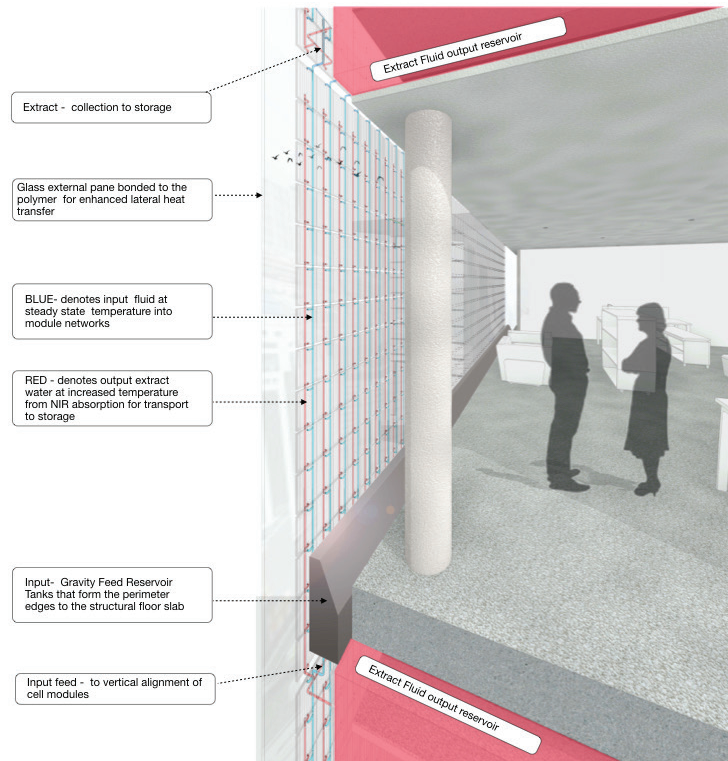


FIG. 7 Section through a building layer with a Capillary Glazed System

Fig. 6 illustrates a repeatable multi-module approach to forming a NIR filtering network to create a geometry system. As each module is independently regulated, this acts as a stop band block to boundary conditions as a performance metric of conductivity, convection, and thermal radiation. This collective approach simulates the structure of a tree by synchronizing network geometry in response to solar radiation intensity. The density of the geometry modules would increase or decrease depending on solar modulation and the requirement need for optical clarity (Fig. 7).

This NIR regulation, by absorption, will heat up the polymer through solar high radiation that will introduce increased thermal stresses within the material. These stresses are managed using precise hydrodynamics control of the microfluidic platform networks. The control of a fluid in volume networks, in comparison to full chamber flooding, enables greater management of thermal absorption to enhance the cooling of the polymer. With increasing solar radiation loading, the module cell geometry spatial separation will become finer and finer as the unit spacing distances reduce to form an overall coherent, maximised-density module pattern. Conversely, as solar radiation decreases, the spacing module pattern will increase to a point at which solar-energy modulation is not needed. This will result in geometry distinctions between building surfaces in a capillary glazing approach method that will be defined by surface function response, as illustrated in Fig. 8. The geometry configuration is a radiant balance between atmosphere and thermal comfort, using module cells that are synchronised to solar radiation load, as a thermal conductance system. A repeatable cell pattern will form the surface of the façade by the deployment of multiple units. Module geometry transformations are set against a changing environmental background aligned to synchronising NIR filtering (Figs 8 & 9).



FIG. 8 Multiple parallel-aligned module cells for maximised low transition temperature

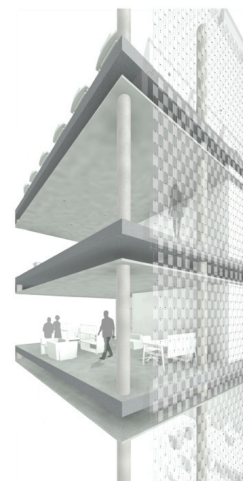


FIG. 9 Module cells with spatial separation for reduced solar radiation load

Figs 8 & 9, illustrate multiple parallel-aligned module cells as a heat seeking system that uses the optimisation parameters of visible transmittance and transition temperature for air conditioning reduction demands. It works as a collective unit that is synced to the user energy demand vector (heating, cooling) through building management monitoring. Figs. 8 & 9 show this geometry systemised solution. However, using NIR absorption glazing as a heat transport method could be optimised for enhanced areas for transparency and functional properties.

3.1 GEOMETRY TRANSFORMATION OF MODULE CELLS

Each module cell is individually autonomous, and would be regulated through flow control measures in relation to fluidic temperature increase within multiple network patterns. These cells are aligned vertically to block IR solar radiation at high temperatures. This gives attractive properties for each cell acting as an IR radiation stop band within a collective formation to maintain low pumping pressures and unified flow at each network entrance of multiple entrance points. These are difficult issues to resolve in maintaining equalised flow distribution for solar absorption. This method would enable operational performance cell tracking through Δt to detect solar radiation properties and the parameters for transition temperature. This approach would advance variant distribution patterns (Fig. 10) to transform transparent façades.

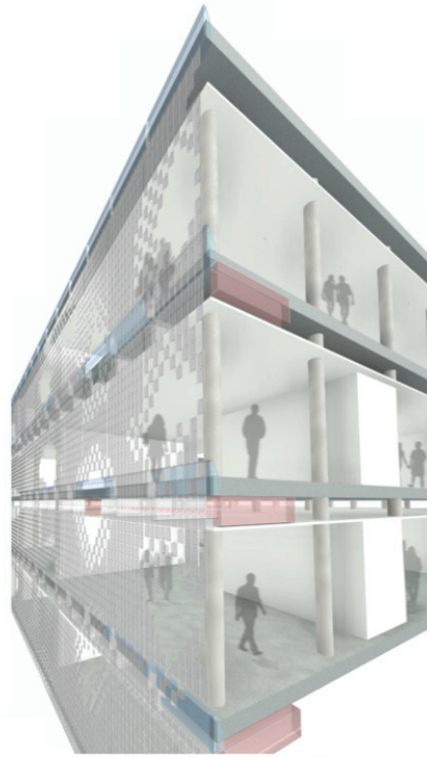


FIG. 10 Transformable module cells networks for solar modulation

This distribution system is a dynamic envelope that is nested to performance change by the hour, season, and weather conditions.

4 CONCLUSION

Global government targets for energy consumption reduction, and increasing uncertainty in the climate, all convey on a clear need for a solution for façades that has greater compliance to such standards. This has been determined to date through thin film reflecting metal oxide layers, electrochromic, and transparent insulation materials. These approaches also reduce the visual contact and optical benefits of view, colour, and light intensity that cannot not be underestimated for human well-being. The research demonstrates a material microfluidic platform of multiple cell geometry as a NIR absorption solution to enhance solar modulation properties, by employing the strategy of fluidics to control and manage multiple microfluidic based module cells to drive the assembly formation of a fully glazed façade as a stop band block for infrared IR solar radiation.

The regulation and management of a material is advanced through multiple networks in response to high solar radiation, by changing the synchronising geometry pattern that enhances distributed NIR filtering to create autonomous optic material surfaces for adaptive performance.

Acknowledgements

Colleagues within BASF SE Advanced materials and system research, Germany, who are referenced within this paper. Thank you to Dr. Robert Barber for his support and advice from Scientific Research Facilities Council, UK government facility SRFC, Daresbury, UK, and to our reviewers who have given formative feedback to progress this paper.

References

- Alston, M.E. (2017). Optimal Microchannel Planar Reactor as a Switchable Infrared Absorber: (invited manuscript) *MRS Advances. Nanomaterials*. Vol. 2, 14, pp. 783-789
- Alston, M.E. & Barber, R. (2016). Leaf venation as a resistor to optimize a switchable IR absorber. *Scientific Reports* 6, 31611; doi: 10.1038/srep31611.
- Blonder, B., Violle, C., Bentley, L. P., & Enquist, B. J. (2011). Venation networks and the origin of the leaf economics spectrum. *Ecology Letters*. 14, pp. 91–100.
- Chow, T.T., Chunying, L., & Zhang, L., (2011) Thermal characteristics of water-flow double-pane window. *International Journal of Thermal Sciences*, 50: 140-148.
- Chow, T.T., & Chunying, L., (2013) Liquid-filled solar glazing design for buoyant water-flow. *Building and Environment* 60: 45-55.
- Dengler, D., & Kang, J. (2001). Vascular Patterning and Leaf Shape. *Plant Biology, Elsevier Science*. 4, pp. 50-56.
- European Parliament Directive 2010/31/EU (2010). European Parliament and of the Council of 19 May 2010 on the energy performance of buildings (recast), *Official Journal of the European Union* 53 (2010) 13.
- Feugier, F.G., Mochizuki, A., & Iwasa, Y. (2005). Self organization of vascular systems in plant leaves: inter-dependent dynamics of auxin flux and carrier proteins. *Journal of Theoretical Biology*. 236, pp. 366–375.
- Hens, H. (2011). *Applied Building Physics, Boundary Conditions, Building Performance and Material Properties*. Berlin: Ernst + Sohn.
- Katifori, E., Szollosi, G.J., & Magnasco, M.O. (2010). Damage and Fluctuations Induce Loops in Optimal Transport Networks, *Physical Review letter*, PRL 104,04874.
- Knaack, U., Klein, T., Bilow, M., & Auer, T. (2014). *Façades, Principles of construction*. Basel: Birkhäuser Verlag GmbH.
- Lopez, T., Gimenez-Molina, C (2012) Influence of double glazing with circulating water chamber on a thermal energy saving in buildings, *Energy and Buildings*, 56, pp.56-65
- Nestle, N., Pulbere, S., & Alston, M.E. (2018), Possible benefits of capillary flow glazing in translucent wall elements, *Facade 2018 – Adaptive!*, Proceedings of the COST Action TU1403 – Adaptive Facades Network Final Conference, Luzern.
- Oh, K.W., Lee, K., Ahn, B., & Furlani, E.P. (2010). Design of Pressure-driven Microfluidic Networks using Electric Circuit Analogy. *Lab on a Chip*. 12, pp.515-545.
- Stopper, J., Boeing, F., & Gstoehl, D., (2013) FluidGlass Façade Elements: Influences of dyeable Liquids within the Fluid Glass Façade, *Energy Forum on Solar Building Skins, Bressanone*.
- Turing, A. M. (1952). The Chemical Basis of Morphogenesis, *Philosophical Transaction of the Royal Society of London, Series B, Biological Science*. 237, 641, pp 37-72.

COPYRIGHT NOTICE

Author(s) hold their copyright without restrictions.

The PLUG-N-HARVEST Façade: A Second Skin with Active and Passive Components

Verena Dannapfel¹, Tanja Osterhage², Maike Klein², Rita Streblow², Marius Vontein³, Dirk Müller², Markus Kuhnhenne³

- 1 E.ON Energy Research Center, Institute for Energy Efficient Building and Indoor Climate, RWTH Aachen University, Aachen, Germany, email: verena.dannapfel@eonerc.rwth-aachen.de
- 2 E.ON Energy Research Center, Institute for Energy Efficient Building and Indoor Climate RWTH Aachen University, Aachen, Germany
- 3 Institute of Steel Construction, Sustainable Metal Building Envelopes, RWTH Aachen University, Aachen, Germany

Abstract

The construction of office buildings in particular, as well as multi-family dwellings, are largely based on regular planning grids, and the widths of such grids appear to be repetitive across Europe.

In the EU project, PLUG-N-HARVEST, a multi-modular façade system for refurbishment, based on these planning grids, is developed. To achieve a comprehensive improvement of the building's energy efficiency, different solutions for active and passive energy demand reduction, as well as harvesting of heat and power were combined, while also taking into account the existing building structure, climatic region, and usage profile.

The PLUG-N-HARVEST façade is designed to enclose the existing façade like a second skin. Thus, the remaining protection provided by the existing outer shell allows continuous usage. The modular approach enables economic efforts by serial production with a high degree of prefabrication and thus shortened assembly time. At the same time, the toolkit design follows the principles of the circular economy. In visual terms, various façade surfaces will be available to allow both an orientation to the existing building and an aesthetic reorientation.

In 2019, pilot buildings in Greece, Spain, the United Kingdom, and Germany aim to show the adaptability of the modular toolkit to different façade geometries and to assess its ecological and economic benefits.

Keywords

Refurbishment, Modular, Circular Economy, Renewable Energy Sources (RES), Building Integrated Photovoltaics (BIPV)

DOI 10.7480/jfde.2019.1.2772

1 INTRODUCTION – CHANCES OF A MODULAR TOOLKIT FOR THE REFURBISHMENT OF FAÇADES

Around 75 % of the European building stock is deemed energy inefficient by the European Commission (European Commission, 2016). Buildings are responsible for 38 % of the EU's CO₂ emissions and, at 40 %, its largest final energy consumer (European Commission & Joint Research Center, 2015). To meet the EU's energy efficiency targets for 2050, a constant minimum renovation rate of 3 % is required (Europäisches Parlament, 2018). This means that it is necessary to triple the average rate of 1 % in 2011 (BPIE, 2011).

How can refurbishment become more attractive?

The construction of office buildings in particular, as well as multi-family dwellings, are largely based on regular planning grids. Throughout Europe, the widths of grids appear to be repetitive as they are based on the Euromodule or masonry sizes, which are consistent across several countries. The idea of the EU-project PLUG-N-HARVEST is to develop a modular façade toolkit, based on these typical grids. This enables economic advantages by serial production with a high degree of prefabrication and thus shortened assembly time. Moreover, the system is designed for exterior application to face obstacles against refurbishment beyond pure investments, namely the wish to allow the ongoing use of a building during refurbishment (dena, 2017), which is enabled by the remaining protection provided by the existing outer shell.

The project PLUG-N-HARVEST is funded by the European Research and Innovation Programme Horizon 2020 and started in September 2017 with a project duration of 51 months. The international project consortium consists of research, industrial, and local government partners from Germany, Greece, Spain, the United Kingdom, and Romania, while the Greek Centre for Research and Technology Hellas (CERTH) has the leadership. In Germany, a cross-institutional team of the RWTH Aachen University of architects, civil engineers, and mechanical engineers is responsible for the technical and architectural design.

As mentioned before, one potential market for the PLUG-N-HARVEST system can be found in offices. In Germany, 65% of the office building stock was built before 1978 and thus before the implementation of the 1st German Heat Saving Ordinance (dena, 2017). In different European countries, like the United Kingdom, the Netherlands, or Germany, from 1950 to 1970, offices were largely built in skeleton construction or with storey wide ribbon windows (Ebbert, 2010). A typical U-value for mullion-transom-façades and metal windows of this building age can be assumed to 4.3 W/(m²K) (BMU & BMWi, 2015). To put this into perspective: The valid German energy saving ordinance (EnEV) 2014/2016 specifies a maximum U-value for windows of 1.3 W/(m²K). This serves as an indication of the improvement potential in terms of transmission losses. Nevertheless, the central elements of modern office refurbishments are mechanical ventilation, heating, and cooling (dena, 2017). Improvements in the building technology achieve energy as well as life cycle cost savings and increased user comfort. That's why a central element for the energetic improvement is the thermal conditioning of buildings. In Germany, it accounts for about 27% of the primary energy consumption (dena, 2018).

Façade systems that are entirely passive can achieve final energy savings up to 50% (dena, 2016). Complementary technology, such as decentralised ventilation units with heat recovery, shading systems, or collectors for renewable energies can exploit further saving potentials. The modules of the PLUG-N-HARVEST façade include both passive components, like insulation or windows, and

active components for ventilation, heating, and cooling. In addition, the PLUG-N-HARVEST concept can also be transferred to multi-family dwellings, which make up 40 % of the German living space (dena, 2018) and of which, similar to the office sector, about 60 % was built before 1978 (dena, 2018).

The individual modules of the PLUG-N-HARVEST façade, as well as their components, are separately exchangeable, which enables the implementation of a leasing model and supports a further project objective, namely compliance with the principles of the circular economy, by the recyclability of complete modules, components, and materials. Thus, PLUG-N-HARVEST has the potential to overcome existing obstacles to refurbishment, while being economically advantageous to existing solutions.

2 METHODOLOGY – ANALYSIS OF STRUCTURES AND REQUIREMENTS

The RWTH Aachen University is responsible for the modular toolbox design, dynamic simulations, and laboratory testing of the prototypes, as well as the German pilot study. Therefore, civil engineers, mechanical engineers, and architects from the Institute of Steel Construction - Chair of Sustainable Metal Envelopes and the E.ON Energy Research Center - Institute for Energy Efficient Buildings and Indoor Climate, work together in collaboration.

The PLUG-N-HARVEST design concept is based on a constructional analysis of offices and multi-family dwellings in Europe. Office buildings mostly follow country-specific or European standardised horizontal grids. Fig. 1 shows two examples of office buildings with the same horizontal grid, one with ribbon windows and one with a mullion-transom façade, which were typical construction designs between 1950 and 1970 in several countries in Europe (Ebbert, 2010). Due to fall protection regulations, the balustrades are also of similar heights, with a minimum of 90cm. Differences can be found in the storey heights, as they depend on the individual room height, as well as floor and false ceiling constructions. Some residential and office buildings do have vertical projections in the external wall, for example oriels or balconies, which interrupt vertical grids and need to be taken into account in the design.



FIG. 1 Regular horizontal and vertical grids of office buildings

A closer look at European grids shows that they are based either on the Euromodule, which was implemented by ISO 1006 in 1973, or on a country-specific basic module derived from masonry sizes (see Fig. 2). This leads to different extension grids as well as typical façade grids based on workspace regulations. The structural grid can be a multiple of the horizontal façade grid, for example, in skeleton construction.

	Standard	Basic Module [cm]	Extension Grid [cm]	Horizontal Facade Grid [m]	Structural Grid [m]
European Union from 1973	Euromodule ISO 1006	10	60	1.20	7.20
				1.50	7.50
Germany (additional)	Masonry Size DIN 4172	12.5	62.5	1.25	7.50
				1.50	
United Kingdom (additional)	Masonry Size BS 5628	11.25	67.5	1.35	...
...

FIG. 2 European basic modules and common grids

In the sector of residential buildings, regular grids are used in many objects, but as shown in Fig. 3, they have divergent measurements for the horizontal and the vertical grids from one object to the other. Only the balustrades remain at a minimum height of 90 cm.



FIG. 3 Regular grids in multi-family dwellings without repetitive measurements

The possibility to assemble an additional façade in front of the existing one is directly related to the existing load-bearing structures and its remaining capacity. Skeleton structures transfer loads horizontally to the primary load-bearing structure, while massive wall constructions are part of the primary structure themselves. Potential fixing points of the primary or secondary load-bearing structure need to be accessible. Therefore, existing external insulation or cladding must be partly removed. For both skeleton and massive construction, fixing to the ceiling construction could be a suitable solution, if its remaining load bearing capacity is sufficient. The energetic quality of buildings can be increased either by the reduction of the final energy demand or by the substitution of fossil fuels by renewable energy sources (see Fig. 4).

As mentioned in the introduction, transmission losses are having a high impact on the energetic demand of a building. A German study shows that improving the quality of windows and external walls achieves a final energy saving of up to 50 % (dena, 2016), and in office buildings in particular, where large areas of the façade have a poor U-value, about three to four times worse than the minimum standard for new buildings, the potential for energy saving is high. Each European country has its own U-value requirements that are in accordance with its climatic region and, usually, additional restrictions for the building's primary energy demand and emissions. In the Mediterranean climate, for example, the prevention of summerly overheating may have a higher priority than heating.

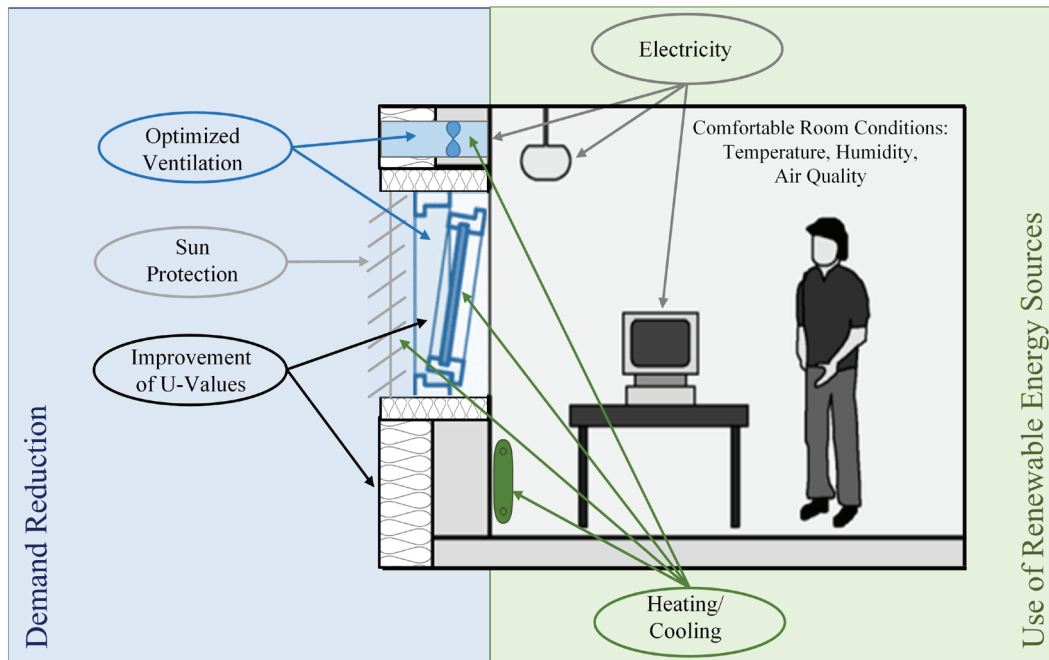


FIG. 4 Improved energetic quality by demand reduction and the use of renewable energy sources

External sun protection is an appropriate measure in this case. Furthermore, optimised ventilation, for example demand-led or with heat recovery, is capable of reducing heat losses, while keeping or increasing the user comfort.

Renewable energy sources can be used to supply electricity or heat. To harvest electricity within a façade, building integrated photovoltaics (BIPV) or building applied photovoltaics (BAPV) are conceivable. Thermal conditioning can be done with the support of solar thermal collectors to provide heated water or air and electrical devices like infrared heaters or cooling units. In terms of aesthetic requirements, non-residential buildings tend to favour modern surfaces, like glass, aluminium, or partly visible technology like PV-cells, while residential buildings tend towards an appearance that is adapted to the surroundings, with subdued and natural colours (white, brown, terracotta) and low reflection. Additionally, local building authorities set guidelines for certain districts.

3 EXPERIMENT / RESEARCH – DEVELOPMENT OF THE PLUG-N-HARVEST MODULAR TOOLKIT

3.1 MAIN ELEMENTS

Fig. 5 shows the main elements of the PLUG-N-HARVEST system. The idea within the PLUG-N-HARVEST design is to use recurrent horizontal grids of offices and multi-family dwellings to determine fixed sizes of modules, which then incorporate passive and active components. Site-measured elements can cover differences in storey heights and additionally function as an installation channel for media supply and control, as well as a fire barrier between storeys. The module's frame is made from aluminium. It has fixing points on the top and on the sides and thus can be installed on horizontal or vertical substructures, which transfer the Main elements of the

PLUG-N-HARVEST system additional loads of the system onto the existing load-bearing structure, or to an additional foundation, with a horizontal locking position only. The use of a substructure is not only due to static reasons. It also enables the separate exchangeability of the modules for technical reasons or because of changes in requirements. Nevertheless, their installation needs to be airtight and secure. So far, within the project, 1.10 m, 1.20 m, and 1.60 m have been fixed as the widths of modules, as well as 90 cm for the height of the balustrade module. Further module heights are based on typical window sizes. The modules' design and choice of components are based on the principles of the circular economy.

In the case of divergent or lacking grids, as typical in small residential buildings, the use of balustrade modules in combination with a conventional façade system opens the possibility to add efficient building technology and energy harvesting components to an existing building with short planning processes and under continuous usage.

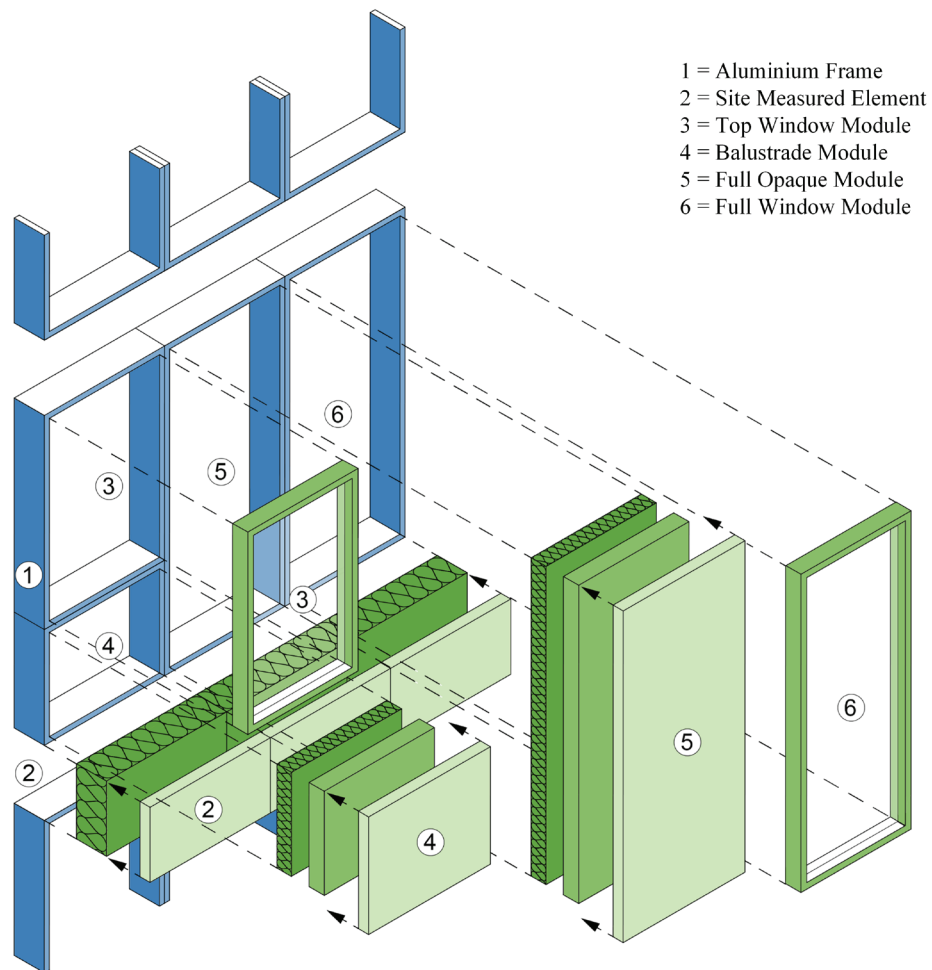


FIG. 5 Main elements of the PLUG-N-HARVEST system

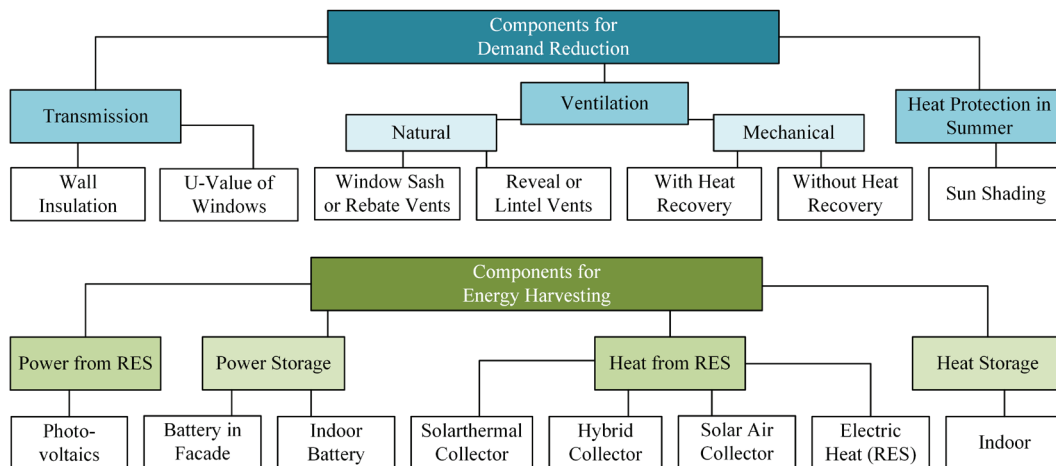


FIG. 6 Components for demand reduction and energy harvesting

3.2 COMPONENTS

As mentioned in Chapter 2, measures to increase the energetic quality of a building can focus on either the demand reduction or the use of renewable energy sources (RES), which shall be provided locally by energy harvesting within PLUG-N-HARVEST. Components from both approaches have been examined. Those which fulfil the technical requirements of security and noise regulations, and which fit inside the determined module sizes, are listed in Fig. 6. Market available products got collected within a database. Their suitability in terms of circular economy is currently under investigation.

The first approach towards the module's depth is 30 cm. The first step in the choice of components is the determination of the required additional insulation by taking the module's frames and substructure into account. This leads to an object-specific free space for technical equipment or additional insulation. In the case of further requirements, for primary energy demand for example, these were fulfilled primarily before the client could choose further components based on his personal preferences. All components will remain separately exchangeable in the cases of changes in use, the end of the component's service life, or the end of a leasing contract. The interaction with the interior is made by drilling holes for media supply, like an air duct with an outlet and heat recovery (HR), and for control purposes as well as through a supplementary connection to the technical room for the potential storage of heat and power or network feeding.

The claddings can be architectural or technical and do partly overlap with the aluminium frame. They need to be easily removable to be exchanged, but also to access the components in behind and the installation duct within the site measured element. Although different cladding types do have different cladding depths, the leading edge of the façade needs to remain in the same position. Therefore, deep claddings are added by using an architectural frame, so they can leap between the profiles of the aluminium frame. The remaining differences between the individual claddings can be covered by adjusted rear ventilation gaps. For the windows, additional or substitutional solutions are conceivable. Furthermore, an option with only a 'hole' in front of the existing window will be evaluated. An additional window could be, for example, sliding or opening outwards. Through this approach, the quality of the existing windows is taken into account and therefore, the costs and the embodied energy of the refurbishment can be kept low.

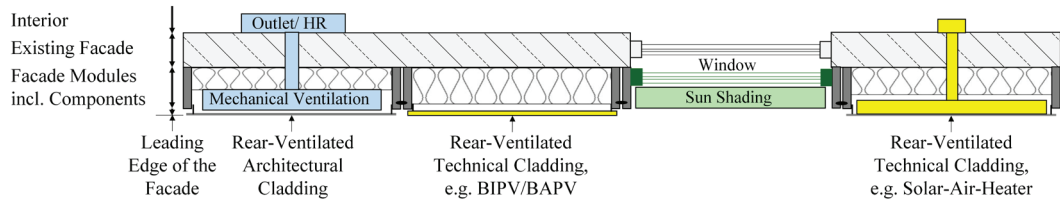


FIG. 7 Examples of different module configurations

During the assembly of the PLUG-N-HARVEST façade, the remaining or subsequent disassembled window protects the interior, so that persistent usage is possible. Each module can be configured from different components, based on country-specific regulations, the existing building's load-bearing structure and energetic quality, as well as individual preferences in terms of costs, aesthetic appearance, and ecological performance. One example of such a configuration is shown in Fig. 7. As mentioned before, there are various aesthetic requirements for the appearance of non-residential and residential buildings. While the possibility for purely architectural claddings is well known, technical claddings, like building integrated or building applied photovoltaics (BIPV/ BAPV), also offer manifold surfaces to meet those requirements.

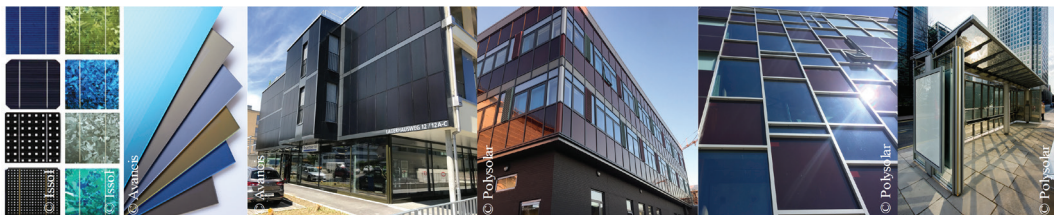


FIG. 8 Modern surfaces with photovoltaics

Fig. 8 shows different modern surfaces with photovoltaic technology in use. There is a huge variety of possible colours and patterns available, as well as prints and coatings. Furthermore, semi-transparent BIPVs with daylight transmission up to 70 % are possible, but will not be focused upon in PLUG-N-HARVEST, as the daylight transmitting areas of existing buildings will not be enlarged by the refurbishment and a reduction of the previous light transmission may lead to problems with workspace regulations and decreased comfort.

Fig. 9 and Fig. 10 show photovoltaic products with more subdued colours and non-reflective to low-reflective surfaces, with the help of structured glass surfaces. These are suitable options for residential buildings in particular, as they have a similar appearance to existing surfaces, like plastering or clinker bricks. The left side of the figures shows residential reality, while the right side shows matching implemented PV-solutions.

However, the aesthetic appearance of photovoltaic products is directly linked to its efficiency and cost. In particular, thin film technologies and crystalline cells with coloured applications are accompanied by reduced efficiency under Standard Test Conditions (Green et al., 2018) and higher system costs (Wietschel, Ullrich, Markewitz, Schulte, & Genoese, 2015). Furthermore, toxic ingredients used in specific technologies like arsenide or cadmium can result in poor ecological performance in the case of circular economy (MCDonough Brangart Design Chemistry, 2016). This is the reason why the choice of a specific type should be considered holistically. This is also the focus in PLUG-N-HARVEST.

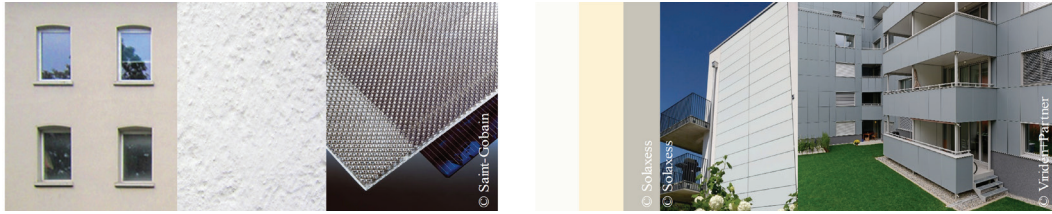


FIG. 9 Photovoltaics with subdued colours, white to grey, and structured glass surfaces for matte appearance



FIG. 10 Photovoltaics with subdued colours, terracotta

4 RESULTS – VALIDATION AND DETAILING OF THE PLUG-N-HARVEST DESIGN

4.1 ARCHITECTURAL AND TECHNICAL DETAILING

At the beginning of 2019, the first prototypes of the PLUG-N-HARVEST system will be realised and examined in the experimental hall of the Institute for Energy Efficient Buildings and Indoor Climate of the RWTH Aachen University; these focus on the constructional details of the modules themselves. Firstly, the design has to be durable and secure, in terms of the stability of the modules as well as the secure fixing of the cladding on them. The fixing needs to resist static and dynamic forces and at the same time must be easily removable for exchange and maintenance of the technical units behind. Secondly, based on the fixed module sizes, the total façade system has to be capable of handling the constructional tolerances. In the vertical direction, these will be covered by the site measured element. In the horizontal direction, the junction between the modules needs to be tolerance-adaptive while at the same time it has to fulfil tightness requirements against wind and rain, as well as after the exchange of a module. Thirdly, movements of the modules caused by temperature and deflection will occur and need to be compensated to avoid rising tensions. In terms of building physics, the prevention of thermal bridges and condensation are the main tasks.

Fig. 11 shows sketches of the PLUG-N-HARVEST design and examples of the current constructional and physical building issues under examination. The laboratory testing on the prototypes will focus on those subjects with the aim to validate or adjust the design concept.

Besides the physical tests, dynamic simulations in Modelica®, as well as CFD (Computational Fluid Dynamics)-simulations, are conducted to prove required ventilation and thermal behaviour. Keeping the project goal of conformity with the principles of circular economy in mind, the design is also examined under their guidelines for separation and selection of materials.

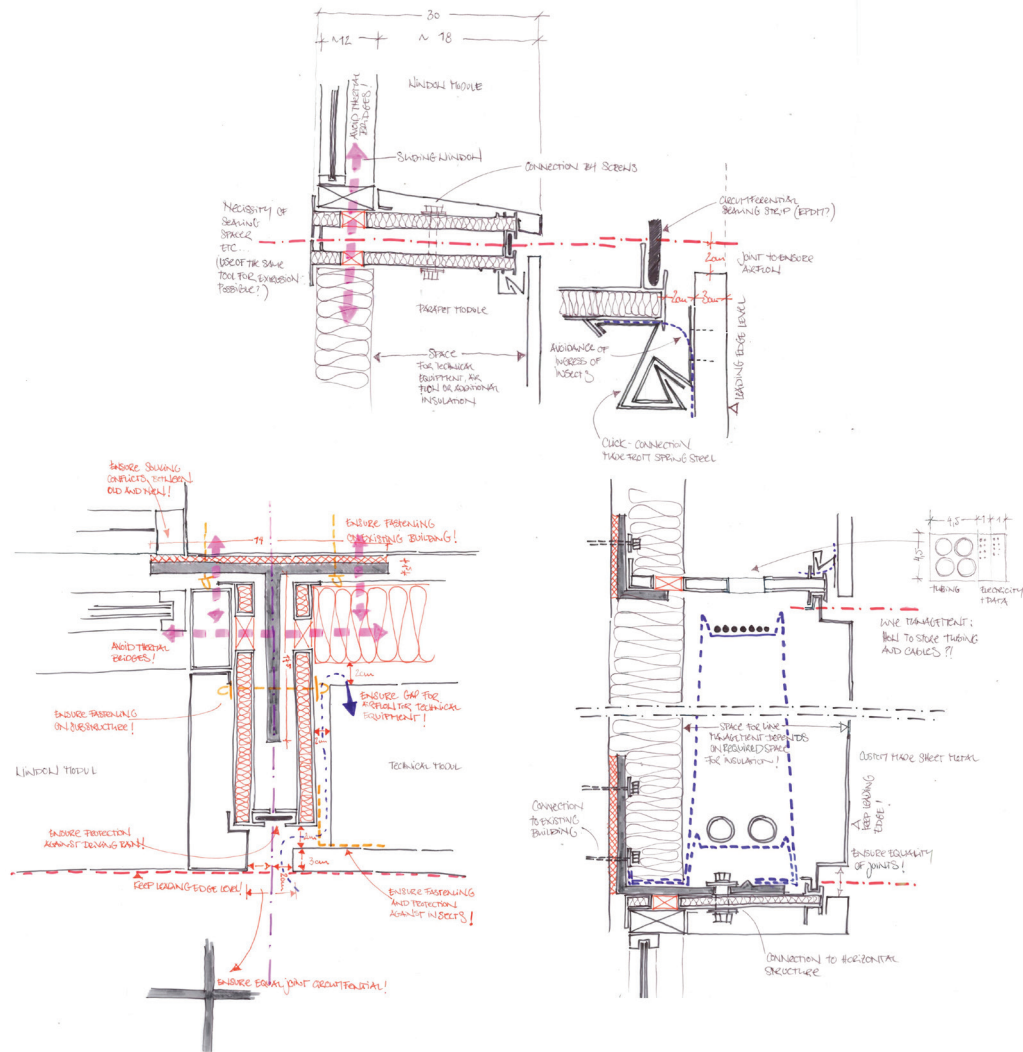


FIG. 11 Sketches and current issues in design details

4.2 SUITABLE BUILDINGS AND SUBSTRUCTURES

The PLUG-N-HARVEST modules are suitable to be fixed to either a horizontal or a vertical substructure, which itself will transfer forces created by the façade extension to the existing load-bearing structure or, if necessary and possible, partly to an additional foundation. The horizontal substructure will be realised by an L-angle and the vertical by a T-profile. In accordance with the modular approach, both substructures' dimensions have been calculated for different combinations of module width or, respectively, static lengths as multiples of these, as well as storey heights, a maximum additional weight of 150 kg/m^2 , and deflection limited to $l/300$. Table 1 shows an extraction of this calculation for the horizontal L-angle.

Furthermore, different qualities and heights of concrete ceilings have been examined in terms of their capability to transfer the resulting forces. The calculation is made for a direct application with dowels and two screws per module into the core area of the ceiling. The resulting minimal

thickness for the ceiling can also be found in Table 1. The table shows that certain ceilings of either insufficient concrete quality or insufficient thickness will not be able to hold the substructure with the attached modules under these boundary conditions. Smaller thicknesses may be possible using more fixation points per module or optimised weight. These options will be examined further over the course of the project. Because the ceiling, as a load-bearing structure of secondary order, works as a load-transferring element, its total capability also has to be approved in accordance with further parameters such as traffic loads. Moreover, the further transfer via the primary structure – pillars or walls – and the foundation to the ground cannot be analysed within the modular toolkit framework and must be proven for each object by an authorised local engineer.

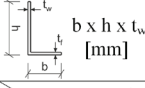

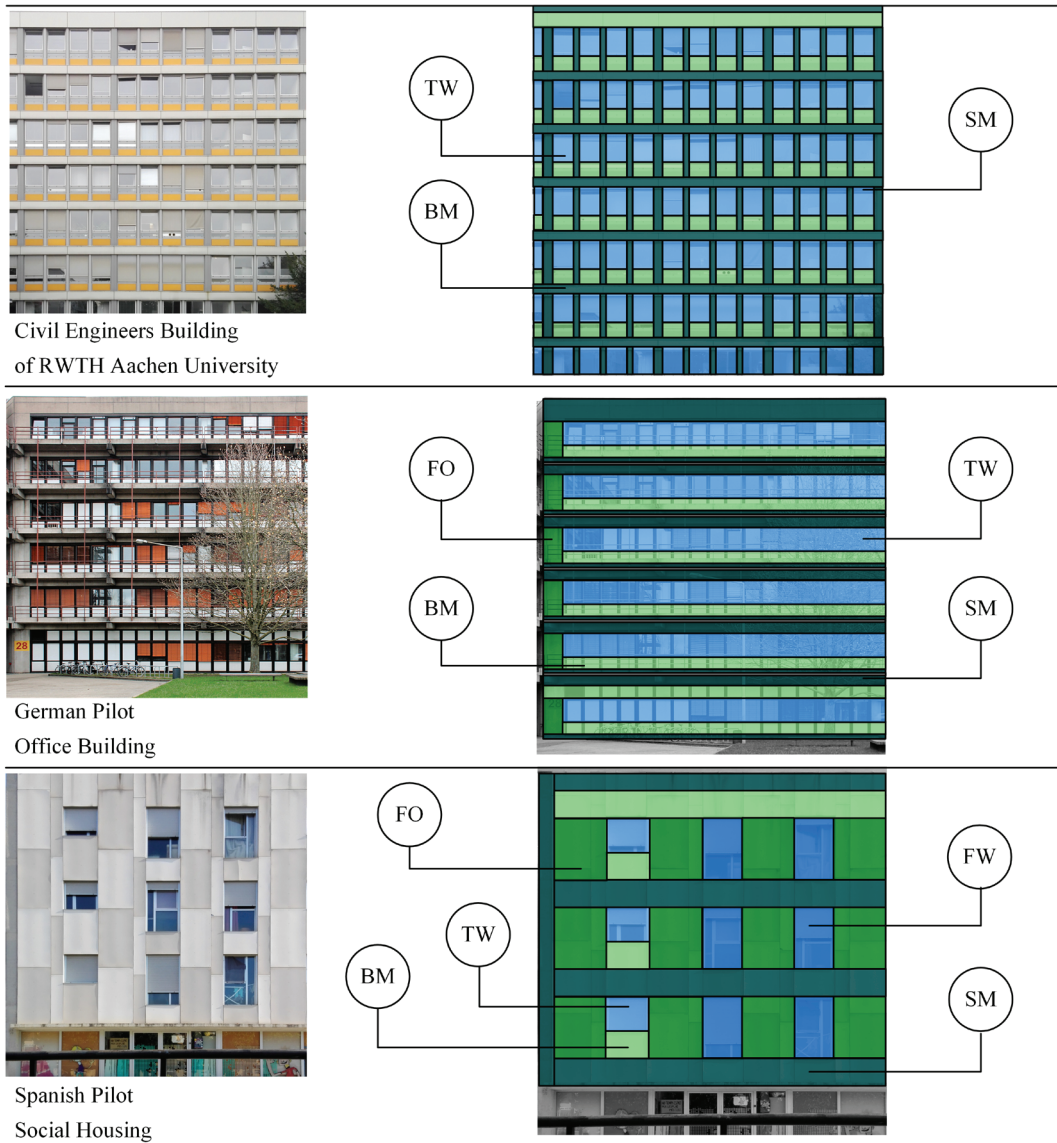
 b x h x t _w [mm]		Dimension of Horizontal Substructure (L-Angle) in accordance to Module Widths „A“ = 1.10 m and „B“ = 1.20 m and limited deflection of l/300					
Storey Height	Static Length	3 x Module Width		5 x Module Width		7 x Module Width	
		„A“	„B“	„A“	„B“	„A“	„B“
3.00 m		150 x 200 x 10	150 x 200 x 10	200 x 200 x 12	250 x 200 x 12	300 x 200 x 12	300 x 200 x 12
3.50 m		150 x 200 x 10	150 x 200 x 10	200 x 200 x 12	250 x 200 x 12	300 x 200 x 12	300 x 200 x 15
4.00 m		150 x 200 x 10	150 x 200 x 10	250 x 200 x 12	250 x 200 x 12	300 x 200 x 15	350 x 200 x 15
		Minimal Thickness of Existing Concrete Ceilings for the Application of Substructure by Dowels in accordance to Module Widths „A“ = 1.10 m and „B“ = 1.20 m, Module Weight ≤ 150 kg/m ²					
Storey Height	Concrete Quality	C 20/25		C 25/30		C 30/37	
		„A“	„B“	„A“	„B“	„A“	„B“
3.00 m		22 cm	22 cm	22 cm	22 cm	20 cm	20 cm
3.50 m		22 cm	> 24 cm	24 cm	24 cm	22 cm	24 cm
4.00 m		> 24 cm	> 24 cm	24 cm	> 24 cm	24 cm	24 cm

TABLE 1 Substructure dimensioning

4.3 APPLICATION EXAMPLES

The PLUG-N-HARVEST modular toolkit can be applied to different types of buildings, which are based on a regular planning grid. Not all grid sizes will be covered by the final toolkit, but the selection will follow a potential analysis and economic criteria. Different application examples are displayed in Fig. 12. The first building shows the Civil Engineers' Building of RWTH Aachen University, where the Institute of Steel Construction, a member of the PLUG-N-HARVEST team, is situated. In the visualised module arrangement the following module sizes were used: Balustrade Module 1.35 m x 0.90 m, Top Window Module 1.35 m x 2.00 m. The second building is the German pilot, an office building in Aachen, with a Balustrade Module of 1.20 m x 0.90 m, Top Window Module of 1.20 m x 1.70 m, and a Full Opaque Module of 1.20 m x 2.50 m. The last building shows the Spanish pilot, a social housing complex near Barcelona, for which the following modules and sizes are used: Balustrade Module of 1.20 m x 0.90 m, Top Window Module of 1.20 m x 1.30 m, Full Opaque Module of 1.60 m x 2.20 m, and a Full Window Module of 1.20 m x 2.20 m.



Legend:
 TW = Top Window Module; BM = Balustrade Module; FO = Full Opaque Module; FW = Full Window Module;
 SM = Site Measured Element

FIG. 12 Application examples for different building types

The implementation of the PLUG-N-HARVEST system at the aforementioned pilots in Germany and Spain and additional residential buildings and offices in Greece and Wales is planned for 2019. The pilot tests will be accompanied by a process of monitoring to examine the building's behaviour, energy demand and supply by energy harvesting, interior comfort, and user satisfaction, before and after the refurbishment. The choice of suitable components including technical equipment, is based on a configuration flowchart, in which country-specific regulations, existing building structures, and energetic quality, as well as personal preferences, are taken into account. The modular approach and the external installation result in high requirements for the installation paths and interfaces. In the same context, a plug-n-play automation, which is able to interoperate with different devices inside the PLUG-N-HARVEST system, as well as existing technology and sensors within the building, is currently under development.

5 CONCLUSIONS – ADVANTAGES OF THE PLUG-N-HARVEST MODULAR TOOLKIT

The PLUG-N-HARVEST concept is a multi-modular toolkit for the refurbishment of the European building stock. It is intended to overcome existing obstacles to refurbishment, such as high investments and temporary vacancy, through large scale production and exterior implementation in front of the existing façade. The combination of components for the reduction of active and passive energy demand and those for renewable energy harvesting enables a comprehensive improvement of the building's energetic quality. At the same time, the design follows the principles of circular economy.

The modular approach has the potential to be economically and ecologically advantageous to existing refurbishment solutions under the preliminary condition that a refurbishment object fits to the system's boundary conditions. Such conditions include, on the one hand, a regular planning grid, which matches one or more of the module sizes that are determined at the end of the project and, on the other hand, the remaining capacity of the existing building's load-bearing structure or the possibility to add a foundation to capture the additional weight of the PLUG-N-HARVEST façade. Especially in the office and multi-family dwellings sector, the PLUG-N-HARVEST system might be an appropriate solution to be introduced at a large-scale.

Though the use of fixed module sizes and their ability to remain separately exchangeable has economic and ecological advantages, it also comes with challenges from a technical perspective, for example, the covering of tolerances or the junction details between the modules and the cladding. Within PLUG-N-HARVEST, suitable solutions to the challenges are developed.

PLUG-N-HARVEST will provide a methodology by which modules can be individually configured based on country-specific requirements for construction and energetic refurbishment, such as U-value requirements, primary energy demand or emissions, object-specific boundary conditions, and an overview of available components set up as product-neutral technology profiles.

Pilot projects in Greece, Spain, the United Kingdom, and Germany will be used to validate the technical implementation of the PLUG-N-HARVEST concept and to assess its ecological and economic benefits. The development of a business plan and the identification of potential exploitation partners complete the approach.

Acknowledgements

We are thankful for the kind permission to use pictures of:

Issol sa/nv, Dison (Liège), Belgium, Products Issol Solar-Terra and Cenit Visual, <http://www.issol.eu>

Avancis GmbH, Torgau, Germany, Product Avancis Powermax Skala, Project Sennareal, Bern, www.avancis.de

Polysolar Ltd., Cambridge, United Kingdom, PS-A and PS-CT-series, www.polysolar.co.uk

Compagnie de Saint-Gobain, Courbevoie, France, Product SGG Albarino S, www.saint-gobain.com

Solaxess SA, Neuchâtel, Switzerland, White Photovoltaics at the refurbishment project Boudry, Switzerland, www.solaxess.ch

Viridén+Partner AG, Zurich, Switzerland, BFE Lighthouse project MFH Hofwiesen-/Rothstrasse in Zurich, refurbishment and

spatial extension with an active solar façade (BIPV) from coloured photovoltaic modules with monocrystalline cells, www.viriden-partner.ch

www.viriden-partner.ch

© European Union

This project has received funding from the European Union's Horizon 2020 research and innovation programme under grant agreement No 768735.

References

- Bundesministerium für Umwelt, Naturschutz und Reaktorsicherheit, & Bundesministerium für Wirtschaft und Energie. (2015). Bekanntmachung der Regeln zur Datenaufnahme und Datenverwendung im Wohngebäudebestand [Publication of rules on data collection and use in the residential building stock]. Berlin.
- Ebbert, T. (2010). Re-Face: Refurbishment strategies for the technical improvement of office façades. (Doctoral dissertation). Delft: Technische Universiteit Delft.
- Deutsche Energie-Agentur GmbH. (2017). Büroimmobilien: Energetischer Zustand und Anreize zur Steigerung der Energieeffizienz [Office properties: Energy status and incentives to increase energy efficiency]. Berlin.
- McDonough Brangart Design Chemistry. (2016). C2CCertified Product Standard V3.1. Charlottesville, Virginia.
- Wietschel, M., Ulrich, S., Markewitz, P., Schulte, F., & Genoese, F. (2015). Energietechnologien der Zukunft [Energy technologies of the future]. Wiesbaden: Springer Fachmedien Wiesbaden.
- Green, M. A., Hishikawa, Y., Dunlop, E. D., Levi, D. H., Hohl-Ebinger, J., & Ho-Baillie, A. W.Y. (2018). Solar cell efficiency tables (version 51). *Progress in Photovoltaics: Research and Applications*, 26, 3-12. Retrieved from <https://doi.org/10.1002/ppp.2978>
- Europäisches Parlament. (2018). Gesamtenergieeffizienz von Gebäuden [Energy performance of buildings]. Brussels.
- European Commission, & Joint Research Center. (2015). Energy Renovation: The Trump Card for the New Start for Europe. Brussels.
- European Commission. (2016). Accelerating clean energy in buildings: Clean Energy For All Europeans. Brussels.
- Deutsche Energie-Agentur GmbH. (2016). dena-Studie: Auswertung von Verbrauchskennwerten energieeffizienter Wohngebäude. Berlin.
- Deutsche Energie-Agentur GmbH. (2018). dena-Gebäudereport kompakt 2018: Statistiken und Analysen zur Energieeffizienz im Gebäudebestand [dena building report compact 2018: Statistics and analyses on energy efficiency in existing buildings]. Berlin.
- Buildings Performance Institute Europe. (2011). Europe's buildings under the microscope: A country-by-country review of the energy performance of buildings. Brussels.

COPYRIGHT NOTICE

Author(s) hold their copyright without restrictions.



JOURNAL OF FACADE DESIGN & ENGINEERING

VOLUME 7 / NUMBER 1 / 2019

- V Editorial PowerSkin 2019**
- 001 Trombe Curtain Wall Façade**
Thomas Wüest, Andreas Luible
- 013 Comparative Overview on LCA Software Programs for Application in the Façade Design Process**
Rebecca Bach, Negar Mohtashami, Linda Hildebrand
- 027 A Study on the Impact of Climate Adaptive Building Shells on Indoor Comfort**
Jacopo Gaspari, Emanuele Naboni, Caterina Ponzio, Adele Ricci
- 041 SMP Prototype Design and Fabrication for Thermo-responsive Façade Elements**
Jungwon Yoon
- 063 Auxetic Structures and Advanced Daylight Control Systems**
Yun Kyu Yi, Ryan Sharston, Dua Barakat
- 075 Impacts on the Embodied Energy of Rammed Earth Façades During Production and Construction Stages**
Lisa Nanz, Martin Rauch, Thomas Honermann, Thomas Auer
- 089 Bio-inspired Transparent Microfluidic Platform as Transformable Networks for Solar Modulation**
Mark E Alston, Uta Pottgiesser, Ulrich Knaack
- 101 The PLUG-N-HARVEST Façade: A Second Skin with Active and Passive Components**
Verena Dannapfel, Tanja Osterhage, Maike Klein, Rita Streblov, Marius Vontein³, Dirk Müller, Markus Kuhnhenne



TU DELFT OPEN
ISSN PRINT 2213-302X
ISSN ONLINE 2213-3038

ISBN 978-94-6366-127-0



9 789463 661270